CHARACTERIZATION AND ANALYSIS OF PLASMA INSTABILITIES IN A 600W PERMANENT MAGNET HALL THRUSTER

THESIS

Samuel D. Wright, Captain, USAF

AFIT-ENY-MS-18-M-308

**DEPARTMENT OF THE AIR FORCE
AIR UNIVERSITY**

AIR FORCE INSTITUTE OF TECHNOLOGY

Wright-Patterson Air Force Base, Ohio

AFIT-ENY-MS-18-M-308

Characterization and Analysis of Plasma Instabilities in a 600W Permanent Magnet Hall Thruster

THESIS

Presented to the Faculty

Department of Aeronautics and Astronautics

Graduate School of Engineering and Management

Air Force Institute of Technology

Air University

Air Education and Training Command

In Partial Fulfillment of the Requirements for the

Degree of Master of Science in Astronautical Engineering

Samuel D. Wright, BS

Captain, USAF

March 2018

DISTRIBUTION STATEMENT A.
APPROVED FOR PUBLIC RELEASE; DISTRIBUTION UNLIMITED.

AFIT-ENY-MS-18-M-308

CHARACTERIZATION AND ANALYSIS OF PLASMA INSTABILITIES IN A 600W PERMANENT MAGNET HALL THRUSTER

Samuel D. Wright, BS
Captain, USAF

Commmittee Membership

Carl Hartsfield, PhD
Chair

Maj. David Liu, PhD
Member

William Hargus, PhD
Member

AFIT-ENY-MS-18-M-308

Abstract

Electric propulsion is an important technology for the future of space operations and exploration. Within the range of electric propulsion devices, Hall Effect Thrusters provide a balance of thrust and specific impulse well-suited for many Earth-centric missions. Hall Effect Thrusters have been studied since their development in the 1960s and have been flown on hundreds of spacecraft, but the intimate details of the plasma behavior within the thruster exhaust plume are still not well understood. Furthering this knowledge may be key to improving thruster design to yield better performance and longer lifetimes. To this end, experiments were conducted to measure visible emissions, plasma potential, and Hall Current from a 600 W permanent magnet Hall Effect Thruster in operation modes that exhibited two well-known plasma behaviors—breathing and azimuthal spokes. Multiple delays and issues with the thruster and laboratory equipment severely limited data collection during the present research, but a number of visible emissions data samples were collected. Data revealed the breathing mode exhibited in the permanent magnet thruster is similar to that in a previously studied electromagnet thruster. Additionally, a trend in the breathing mode was observed that appears to lead to discharge extinction. An azimuthally-varying mode was also identified and compared to the spoke mode exhibited by the electromagnet thruster.

For my ever-supportive wife and son.

Acknowledgments

Much thank is due to my advisor, Dr. Carl Hartsfield for the expert knowledge he shared with me and all of his support through this research. This work would also have been exponentially more difficult without the laboratory technicians and staff, including Mike, Josh, and Jamie.

I would also like to acknowledge Dr. Mitat Birkan of the Air Force Office of Scientific Research for providing funding and support for this research.

Samuel D. Wright

Table of Contents

List of Figures

List of Tables

CHARACTERIZATION AND ANALYSIS OF PLASMA INSTABILITIES IN A 600W

PERMANENT MAGNET HALL THRUSTER

I. Introduction

1.1 Background

One of the primary subsystems of a spacecraft that is often critical to mission completion is propulsion. This subsystem allows a spacecraft to adjust its orbit, to include correcting for orbit injection errors, recovering from the effects of aerodynamic drag and perturbations caused by J2 and third-body effects, enabling rendezvous or intercept of other spacecraft, and, probably most importantly, performing planned orbit changes such as orbit raising to geosynchronous orbit (GEO) or injection into a patched-conic or other interplanetary trajectory. The historic method of space propulsion has been to use chemical thrusters of some description, such as small solid apogee kick motors or chemical bi-propellant rockets. Chemical rockets require relatively large amounts of fuel and oxidizer in addition to a thrust chamber suitable for containing the combustion reactions and a converging-diverging nozzle with a sufficient area ratio to expand the exhaust to provide the desired thrust. Reducing mass is highly desirable for spacecraft, as spacelift costs increase steeply with increasing weight, so lighter propulsion systems have been of great interest throughout the Space Age.

A chemical rocket's mass is heavily dominated by propellant, so a rocket that uses less propellant is likely to have a much lower overall mass. Specific Impulse (I_{sp}) is a measure of total impulse delivered by the rocket per mass (or weight) unit of propellant. Thus, a rocket with a higher I_{sp} can deliver the same total impulse with less propellant compared to a rocket with lower I_{sp}. Electric thrusters also have the advantage of being able to restart thousands of times

1

over their lifetime, as opposed to chemical rockets. This makes the use of electric thrusters very promising; while chemical rockets have I_{sp}s in the 150-400 second range, some electric thrusters have no theoretical limit on I_{sp} and I_{sp} values into the tens of thousands of seconds are achievable today [1].

There is a penalty for increased I_{sp} in electric thrusters, however, in that their power systems require more mass. Hall Effect Thrusters (HETs) have a good ratio of I_{sp} to mass for Earth-based missions, and thus have been studied extensively since their invention. They are typically capable of I_{sp}s from 1100-2000 or more seconds. While they were invented in the United States, most early research was performed in the Soviet Union as much of the US's research focus was on ion engines. The United States first flew a Hall Thruster on orbit in 1998 as part of the National Reconnaissance Office's (NRO) Space Technology Experiment (STEX) program [1]. Research has continued since then, and Hall Thrusters have become more prevalent, though more research and better modelling is required to increase their efficiency.

Hall Effect Thrusters are typically constructed in the form of a channel formed by two concentric cylindrical walls, each with magnets on the side opposite the channel. The back of the channel contains an anode and a gas feed, which are sometimes combined into one piece, and a cathode is mounted on the outside of the channel. The magnets surrounding the channel impose a radial magnetic ($\vec{B}$) field, and an axial electric ($\vec{E}$) field is applied from anode to cathode. The interaction of these fields causes electrons to accelerate in the $\vec{E}x\vec{B}$ direction, trapping them in a drift within the channel. The electrons in the drift are very high-energy, travelling at a velocity roughly 2 % of the speed of light, so when the working fluid (usually Krypton or Xenon) is fed into the channel, the atoms are impacted by these electrons and ionized. These ions are

accelerated by the electric field out of the channel at speeds up to 100 km/s, but usually limited to about 20 km/s [1].

1.2 Motivation

Hall Thrusters have been researched and used for several decades now, but fully understanding the complex plasma behavior that allows them to operate has eluded researchers. Observation of the plasma has been quite difficult with available technologies, and the transience in the plasma behavior has prevented the development of robust, reliable models. As tends to be the goal in most spacecraft research, the goal in Hall Thruster research is to design lighter, more efficient thrusters that require less propellant so more payload can be carried. Current Hall Thruster performance models are generally adequate for analysis of steady-state averages, but fail to predict complex plasma behavioral modes on small timescales [2]. This research aims to collect data from a 600 W permanent magnet Hall Thruster in operation at a high data rate, between 500 kHz and 1 MHz, to observe the plasma behavior on a small timescale and to investigate causal relationships between anomalous diffusion modes and plasma properties. The data will also be compared to similar data from a 600 W Electromagnet Hall Thruster to compare plasma instability behavior and attempt to isolate differences between the thrusters as causal to the behavior of instabilities.

1.3 Scope

The unit being studied will be a Busek 600 W Permanent Magnet Hall Thruster. Data expected to be collected in this research include local plasma potential measured with an emissive probe, Hall current measured with magnetic field sensors, and visible emissions captured with a high speed panchromatic camera, all collected at a very high data rate, between 500 kHz and 1 MHz, and time-correlated. The data from these collections will be compared to

similar data from a 600 W Electromagnet Hall Thruster to determine whether geometric differences are causal to plasma instability behavior. The behavior of plasma instabilities will also be correlated to determine causal relationships between plasma properties and anomalous diffusion modes based on differences in applied electric and magnetic fields in the two thrusters.

1.4 Experimental Methodology

Hall Effect Thrusters require a vacuum environment to operate, so all experiments will be conducted in the vacuum chamber located in The Air Force Institute of Technology's (AFIT) Space Propulsion Application Simulation System (SPASS) Laboratory. This vacuum chamber is approximately cylindrical, with a diameter of 1.8 m and a length of 3.76 m. It is capable of maintaining pressures less than or equal to $3 \cdot 10^{-7}$ torr with no gas flow into the chamber, or approximately $3 \cdot 10^{-5}$ torr while a thruster is in operation [3]. The Busek 600 W Permanent Magnet Hall Thruster will be mounted to a translational stand inside the chamber.

During experiments, an emissive probe will be placed in the plume to measure local plasma potential, magnetic field sensors will be used to measure Hall current, and a high-speed panchromatic camera will be used to capture visible emissions.

II. Background

2.1 Rocket Propulsion Basics

     As with all propulsion, rocket propulsion has its theoretical roots in Newton's second law. As forces are applied to a system, the momentum of the system changes at a rate equal to those forces. This is represented in Equation 2.1:

$$\sum \vec{F} = \frac{d}{dt}(m\vec{v}) \tag{2.1}$$

Assuming a rocket starts with a given mass m and velocity v and no external forces are applied, then there is no change in total momentum within the system; this is known as conservation of momentum. This assumption is valid when pressure effects of the rocket exhaust are negligible and the rocket is operating in the absence of atmospheric drag, both of which are the case for Hall Effect Thrusters, which require near-vacuum conditions to function and operate at very low exhaust pressures. When the rocket is firing, mass dm is ejected at velocity v_e as in Figure 2.1 and the total momentum can be shown to be conserved as in Equation 2.2:

$$mv = (m - dm)(v + dv) + dm(v - v_e) \tag{2.2a}$$

or, expanded,

$$mv = mv - v\,dm + m\,dv - dm\,dv + v\,dm - v_e\,dm \tag{2.2b}$$

where dv is the increase in velocity of the rocket. Higher order terms can be neglected, and this can be simplified and examined with respect to time in Equation 2.3:

$$v_e \frac{dm}{dt} = m \frac{dv}{dt} \tag{2.3}$$

The rate of mass ejection from the rocket is equal in magnitude to the rocket's change in mass, but the rocket's change in mass ($\dot{m}$) is negative. Simplifying some more, $\frac{dv}{dt}$ is equal to the rate of

change in the rocket's velocity over time, or acceleration (a). Thus, Equation 2.3 is equivalent to

Equation 2.4:

$$ma = -v_e\dot{m} \tag{2.4}$$
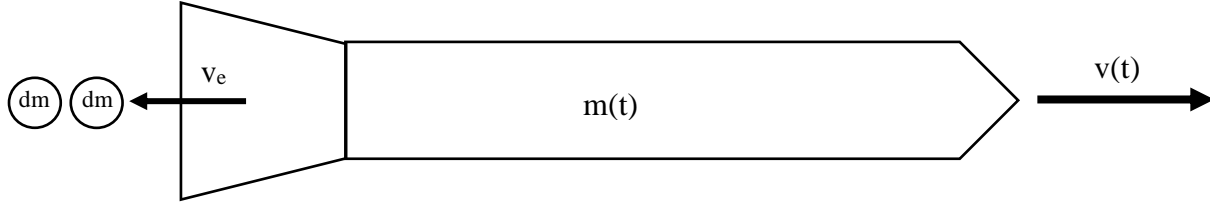
Figure 2.1: Ideal Rocket System

When the system is defined such that the exhaust is excluded from the system under

consideration, the same equations hold, but there is now a non-zero force acting on the system.

To satisfy Equations 2.1 and 2.4 this force can be defined as the thrust according to Equation 2.5:

$$T \equiv v_e\dot{m} \tag{2.5}$$

Still ignoring higher order terms, Equation 2.2b can be integrated from the rocket's initial

mass and velocity, m_0 and v_0, to its final state, m_f and v_f. In representing the result of this

integration, it is useful to introduce one of the most useful parameters for characterizing rocket

performance, I_{sp}, defined in Equation 2.6:

$$I_{sp} \equiv \frac{T}{g_0\dot{m}} = \frac{v_e}{g_0} \tag{2.6}$$

where g_0 is a constant defined as the acceleration due to gravity at the Earth's surface,

9.80665 m/s^2. Using this definition, the change in velocity, Δv, induced by a rocket as it expels

mass is given by Equation 2.7:

$$\Delta v = I_{sp}g_0 \ln\left(\frac{m_0}{m_f}\right) \tag{2.7}$$

This equation is known as the ideal rocket equation [4]. Space missions and maneuvers are

commonly characterized by the amount of velocity change required to complete them, so

6

Equation 2.7 allows one to determine the amount of propellant required to complete a given maneuver for a rocket with a particular I_{sp}.

2.2 Plasma Basics

While chemical rockets operate within the realm of normal fluid mechanics and compressible flow, Hall Effect Thrusters rely on electromagnetic forces for their operation, as will be discussed further in a future section. For this reason, the working fluid in a Hall Effect Thruster is a gas that is ionized in the thruster, resulting in a plasma. A plasma is the state of matter in which electrons are separated from atoms or molecules, leaving these particles with a net charge. For the purposes of the present research, the gas being ionized consists of a single monatomic noble gas; the atoms therein will be stripped of one or more electrons, resulting in a field of positively charged ions and a number of electrons equal to the sum of the charge of all of the ions.

2.2.1 Quasineutrality

In the absence of other forces, and assuming the ions and electrons do not recombine, these ions and electrons will assume their lowest-energy configuration, which is uniform distribution throughout the vessel in which they are contained, if wall effects are neglected. In this configuration, any volume large enough to statistically represent the distribution of particles in the vessel as a whole will have no net charge. This is known as quasineutrality [5]. Deviations from this uniform distribution will introduce internal forces in the plasma seeking to reinstate the minimum energy configuration of the particles. Such forces have been suggested as contributors to various types of plasma instabilities, including those that are observed within Hall Effect Thruster exhaust plumes, although the cause of variations in the distribution of charge in the plasma has not been explicitly determined [1].

2.2.2 Larmor Radius

Larmor radius is a plasma parameter that is of particular import in understanding plasma physics as it applies to Hall Effect Thrusters. When a charged particle is exposed to an electric field ($\vec{E}$) and a magnetic field ($\vec{B}$), the particle experiences an acceleration according to the Lorentz force equation, shown in Equation 2.8 [1]:

$$\vec{F} = m_p \frac{d\vec{v_p}}{dt} = q_p(\vec{E} + \vec{v_p} \times \vec{B}) \tag{2.8}$$

where q_p, m_p, and $\vec{v_p}$ are the charge, mass, and velocity of a particle, respectively. Ignoring the electric field, this equation describes a particle acceleration that is always orthogonal to the particle's direction of motion and the magnetic field; the particle's motion, then, can be described as the result of the centripetal force experienced by the particle as it orbits a magnetic field line. This allows one to solve for the radius of the motion of a particle, also known as the Larmor radius, by Equation 2.9 [1]:

$$r_L = \frac{m_p v_\perp}{q_p B} \tag{2.9}$$

where $v_\perp$ is the component of the particle's velocity orthogonal to the magnetic field.

2.2.3 Ionization Mechanisms

Generally speaking, a gas can become ionized when a sufficient amount of energy is imparted to the particles therein. This energy transfer typically results from the impact of a highly energetic charged particle or photon with a neutral atom. The energy that needs to be transferred to a particle in this impact in order to ionize the particle varies by species and is known as the species' ionization potential. Particles may also be ionized multiple times; the result of this is an ion that has a charge greater than +1electron unit and a number of free electrons equal to the resulting charge of the ion. Each additional ionization requires more

energy than the previous, typically almost double, as shown in Table 2.1 for the two species of

interest in the present research, Xenon and Krypton.

Table 2.1: Ionization Potentials for Species of Interest [1,6]

Species	First Ionization Potential (eV)	Second Ionization Potential (eV)
Xenon	12.1299	21.2100
Krypton	13.9996	24.3590

While multiple ionizations are not uncommon in Hall Effect Thruster operation, they are not

desired and contribute as a loss mechanism. Thus, the ionization mechanism in the thruster,

which will be discussed in a future section, must be capable of imparting 12.1299 eV of energy

into neutral atoms when running on Xenon, or slightly more energy, 13.9996 eV, when running

on Krypton. It is also desirable for the ionization mechanism to have a low probability of

imparting energy in excess of the propellant's second ionization potential to singly ionized

particles.

2.2.4 Gas/Plasma Photon Emission

When energy is imparted to a gas by collision of high energy particles with neutral atoms,

some amount of excess energy is provided to the atom. As the energy is absorbed by the atom,

the atom's electrons will occupy higher energy levels or, if enough energy is absorbed, an

electron will be separated from the atom, ionizing it, as discussed above. As with a

non-quasineutral plasma as discussed above, the atom cannot maintain this higher energy state

and will naturally return to its base energy state. In doing so, the atom must release energy,

which it does by emitting a photon. The energy states achievable to the atom are discrete, so

emitted photons have a precise energy associated with each quantum leap. This means that the

spectrum of this emission is unique to each species, a fact that can be helpful in identifying what species are present in an energized or ionized gas flow. Generally speaking, the predominant wavelengths present in emissions from energized Xenon are visible to the human eye in the blue range, while energized Krypton emissions are more visible in the violet range [7]. In the current research, this phenomenon was observed and used to determine the status of the thruster under different operating conditions, which will be discussed in a later section.

2.3 Hall Effect Thruster Basics

As shown in the ideal rocket equation above, the I_{sp} achievable by a rocket is a significant factor in its ability to perform maneuvers. I_{sp} is directly proportional to exhaust velocity, so for maneuvers that require a large Δv, chemical rockets, which are limited in exhaust velocity by the thermodynamic energy available in the propellant, are not always the best solution. A different class of rockets, known as electric thrusters, rely on electromagnetic forces to propel ions to generate thrust and often offer improvements in I_{sp} by orders of magnitude over chemical rockets, allowing them to perform higher Δv maneuvers or perform the same maneuvers with significantly less propellant than their chemical counterparts.

Hall Effect Thrusters are one type of electric thruster, specifically belonging to the subcategory of electrostatic thrusters. As opposed to chemical rockets' limit of about 450 s of I_{sp}, Hall Effect Thrusters can achieve I_{sp}s of around 2,000 s [1]. Electric thrusters offer a few other major benefits over chemical rockets as well. Propellant for chemical rockets is often caustic, highly reactive, and/or toxic, either before or after being combusted, or both, and may require highly specialized storage tanks; electric thrusters, on the other hand, typically use inert gases safely storable at high pressures, making them generally much safer than chemical rockets. Electric thrusters can also use any available power source the spacecraft can collect. This leads to

10

one major obstacle, however, in that this power must be conditioned for use by the various thruster components, which requires a significant amount of mass above the mass of the thruster itself. The thrust generated by the engine is also dependent upon the amount of electric power available to it, and at typical power generation levels for vehicles on orbit, this is extremely low compared to chemical rockets.

There are a number of research areas of interest regarding Hall Effect Thrusters, including new configurations such as non-cylindrical channels, multiple concentric channels served by the same sets of magnets, and thrusters with improved magnetic shielding. All of these are variations on the more traditional coaxial Hall Effect Thruster design, which consists of inner and outer cylindrical hubs containing magnets, shielded behind ceramic insulators, and a gap between them forming the cylindrical Hall Current channel. This traditional design is the type of thruster that was studied in the present research, with one exception. For enhanced tunability and ease of use, most thrusters have been designed with electromagnets, while the thruster under study here uses permanent magnets, which offers some power savings and significant mass savings. The operating principles of this type of thruster as well as the theory invoked in the present research will be outlined in the below sections.

2.3.1 Theory of Thruster Operation

Figure 2.2 shows two views of a Hall Effect Thruster, the left looking at the exhaust channel and the right showing a cross-section thereof. Features of interest are labeled in one or more parts of the figure, but it is important to note that the operation of the thruster is approximately radially symmetric, so features labelled in one part of the figure can be assumed to also be uniformly distributed around the channel. In most cases, the features are also distributed uniformly across the channel width, so most parameters are assumed to be constant

11

both radially and azimuthally, but the operation of the thruster will cause variations in the axial direction.
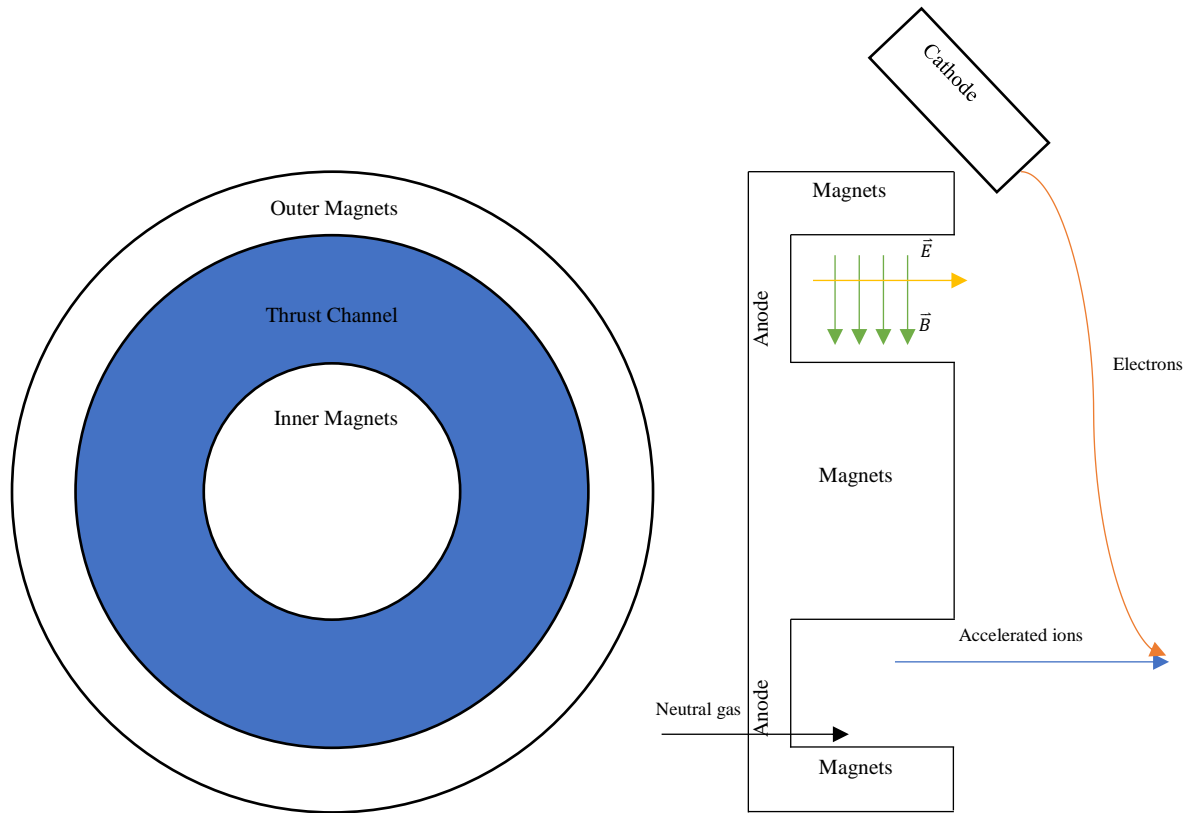
Figure 2.2: Hall Effect Thruster Diagram

The back of the channel, seen on the left side of the cross-section diagram above, is comprised of an anode and gas distribution plumbing. During operation, a positive voltage is applied to this anode with respect to the externally mounted cathode, which is held at the ground potential. This creates an electric field in the axial direction, directed out of the channel. The magnets that surround the thrust channel impose a radial magnetic field oriented toward the center of the thruster. These magnets may be electromagnets or permanent magnets; the thruster under study in the present research utilizes permanent magnets. The externally mounted cathode emits electrons, which are attracted to and flow toward the anode due to the imposed electric

field. The interaction of the electric and magnetic fields in the thruster channel, however, trap these electrons and cause them to drift in the $\vec{E} \times \vec{B}$ direction, which leads them to form a closed current within the channel, as would be expected based on Equation 2.8. This current is known as the Hall Current and will serve as the ionization source for the thruster. The velocity of the electrons in this can be calculated by crossing both sides of Equation 2.8 by $\vec{B}$, resulting in Equation 2.10 [1]:

$$\vec{v}_e = \frac{\vec{E} \times \vec{B}}{\left\| \vec{B} \right\|^2} \tag{2.10}$$

For the coaxial design of the Hall Effect Thruster under study, the electric and magnetic fields are orthogonal at all points in the channel, so the bulk motion of the electron drift is around the channel. For typical electric and magnetic field strengths, the magnitude of this velocity is around 2 % of the speed of light, so the electrons in this drift are very energetic [1].

While the bulk flow of the electrons is circular about the channel, the motion described in Equation 2.8 also contains a component that can be described as an orbit around magnetic field lines. Thus, the motion of an individual electron follows a helical path as shown in Figure 2.3. The minor radius of the helix is equal to the Larmor radius of the electrons as calculated in Equation 2.9.
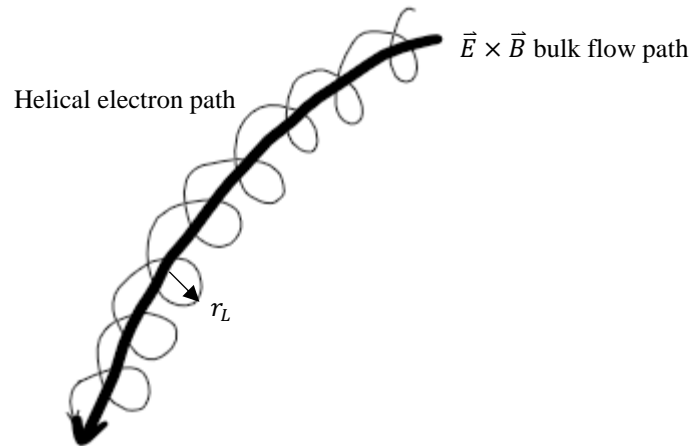
Figure 2.3: Electron path in Hall Current

This reveals an important design consideration in Hall Effect Thrusters—in order to keep the electrons trapped within the thruster channel, the channel width and depth must be much greater than the Larmor radius, otherwise the electrons may either impact the channel walls, interrupting the current, or they may escape the influence of the electric and magnetic fields, opening the electron drift.

While this cloud of high-energy electrons is drifting in the channel, neutral gas is being injected into the channel by the gas distributor on the anode side. The electrons impact the neutral atoms, ionizing them, resulting in a positive ion and a free electron. The free electrons become trapped in the Hall Current, while the electric field across the channel axis propels the positive ions out of the thruster. While the positive ions are affected by the same Lorentz force as the electrons, they have a much larger Larmor radius due to their much larger particle mass, as described in Equation 2.9, so they are not trapped in the channel like the electrons are. In fact, the effect of the magnetic field on the path of the ions is negligible; they are effectively propelled axially by the electric field. When the positive ions are expelled, they must be neutralized to prevent charge build-up on the spacecraft. The cathode serves this purpose during thruster operation, and the electrons it expels are replenished as more neutrals are ionized in the channel.

Electrons in the Hall Current lose energy when they impact and ionize neutrals, so they slowly

drift toward the anode before being ejected as part of the discharge current.

2.3.2 Theory of Cathode Operation

The purpose of the cathode in the Hall Effect Thruster system is to provide electrons to

start the Hall Current and to provide electrons to neutralize the exhaust plume of the thruster

during operation. A number of different mechanisms for electron emission are suitable for

employment in a Hall Effect Thruster cathode, and many different types are commercially

available for this purpose. The type of cathode used in the present research is a hollow cathode,

so named because its construction is a hollow cylinder. Inside the cylinder is a low work function

insert, which emits electrons with relatively low energy input. To achieve electron emission, the

cathode must first be heated, which is accomplished by running a current through a heater wire

wrapped around the tube. Once sufficiently heated, the cathode is ignited and neutral propellant

flowing through the cathode is bombarded by electrons, creating a plasma. A positively charged

electrode called the keeper draws electrons out of the cathode tube, at which point the positively

charged ion plume from the thruster channel attracts the electrons and ions recombine with

electrons, resulting in a neutral plume.

2.3.3 Thruster Losses and Efficiency

There are a number of measures of efficiency for Hall Effect Thrusters. The most

commonly used overall efficiency term is expressed as in Equation 2.11 [1]:

$$\eta_T = \frac{T^2}{2\dot{m}P_{in}} \tag{2.11}$$

where T is Thrust, $\dot{m}$ is the total mass flow to both the cathode and anode, and P_{in} is the total

power input to all thruster components, including discharge power and cathode heater and

keeper. In electromagnet thrusters, this also includes power to the magnets, but the thruster under

study does not have this additional power requirement, which should be realized as increased overall efficiency. This measure of efficiency varies slightly based on the exact cathode setup being used, so to better characterize the thruster itself, a parameter called anode efficiency, as calculated in Equation 2.12, can be used [1].

$$\eta_a = \frac{T^2}{2\dot{m}_a I_d V_d} \tag{2.12}$$

where $\dot{m}_a$ is the mass flow to the anode and I_d and V_d are the discharge current and potential, respectively.

2.4 Anomalous Diffusion

Plasma systems in the "classical" model are assumed to experience diffusion inversely proportional to the square of the magnetic field strength. Commonly, however, diffusion is observed in many systems to be inversely proportional to the magnetic field strength, an increase compared to the "classical" model [5]. This anomalous diffusion is observed in Hall Effect Thrusters as higher-than-expected flow of electrons to the anode [8-9]. The minimum current required to flow to the anode is equal to the beam current, and some collection of electrons near the anode is expected in order to preserve the quasineutrality of the plasma, but cause of the higher flow of electrons to the anode commonly seen in experiments is not definitively known. Previous research has suggested that Bohm diffusion or electron-wall conductivity may be to blame; these will be discussed in more depth below [9-12].

Bohm diffusion is observed in Hall Effect Thrusters, but, while it is generally assumed to result from instabilities in a plasma system, its exact cause is unknown. Janes and Lowder propose anomalous electron diffusion is impacted by the electric field variations generated by electron density perturbations according to Gauss's Law as described in 2.2.1 [9]. Morozov postulated collisions between electrons and the thruster wall can change the azimuthal velocity

of the electrons, causing deviations from the expected diffusion patterns; specifically, electrons are made able to drift toward the anode in a layer about as thick as the Larmor radius for electrons [10]. While this behavior has been experimentally observed, measurements have shown it does not adequately account for the high electron conductivity observed [11-12]. Regardless of the cause of this phenomenon, it has been associated with decreased Hall Effect Thruster efficiency and increased wear on the thruster, resulting in shortened lifetime [1-3].

2.4.1 Hall Thruster Instability Modes

The exhaust plume of a Hall Effect Thruster in operation appears to the human eye to consist of a stationary, quiescent plasma, which is why they are also referred to as Stationary Plasma Thrusters. Many experiments have been conducted with various measurement techniques, however, that reveal many instabilities and oscillations occurring within this plasma plume, particularly at high frequencies [13]. Some instabilities are tied to the anomalous plasma diffusion modes described above; therefore, research has been ongoing to better understand these phenomena, their underlying physical mechanisms, and their precise effects on thruster performance and lifetime. Current models of Hall Effect Thruster operation have not been able to account for these effects due to the current lack of understanding of the phenomena, but their inclusion could drastically improve modelling of Hall Effect Thrusters, allowing improved thruster design [3]. Developing models for these phenomena is outside the scope of the present research, but attempts will be made to produce them in order to observe and characterize them via an array of sensors.

2.4.2 Breathing Mode

During Hall Effect Thruster operation, the discharge current amplitude is observed to oscillate with frequency between about 1 and 30 kHz [13]. This oscillation is called the breathing

mode, and is the most well understood instability mode in Hall Effect Thrusters. Research has also shown that these variations in discharge current are accompanied by oscillations in plume optical intensity, plasma potential in the plume, and magnetic field strength in the thruster channel [3]. There is a theoretical explanation that describes an ionization rate that is too fast for the gas diffusion rate to keep up. This very fast ionization rate ionizes the available neutrals in the channel very quickly. As a result, too few neutrals are now immediately available to be ionized and fewer electrons are available because fewer are being produced in ionizing collisions, so the ionization rate decreases until the channel is sufficiently replenished with neutral atoms, at which point the ionization rate increases, beginning the breathing cycle again [14].

2.4.3 Spoke Mode

Also known as ionization instability, the spoke mode is another prominently studied plasma instability mode in Hall Effect Thrusters. This mode has been observed using Langmuir probes to measure electron density, where it appeared as a single major density fluctuation that travelled azimuthally in the $\vec{E} \times \vec{B}$ direction in the thruster channel at about 20 % of the predicted Hall Current velocity [9]. While higher frequency oscillations were also observed within these spokes, gross electron diffusion has been shown to exhibit an inverse square proportionality to frequency, so higher order oscillations have been assumed to be negligible [9].

Spokes have also been observed in the high speed visible imagery of Hall Effect Thrusters as bright spots rotating about the thruster channel [3,15]. Azimuthal spokes have been associated with regions of higher discharge current, and this phenomenon has been theorized to allow electron transport across magnetic field lines, forming currents with appropriate magnitudes to explain observed Bohm diffusion [8,9]. While this mode can explain some

anomalous diffusion in Hall Effect Thrusters, its cause is not yet known; numerical modelling has been successful in reproducing aspects of the phenomenon but determining the underlying cause will likely require additional experimental research [16].

Spokes have also been tied to decreased thruster lifetime and efficiency as a mechanism that may cause incomplete propellant ionization within the thruster channel [17]. These effects contribute to the spoke mode's presence at the forefront of active research in the field.

2.4.4 Other Instabilities

Higher frequency oscillations in Hall Effect Thruster operation have been observed and likely have some effect on thruster performance, with frequencies on the order of MHz or higher [13]. Oscillations of such high frequencies would require even more advanced equipment than that used to observe breathing and spoke modes. These higher frequency phenomena also have lower amplitudes than the aforementioned modes and, as such, are not currently as critical to understanding plasma instability modes.

2.5 Instrumentation

There are three primary instruments that will be used to characterize the Hall Effect Thruster under study in the present research. These instruments are the same used in Cunningham's work on an electromagnet Hall Effect Thruster [3]; the methodologies from that research will be employed in studying the permanent magnet Hall Effect Thruster that is the subject of this research in order to facilitate comparison between the two thrusters. The sensors that will be used are a high-speed camera that will be used to collect visible emission data, an emissive probe used for collecting plasma potential data, and a magnetic sensor array that will provide data that can be used to calculate Hall Current information.

2.5.1 High Speed Camera

The plasma instabilities found in Hall Effect Thrusters have been observed to induce oscillations in the intensity of visible emissions from the thruster [15]. For this reason it is desirable to capture visible emissions from the thruster channel at sample rates high enough to accurately display high frequency oscillations in the visible intensity of the plasma without aliasing. For the purposes of the present research, video will be captured at rates up to one million frames per second (Mfps), which is adequate for capturing the oscillations of the breathing mode and the motion of spokes in the spoke mode; these modes have frequencies up to about 30 kHz and 70 kHz, respectively [13,18]. This video data will be of particular use in studying the spoke mode, as the other sensors being used only take measurements in a single location; since the spoke mode consists of azimuthal variations, a view of the entire thruster face at each sample will provide additional context to the other measurements.

While the features of interest are occurring in the thruster channel, which is where the camera will be focused, the positioning of the camera outside the vacuum boundary and downstream of the thruster will cause the camera to capture any visible emissions along the path from the thruster to the camera. This has been described as the "integration of light throughout the plasma plume," and will make any visible phenomena that happen along a single path from the thruster to the camera appear coincidental and thus indistinguishable [15].

2.5.2 Emissive Probe

As ions in the thruster exhaust plume move downstream, their charge distribution forms a potential, known as the plasma potential. Measurement of this potential is important in determining ion and electron populations and their movements. There are a few instruments that can accomplish this task, but the emissive probe is the best for this application, as it is

appropriate for use in moving streams of plasma and has very high temporal resolution if the correct methodology is used. The appropriate methodology was developed by Kemp and Sellen and makes use of a large load resistor to allow the potential of the probe to float, or vary relative to the laboratory ground [19]. The filament of the emissive probe is heated to the point of electron emission, and the the floating potential of the probe, V_f, is then related to the plasma potential, V_p, the ion saturation, electron saturation, and electron emission currents, $I_{s,i}$, $I_{s,e}$, and $I_{e,e}$, as well as the electron temperature, T_e, according to Equation 2.13 [20]:

$$V_f = V_p - T_e \ln\left(\frac{I_{s,e}}{I_{s,i}+I_{e,e}}\right) \tag{2.13}$$

It is clear from this that the floating potential measurement approaches the plasma potential when the electron emission current approaches the electron saturation current, both of which are higher than the ion saturation current. Error is also introduced on the order of the plasma electron temperature because of the difference in energies of the electrons emitted from the probe and those in the plasma plume [20]. The frequency response of the probe measurement is considerably higher than the resolution required to observe the phenomena of interest, up to the low RF frequency range, so with the aid of a data acquisition device capable of sampling at a high enough rate, time resolved plasma potential measurements at high sampling rates are possible [19].

2.5.3 Magnetic Sensor

During Hall Effect Thruster operation, it is useful to measure the Hall Current density within the thruster channel. To avoid interfering with and altering the current, a non-intrusive measurement method is required. During modes in which the Hall Current is steady, this can be done by taking magnetic field measurements and applying the Biot-Savart law, which describes

the magnetic field at one location, $\vec{B}(\vec{r})$, due to a current distribution at another location, $\vec{J}(\vec{r}')$, as in Equation 2.14:

$$\vec{B}(\vec{r}) = \frac{\mu_0}{4\pi} \oint_{Q'} \frac{\vec{J}(\vec{r}') \times \vec{r} - \vec{r}'}{||\vec{r} - \vec{r}'||^2} dQ' \tag{2.14}$$

where μ_0 is the permeability of free space and Q' is the volume containing all current elements [21]. As mentioned above, this assumes a steady current, which implies that use of this conversion cannot be applied during analysis of the spoke mode, as azimuthal variations in Hall Current are present. For the present research, no attempt will be made, therefore, to analyze Hall Current during spoke mode operation due to this limitation. Measurements of spoke mode Hall Current will require either a different collection method or a different conversion scheme from magnetic field data that does not require the steady assumption.

Because the measurements being collected in the present research are of magnetic field strength at some location, the inverse of the problem solved by Equation 2.14 is required in order to calculate the current that induced that magnetic field. The methodology for performing this inverse solution that follows was developed by Rubin for Hall Effect Thruster diagnostics and has been applied by Mullins et al [22,23].

The first step in solving the inverse problem is to solve the direct problem. In the current application, the magnetic sensor is oriented such that it is capable of measuring in the radial and axial directions, thus the solution plane for the sensor is the r-z plane. By assuming all current measurable by the magnetic sensor array is steady, axisymmetric, and intersects the solution plane, Equation 2.14 reduces to the following [3]:

$$B_r(\vec{r})\widehat{e_r} + B_z(\vec{r})\widehat{e_z} = \frac{\mu}{4\pi} \oint_{E'} \frac{-J_\theta(\vec{r}')(z-z')\widehat{e_r} + J_\theta(\vec{r}')(z-z')\widehat{e_z}}{(r-r')^2 + (z-z')^2} dr'dz' \tag{2.15}$$

Assuming that the area of integration can be divided into n areas of piecewise constant current density, the currents can be passed outside the integral and the radial and axial components of the magnetic field may be considered separately, as in Equations 2.16 [3]:

$$B_r(\vec{r}) = \sum_{i=1}^{n} \frac{\mu J_{\theta,i}}{4\pi} \oint_{E_{i'}} -\frac{z-z'}{(r-r')^2+(z-z')^2} dr' dz' \tag{2.16a}$$

$$B_z(\vec{r}) = \sum_{i=1}^{n} \frac{\mu J_{\theta,i}}{4\pi} \oint_{E_{i'}} -\frac{r-r'}{(r-r')^2+(z-z')^2} dr' dz' \tag{2.16b}$$

where i is the index of the current element being considered. Because each sensor the in the array being used only measures in either the radial or axial direction, only one of Equation 2.16 needs to be evaluated for each one. The sensors are also stationary, so the position and area components in the integral will be constant for each sensor. Therefore, a constant coefficient, A_{ij}, can be determined for each sensor and each current element being examined that incorporates the relative position of the sensor and current element, the size of the area being considered, and the permeability of the space between the sensor and the current element. From these coefficients, a Green's matrix of coefficients, A, can be formed that relates the vector of currents in area elements, $\vec{J}$, to the vector of magnetic sensor readings, $\vec{B}$, as in Equation 2.17 [3]:

$$A\vec{J} = \vec{B} \tag{2.17}$$

The calibration process that will be used to determine the values of A_{ij} for the non-operating background case will account for the magnetic field imposed by the permanent magnets in the thruster, but not the magnetic field induced by the electric field between the anode and cathode [22,23].

The direct solution found in Equation 2.17 is a good starting point for solving the inverse problem, but for the conditions of the present research, in which 8 magnetic sensor locations are being used to solve for 80 current elements, the system is greatly underdetermined. Cunningham first examined a linear least-squares method to solve the inverse problem, but the results

obtained from this method were not physically meaningful [3]. Instead, a matrix regularization scheme using Tikhonov's method will be used to find $\vec{J}$ by minimization:

$$Min\left(\left|\left|A\vec{J} - \vec{B}\right|\right|^2 + \lambda^2 \left|\left|L\vec{J}\right|\right|^2\right) \tag{2.18}$$

where L is a discrete smoothing matrix known as the Tikhonov regularization operator and λ is a regularization parameter. L is determined by making assumptions about the desired solution and includes constraints that limit current to be non-negative and equal to zero at the wall and the upstream and downstream limits of the solution space. These constraints, specifically the zero-current condition applied to the upstream and downstream boundaries, assume a priori knowledge of the location of current phenomena and are not physically expected. Even the zero-current assumption at the walls, which is supported by the ceramic-insulator construction of the channel, is known to be inaccurate, as electron collisions with the wall, which represent a current there, have been observed as an erosion mechanism in Hall Effect Thrusters [1]. Despite these limitations, which will induce some error, this solution method has provided better results than other attempts, and will be useful in examining many effects, including the breathing mode [23]. The resulting regularization operator based on these assumptions is shown in Equation 2.19 [24]:

$$L = \left|\left|\frac{d^2 j}{dr^2}J\right|\right|^2 + \left|\left|\frac{d^2 j}{dz^2}J\right|\right|^2 + \left|\left|\frac{d^2 j}{drdz}J\right|\right|^2 \tag{2.19}$$

A range for the value of the regularization parameter, λ, will be calculated in the solution of the minimization problem found in Equation 2.18. From here, a solution that minimizes $\ln\left|\left|A\vec{J} - \vec{B}\right|\right|^2 + \ln\left|\left|L\vec{J}\right|\right|^2$ will be chosen. Performing this optimization at every timestep is extremely computationally intensive but finding λ at one timestep and using the same value for the entire dataset has been shown to be an acceptable alternative, avoiding degradation of the solution [23].

As mentioned previously, a calibration process will be required in order to determine the Green's matrix, A. This process will be outlined in greater detail in the following chapter. From this point, the Hall Current can be derived based on magnetic field measurements.

2.6 Motivation

The motivation for the current research is to gain some insight into the behavior of the plasma discharge of a Hall Effect Thruster operating in various modes that exhibit anomalous plasma diffusion. In particular, this work aims to apply the methodologies used by Cunningham on an electromagnet thruster to a permanent magnet thruster. These methodologies include applying commonly used high-frequency measurement techniques and time-correlating them so multiple thruster characteristics can be compared at high sample rates. This data may prove useful to model developers, allowing them to incorporate more of these high frequency phenomena that decrease thruster performance and lifetime. These improved models will help pave the way for improved thruster design.

III. Methodology

3.1 Chapter Overview

This chapter will describe the experimental setup and methodologies used to acquire data for this research. This will include the article under study and related components, laboratory environment and equipment, data collection equipment and techniques, and data processing and analysis techniques. Not all of the below methodologies were able to be used on new data collected in this research but are applicable to the past research that is also addressed in this paper and will be useful in future research.

3.2 Article Under Study

The setup of the article being studied in this research includes the following Hall Effect Thruster, Hollow Cathode, and peripheral equipment.

3.2.1 Hall Effect Thruster

The Hall Effect Thruster being studied in the present research is a 600 W unit that uses permanent magnets to generate its magnetic field. It was designed and manufactured by Busek Co. Inc. and is designated BHT-600 PM; it is shown in Figure 3.1. The device in front of the right side of the thruster is a magnetic sensor array and is not part of the thruster itself. This thruster is designed for use on a wide array of satellites. Its relatively simple design compared to electromagnet models increase the possibility for it to be used on small satellites, on the order of 10 kg, but it is also suitable for use on spacecraft up to several hundred kilograms. According to Busek, the thruster is capable of generating 40 mN of thrust with an I_{SP} of approximately 1,500 s and an efficiency of 40-55 % for typical operation [25]. These are theoretical values determined analytically so actual/laboratory conditions, as well as the effect of the cathode, will likely cause actual values for I_{SP} and efficiency to decrease. If thrust was to be measured, its value may be

26

artificially higher in the laboratory environment, as the pressure of the vacuum chamber is higher

than that of the intended operating environment. The increased density in the chamber provides

more matter for the accelerated ions to interact with and may increase the force provided by the

exhaust as measured by a thrust stand. For the present research, these artifacts of testing in the

laboratory are not of interest, as thruster performance characteristics are not currently under
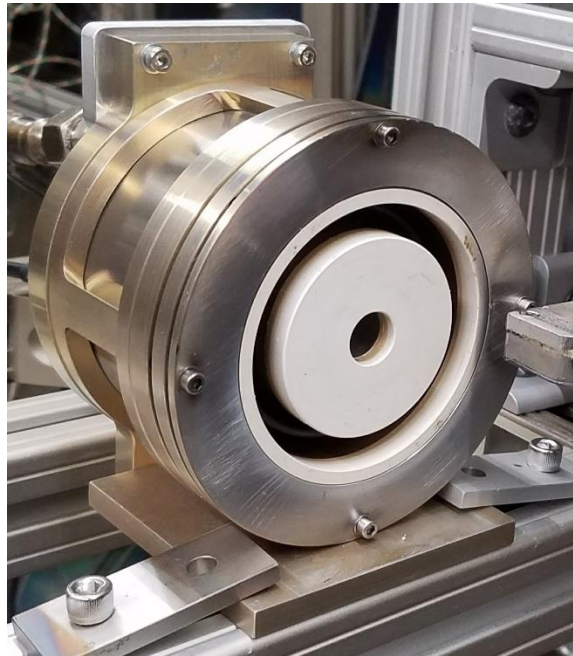
study.

Figure 3.1: BHT-600-PM

The primary difference between this thruster and similar thrusters that have been studied

previously at AFIT, as in [3], is the source of the magnetic field in the thruster channel. Many

traditional Hall Effect Thrusters utilize electromagnetic coils to generate a tunable magnetic

field, which enables easier thruster startup and provides an extra adjustment point to achieve

desired operating conditions. The downside to electromagnets is that the coils that they require

are immensely heavy, bulky, and require an appreciable amount of power to generate the

required field. For comparison, the BHT-600, a Hall Effect Thruster with the same discharge

power rating and a similar channel radius that uses electromagnets, is shown in Figure 3.2. The

variability of magnetic fields formed by electromagnets also complicates development of

magnetic shielding to help reduce insulator erosion, a major area of design research that aims to

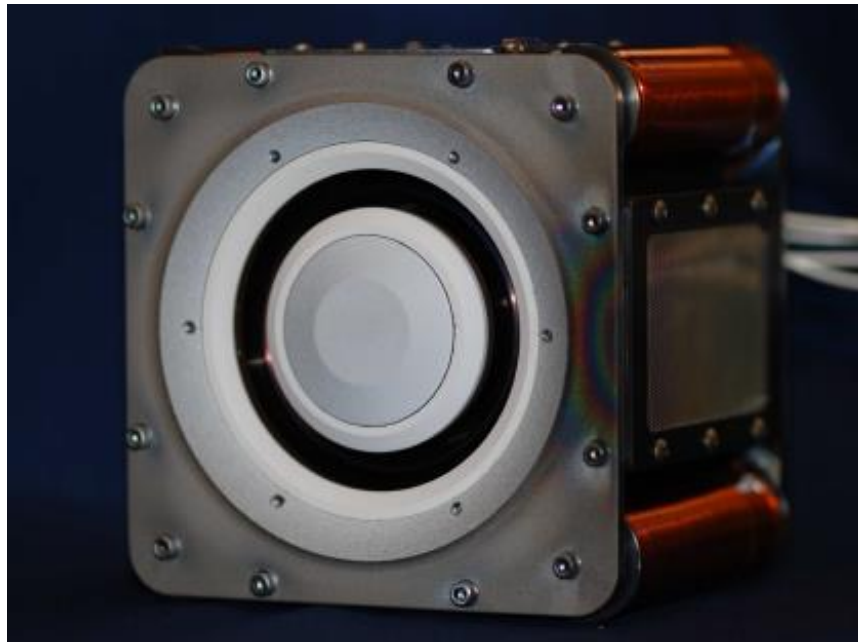significantly improve thruster lifetime.

Figure 3.2: BHT-600 [26]

In an effort to reduce mass and volume and increase the applicability of Hall Effect

Thrusters to small satellites, the BHT-600-PM was designed to use Samarium-Cobalt (SmCo)

magnets to generate a fixed magnetic field. According to Busek, this affords a mass savings of

around 70 %, which is significant in spacecraft systems and can directly increase the amount of

mass available for a satellite's primary payload [25]. Use of permanent magnets also simplifies

incorporation of magnetic shielding, which can significantly decrease the frequency of electron-

wall collisions and therefore erosion of the channel wall insulator, leading to greatly improved

thruster lifetimes. Some of the negative aspects of using permanent magnets include lack of

tunability of the magnetic field, which will be discussed more below, and susceptibility to

damage from high temperatures, above 450 °C specifically, leading to demagnetization of the

permanent magnets [25].

3.2.2 Hollow Cathode

Busek Co. Inc. manufacturers a hollow cathode designed to be mounted along the

centerline of the BHT-600-PM, but this cathode was not available for use in the current research.

Instead, a top-mounted BHC-1500, also manufactured by Busek, was used. Figure 3.3 shows this

cathode mounted on the thruster. This substitution has not been previously studied for this

particular thruster, but a study on another thruster showed that using an external cathode

compared to an internal one causes an increase in cathode coupling voltage and an associated

total thruster efficiency decrease of 2-3 % [27]. This is not expected to be of consequence in the

current research, as efficiency is not being examined; however, future research on the differences

in spoke generation between these two cathode arrangements could prove insightful.
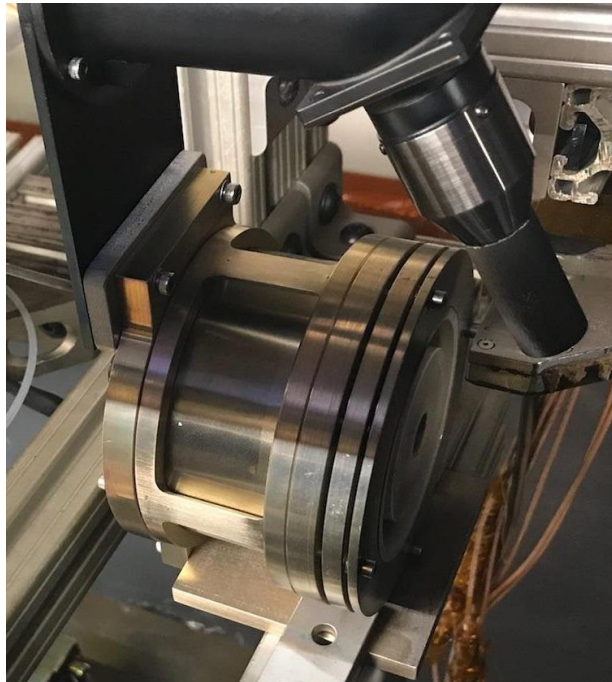

Figure 3.3: BHC-1500 mounted on BHT-600-PM

The BHC-1500 hollow cathode has been used in past research on similar thrusters, and has flight legacy, having been flown on Air Force Research Laboratory's TacSat 2 satellite [28]. The BHC-1500 consists of a porous Tungsten hollow insert impregnated with a Barium-Calcium-Aluminate mixture, which gives the cathode its desirable low work function emitter properties. The cathode is heated to its ignition temperature of 1,000 to 1,200 °C by a coaxial Tantalum swaged heater wire with a current of up to 10 A running through it [28]. The cathode is mounted to the thruster with a mounting bracket that was designed and manufactured in AFIT's machine shop in the course of past research.

The Barium-Calcium-Aluminate mixture present in the cathode is susceptible to degradation by exposure to Oxygen and, more prominently, water vapor. In particular, the lifetime of the cathode is significantly reduced when the cathode is heated in the presence of such atmospheric gases. Before the current experiments began, the cathodes available all showed signs of such degradation (the primary sign being increased resistance to ignition) and were sent back to the manufacturer to be refurbished, a lengthy process that had to be completed before the thrusters under study could be operated.

3.2.3 Power Processing

While the omission of electromagnet circuits simplifies the electrical requirements of the BHT-600-PM compared to similar electromagnet thrusters, there are still many electrical components with varying power requirements involved in its operation. The complexity of the electrical equipment required for a Hall Effect Thruster can be daunting in terms of mass and size, and even with the exclusion of electromagnet circuits, the BHT-600-PM requires power supplies capable of supporting high voltage requirements such as the anode discharge and the

cathode keeper, as well as the relatively low voltage requirement of the cathode heater. For this

research, this task is accomplished by Sorensen DCS33-33E and DCS55-55E power supplies.

Because of the various voltages and currents required by the different components, a

Power Processing Unit (PPU) is also required. For this research, the power is processed by a

PPU designed and provided by Busek Co. Inc., designated model BPU-600. This PPU is

controlled by software run from a PC running Windows XP. The software has the capability to

run thrusters automatically with predetermined settings and also has an "Operational Mode,"

which allows the adjustment of a variety of thruster power parameters, including discharge

voltage, electromagnet circuit current (not applicable for BHT-600-PM), cathode heater current,

and cathode keeper current. The software also displays the actual values for these and other

thruster power parameters. The software interface during operation is shown in Figure 3.4. Take

note that this interface has been used for a variety of other thrusters and, as such, displays

options for and readouts of parameters that are not applicable to the thruster under study in the
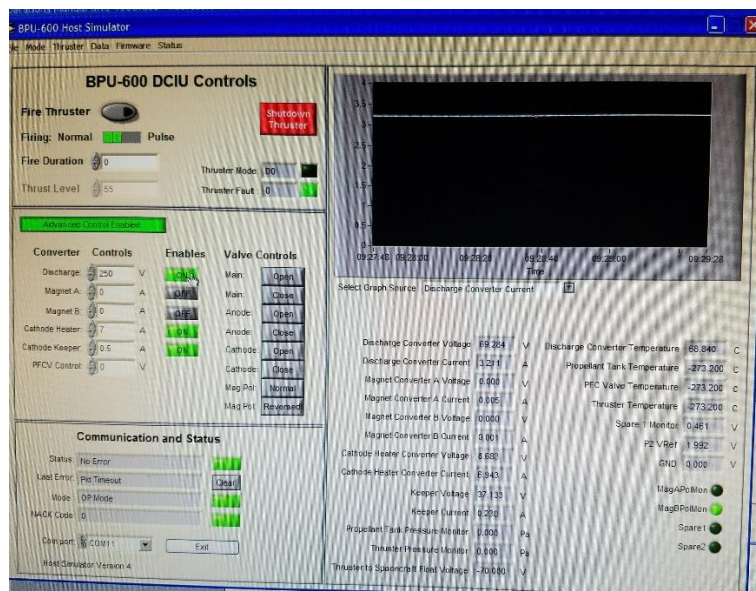
present research.

Figure 3.4: BPU-600 Control Software

The power equipment is all rack-mounted along with patch panels that facilitate switching operation between the thruster under study here and another thruster being studied by another student. This rack is pictured in Figure 3.5. The Sorensen power supplies are toward the bottom of the rack—the first and third units below the shelf with the oscilloscope, and the BPU-600 is visible behind the oscilloscope.

Figure 3.5: Power Supply and Mass Flow Control Rack

3.2.4 Mass Flow Control

Another important parameter that significantly impacts Hall Effect Thruster operation is the mass flow of propellant provided through the cathode and the anode. For the current research, these parameters are controlled by MKS mass flow controllers, one with a maximum flow rate of 10 standard cubic centimeters per minute (SCCM), which feeds the cathode, and the other with a maximum flow rate of 50 SCCM, which feeds the anode. These flow controllers are collocated with and fed by propellant tanks located outside of the vacuum boundary. The mass flow controllers are shown in figure 3.6. They are controlled by an MKS type 247 4-channel readout, visible in Figure 3.5 on the shelf above the oscilloscope.

Figure 3.6: Mass Flow Controllers

The source of propellant gas are tanks connected to the mass flow controllers through a switching system so either of two tanks can be used. The current setup has one Krypton tank and one Xenon tank connected, both 99.9999 % pure laboratory grade gases. The switching system allows either gas to be used, but care must be taken to prevent backflow of gas into the other tank by ensuring that the switching circuit's pressure has fallen below the tank pressure of the other gas before switching to that gas. During the course of this research, the Xenon tank maintained a

pressure of about 650 psi and the Krypton tank maintained a pressure of about 850 psi. While

Xenon was primarily used to operate the BHT-600-PM, Krypton was commonly used to operate

another Hall Effect Thruster under study in the same facility, so the feed switching system was

frequently used. The tanks, switching system, and mass flow controllers can be seen in Figure
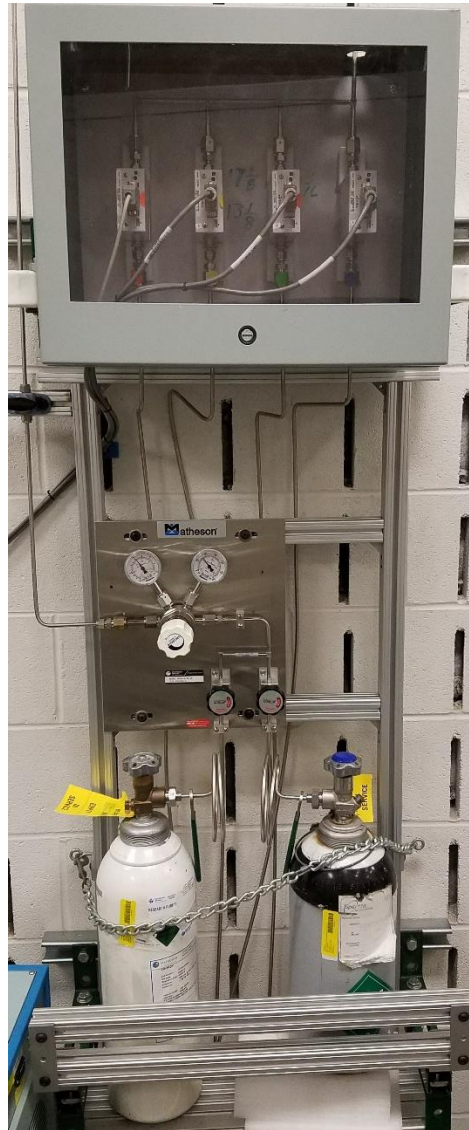
3.7.

Figure 3.7: Propellant Feed System

The pressure from the tanks was regulated to 20 psi and fed into the mass flow

controllers. At the beginning of the research period the mass flow controllers fed into the vacuum

chamber boundary using flexible plumbing; to reduce the likelihood of leaks and air contamination into the lines, these lines were replaced with stainless steel hard lines terminated with Swagelok VCR fittings. Inside the chamber, the thruster anode and cathode are connected to these lines through the vacuum boundary by flexible hoses with Swagelok VCR connectors. Flex lines were used for this application because the thrusters needed to be able to be repositioned within the chamber, and while any possible leaks could contribute to a decreased mass flow to the thruster, they wouldn't lead to air contamination because they are within the vacuum chamber.

3.3 Laboratory Equipment

Laboratory equipment that will be described in this section include the facility in which experimentation was completed and equipment used for test purposes but not directly related to operation of the article under study or instrumentation.

3.3.1 Vacuum Chamber

The facility used for this research is a vacuum chamber located in AFIT's Space Propulsion Application Simulation System (SPASS) Laboratory, shown in Figure 3.8. This vacuum chamber is approximately cylindrical, with a diameter of 1.8 m and a length of 3.76 m. During the current research it was observed to maintain pressures less than or equal to $8 \cdot 10^{-7}$ torr with no gas flow into the chamber, or approximately $4 \cdot 10^{-5}$ torr while a thruster is in operation.

Figure 3.8: SPASS Lab Vacuum Chamber

This pressure is achieved and maintained using an Oerlikon/Leybold Vacuum Screwline SP 250 roughing pump, shown in Figure 3.9, and four CVI Torr Master 20 in TM500 (canted to the top left and right, in front in back as seen in Figure 3.8) and one CVI Torr Master 10 in TM250 (mounted on top in Figure 3.8) helium cooled cryopumps. An ExTorr Residual Gas Analyzer (RGA) is used to measure chamber pressure during operation. This RGA is capable of identifying species with masses between 1 and 101 AMU, which includes Krypton at an atomic mass of 83.8, but not Xenon, which has an atomic mass of 131.29. Instead of reading Xenon at 131.29 AMU, an aliasing effect causes the RGA to display Xenon at its half mass, around 65 AMU.

Figure 3.9: Oerlikon/Leybold SP 250 Roughing Pump

Before any experiments were conducted, an extension was installed in the vacuum

chamber to bring its length from 2.5 m to the aforementioned 3.76 m. After this was complete,

the chamber was failing to reach the necessary vacuum pressure when pump-down was initiated.

The first repair method attempted was to replace seals and O-rings around the chamber where

accessible to eliminate a leak as causal to the failure. There is not an easy procedure for leak

testing on a vacuum chamber this large, so replacing the seals that could be replaced and

attempting to pump down again was the best course of action available for this. The issue was

still not remedied, so the prevailing hypothesis was that the existing control mechanisms were

not compatible with the increased chamber volume.

The control system for the pump-down process was not well documented, so a trial-and-

error diagnosis style was used to attempt to remedy the issue. It was clear that a Pirani pressure

gauge mounted on the chamber, pictured in Figure 3.10, sent a control signal to the power board that caused the crossover from the roughing pump to the cryopumps, so the crossover pressure was adjusted based on the new chamber volume, but this alone was not enough to fix the problem. It was observed that the TM250 cryopump mounted on top of the chamber contained a gate valve that separated the pump from the chamber that never appeared to actuate, and a disconnected control wire was discovered that had a serial connection matching temperature monitor connected to the four TM500 pumps, as shown in Figure 3.11. The missing temperature monitor, a Lake Shore Model 211, was connected and revealed that the pump's cryo-head was reaching about 12 K. When pump-down was attempted again, the gate valve was observed to remain closed to isolate the pump from the chamber and allow this cryo-head to achieve its very low temperature. When the Pirani gauge reached its crossover pressure and the temperature monitor recorded a cryo-head temperature below 20 K the gate valve was opened and the chamber pressure dropped significantly. At this point, all five cryopumps were activated and were able to achieve and maintain the required operating pressures.

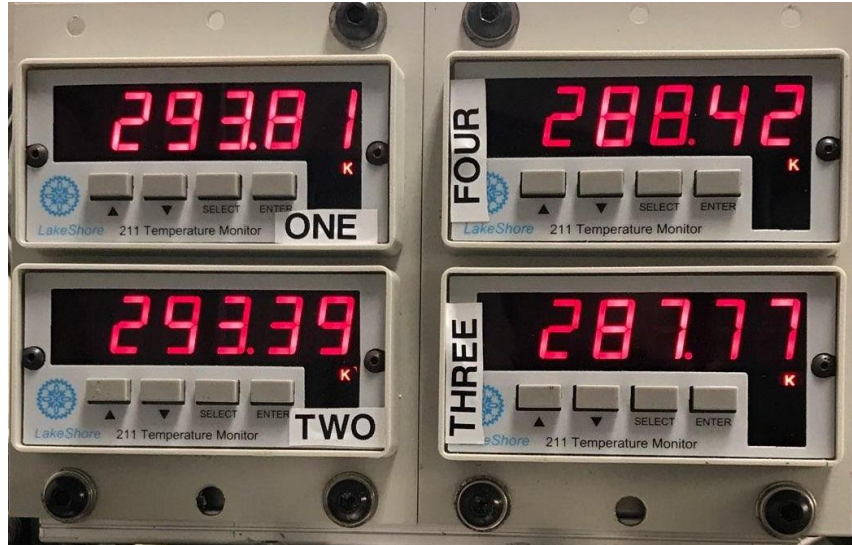Figure 3.10: Pirani Pressure Gauge that Controls Crossover to Cryopumps

Figure 3.11: Lake Shore 211 Temperature Monitors, measuring cyrohead temperature

3.3.2 Chamber Interior Equipment

Inside the vacuum chamber there are two translation stages, one for mounting thrusters, and one for mounting sensors and probes. The thruster stage is seen in the foreground of Figure 3.12 and has three translational degrees of freedom. This stage was located on another sliding platform for greater mobility in the axial direction of the chamber. For the present research, two thrusters were mounted on the stand, next to each other; one is the BHT-600-PM, and the other is a Busek Pseudolinear Hall Thruster being studied by another student. The translation stage X-axis is in line with the axial direction of the thruster and the chamber, the Y-axis moves in the horizontal direction orthogonal to the X-axis, and the Z-axis moves vertically. This stage was used to adjust the position of the thruster between experiments, and to switch which thruster was located in the field of view offered by the chamber viewport but was not used for any experimental purposes.

Figure 3.12: Chamber Interior

The probe translation stage, visible in the background of Figure 3.12, has two horizontal translational degrees of freedom and one rotational degree of freedom for performing scans through the thruster exhaust plume. This stage was not used for the present research, as high frequency temporal variations in the exhaust were of primary interest as opposed to temporally-steady spatial variations in the plume.

3.4 Instrumentation

The below sections detail the instrumentation devices and procedures that were intended to be used during the present research. Due to issues with getting the thruster to fire stably and

reliably, many of these sources were not able to be collected from in the intended manner, as noted in each section.

3.4.1 High Speed Video Camera

In order to collect data on optical emissions at the desired data rate of up to 1 MHz, a high-speed video camera needed to be positioned at one end of the chamber, outside the vacuum boundary, looking at the thruster exhaust plume through a quartz window in the chamber, as seen in Figure 3.13. A Shimadzu Hyper Vision HPV-2 camera was used for this purpose, capable of collecting 102 frames of 312 x 260 -pixel images at rates up to 1 Mfps. A Nikon ED AF-S Nikkor 400 mm lens was used; this lens is wider than the lenses used in previous research and would allow more light to impact the camera's sensor, a panchromatic complementary metal-oxide semiconductor (CMOS). The f-stop on this lens was also set at its highest setting of 2.4 to maximize light incident on the sensor. An even larger lens was desired, but the lens available was not compatible with the Shimadzu HPV-2 camera. The reason the incident light needs to be maximized is that at a collection rate of 1 Mfps, which necessitates an exposure time of 750 ns per frame, very few photons are available to impact the sensor compared to a standard camera with a typical shutter speed. The resulting images from this camera were converted to a series of panchromatic Tagged Image File Format (TIFF) files that were processed as will be described later to generate false color plots of intensity around the entire channel against time.

Figure 3.13: High Speed Video Camera Setup

The HPV-2 was connected to an external triggering circuit as described in a later section to allow for synchronization of optical emission data with other sensor sources. Due to some technological difficulties, not all video samples collected were triggered in this manner.

3.4.2 Emissive Probe

Study of the spoke mode requires some measurements both to be taken at very high frequency and capable of distinguishing between azimuthal position rather than taking an average measurement about the entire thruster channel, as the spokes are observed to travel azimuthally. To accomplish this, an emissive probe can be placed at one position in the plume, and the variation in the plasma potential at this point can be recorded as spokes travel across that azimuth. The emissive probe used in the present research, shown in Figure 3.14, was developed by Plasma Controls and consists of a 0.005 in tungsten filament in a 0.13 mm diameter loop with each end inserted into a copper tube, each of which will act like a lead. These tubes were placed inside a double-bore alumina tube, which was secured to a base, inside which the copper tubes were connected to posts that connect to external BNC connections. The probe is heated to the point of emission by a battery floating with the probe. The probe was mounted on a stand

constructed from 80-20 Aluminum extrusions and placed in front of the thrusters such that they

could be moved using the translational stand to position the emissive probe just within the

plasma plume and just downstream from the thruster. The BNC connections on the probe base

are connected through the vacuum boundary to a control box, shown in Figure 3.15, inside which

the battery that provides the heating potential is located. This box connects to a PicoScope DAQ,

which is connected to a PC, where the probe parameters are controlled and measurements are

stored. These are visible in the bottom of Figure 3.15. The PicoScope is connected to the

triggering circuit that will be described in a later section in order to allow synchronization of

plasma potential data with other data sources.
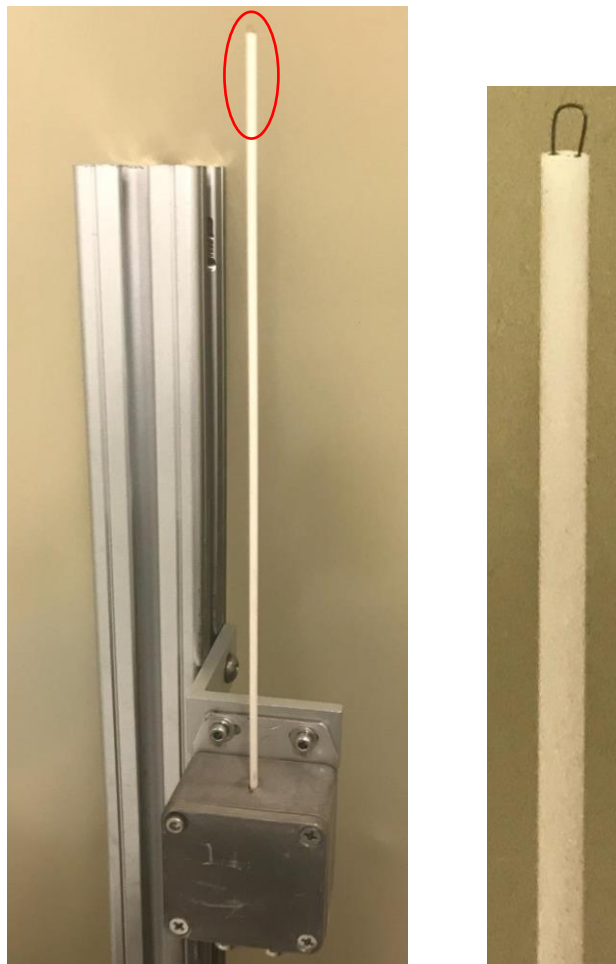
Figure 3.14: Emissive Probe. Right image is detail of area circled in red on left.

Figure 3.15: Emissive Probe Control Box, PicoScope DAQ, and Recording PC

The filament on this probe is subject to very high thermal loads and is susceptible to breaking, similar to an incandescent light bulb filament, but after just a few minutes of testing. For this reason, the emissive probe could not be kept in an operational configuration indefinitely and would only be heated immediately before data were to be collected, which was intended to be done in a stable plasma exhaust. Due to problems with keeping the thruster running long enough for the discharge to stabilize, the conditions for preparing the emissive probe were never met and no plasma potential data were collected.

3.4.3 Magnetic Sensor

To measure magnetic field fluctuations around the thruster, a sensor array developed by Plasma Controls, shown in Figure 3.16, will be used. This probe consists of eight Micro-Magnetics STJ-240 tunneling magnetoresistance (TMR) sensors arranged in a planar array, with four sensors mounted in the radial direction and four sensors mounted in the axial direction. The sensor probe was positioned very close to the thruster plume, as seen in Figure 3.17, in order to attain a sufficient signal to noise ratio. The sensors are contained within a graphite-coated

stainless-steel housing to protect them from the plasma environment, and they are connected to a water-cooling system in the chamber to maintain appropriate operating temperatures. The probe is powered with the required constant voltage by a Li-ion battery located outside the vacuum boundary. The magnetic field data will be collected from all eight sensors simultaneously at 2 MS/s via the NI USB-6366 DAQ.
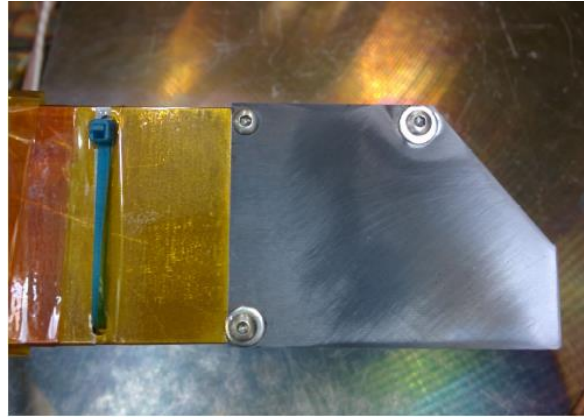
Figure 3.16: Magnetic Sensor Array
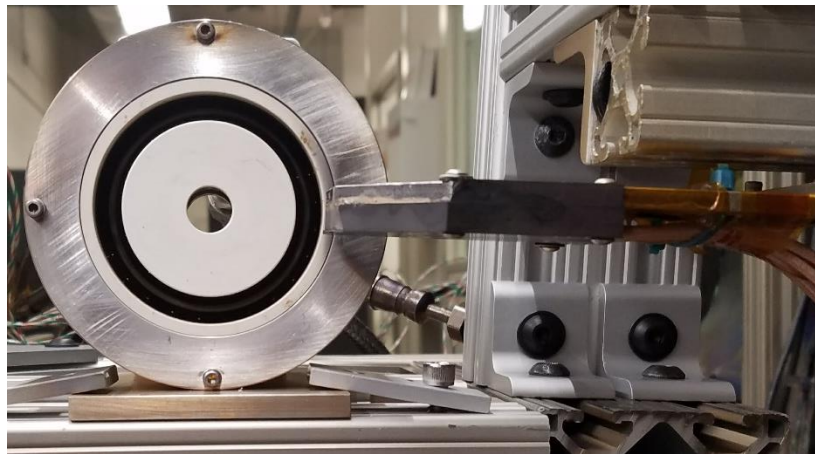
Figure 3.17: Magnetic Sensor Array Positioned on Thruster

This DAQ was connected to the triggering circuit that will be described in a later section but appeared to leave the circuit open; when it was connected, none of the connected sensors responded to any trigger events. For this reason, no magnetic field data were collected upon

trigger by the oscilloscope; instead, some datasets were collected by manually commanding a recording event.

Due to issues with achieving stable thruster discharge during the course of the present research, very few magnetic field measurements were collected and, as mentioned previously, none of them were synchronized with other data collections.

3.4.4 Triggering Mechanism

While the thruster is firing, its discharge current is being monitored by a Tektronix DPO 4032 Digital Phosphor Oscilloscope, visible in Figure 3.5. This device has a trigger feature that can be configured to recognize a specific part of a waveform and send a Transistor-Transistor Logic (TTL) pulse via BNC connection. For this research, this trigger was set to be sent on the rising edge of the breathing mode of the thruster discharge. The other three data collection devices receive the trigger and begin recording data. In past research, this trigger also forced a recording of the discharge current on the oscilloscope, but neither this functionality nor the ability to retrieve any waveform recordings from the oscilloscope were discovered during the present research. The trigger setup allows time synchronization of discharge current data, magnetic sensor/Hall Current data, plasma potential data, and high speed visible emission data to within the timing uncertainty determined in previous research and outlined in Table 3.1 [3].

Table 3.1: Sensor Timing Uncertainty

Sensor	Timing Uncertainty
Magnetic Sensor	± 0.25 μs
Emissive Probe	± 0.008 μs
High Speed Video	± 0. 5 μs

3.5 Data Analysis

This section details the analysis methodology used for each sensor.

3.5.1 High Speed Video Analysis

The TIFF image files from each video collection were processed using Matlab code developed in Cunningham's previous research to facilitate comparison of performance of the thruster under study in the present research with the thruster he was studying [3]. Each frame of video was "unrolled," resulting in optical intensity around the thruster channel being projected onto a vertical line. The bottom and top of this vertical line are the discontinuous point in the unrolling process, at 180°, or the 9 o'clock position on the thruster. This is illustrated in Figure 3.18, but instead of four azimuthal sectors, the channel was divided into 180 2° sectors. This process is based on a technique developed by Sekerak [8]. Each subsequent frame is processed and then concatenated to the result of the image processing from the previous frames on the right side, resulting in time being on the X-axis, ranging from 0 to 102 μs for 1 MHz data, and channel azimuth on the Y-axis, with minimum and maximum scale values representing the 180° point on the thruster, and the middle of the Y-axis corresponding to the 0° point, or the 3 o'clock point. Each pixel contains brightness data averaged over the channel width and a 2° azimuthal swath, over 1 μs of time. False color is applied to the image based on brightness to make differences in intensity more apparent.
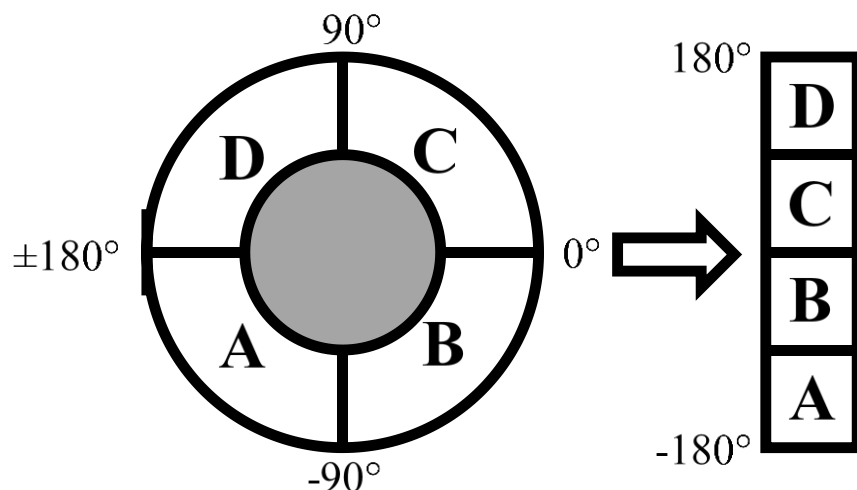
Figure 3.18: Channel Unrolling Schematic

Figure 3.19 shows an example of a fully processed unrolled video. In this plot, the whole

thruster channel can be observed to vary uniformly in brightness with time; in other words, the

channel appears to flash on and off all at once. The azimuthal homogeneity exhibited in this

mode can be seen in the plot as the pixels within each column are approximately uniform in

intensity. Note that coloration is assigned to relative intensity changes according to the colorbar

in the figure, but magnitude of the intensity is arbitrary and may be inconsistent between plots, as

gain is applied as needed to each plot individually to show features of interest.
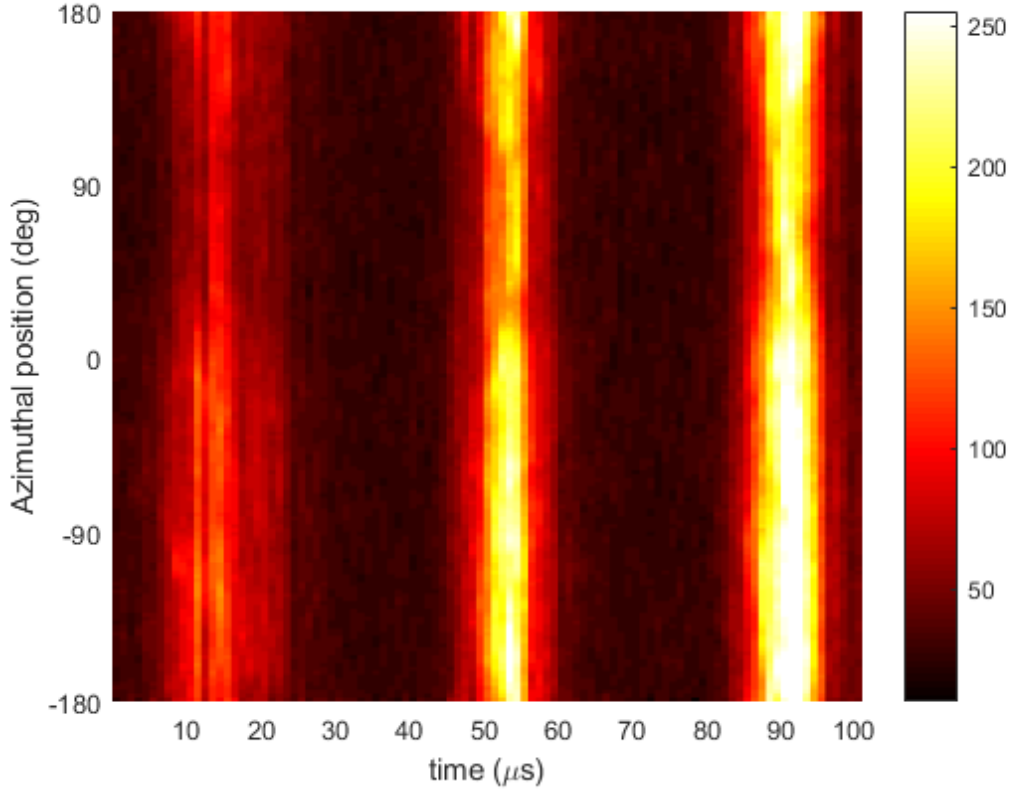
Figure 3.19: Example Unrolled Video Plot: thruster exhibiting breathing mode

3.5.2 Magnetic Data Analysis

The theory relating magnetic field data and Hall Current outlined in Chapter II describes the algorithms and solution methods used to convert the measured data from the magnetic sensor array to Hall Current data for further analysis. While the sensor was sampled at 2 MS/s, Cunningham's research showed there was too much high frequency noise in the data at this sample rate, so the data were downsampled to 250 kS/s using a four point moving average, as in Equation 3.1 [3]:

$$\overline{b_{i'}} = \frac{1}{4}\sum_{i=4(i'-1)}^{4i'-1} b_i \tag{3.1}$$

where $b_{i'}$ is the downsampled value at index i', and b_i is the original value at index i. The data

will also be timeshifted due to this averaging, so the new time for each sample will be 0.75 µs

after the timestamp of the first point in that point's moving average.

In order to make use of the processing algorithms described above, the sensor had to be

calibrated before data was taken. The calibration process consisted of taking measurements while

a set of circular copper coils was moved to different axial locations. These axial locations are

found by using a set of plastic spacers, and the copper coil is fixed in place for each

measurement using a plastic screw and nut system developed for this specific thruster by Hyatt

[29]. This setup is shown in Figure 3.20. At each axial coil position, each of the eight coils were

individually energized and magnetic field measurements were captured at each step. This

calibration procedure allows known currents at known radii and axial positions to be related to

measured magnetic field, as described in Chapter II.
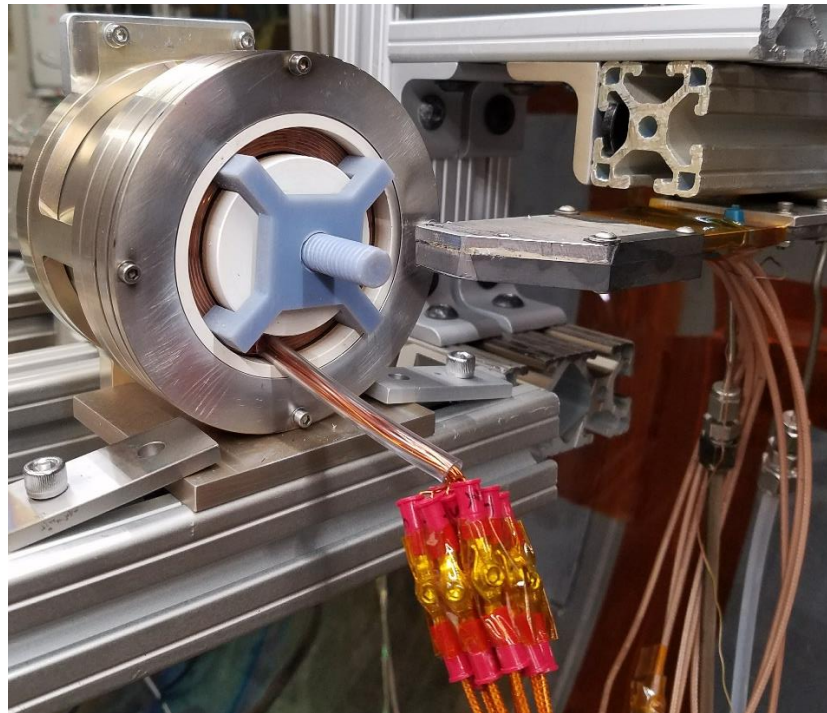
Figure 3.20: Magnetic Sensor Array Calibration Configuration

Using the Green's Matrix calculated from the calibration process, current densities in the

solution plane can be determined using the algorithms in Chapter II. To compare to optical

intensity data, the total current density through the solution plane at 0° azimuth is summed across

all elements. As discussed in Chapter II, this analysis is only meaningful in operating conditions

that meet the assumptions made to relate magnetic field data to Hall Current, which include a

steady current. While this assumption can be considered valid in the breathing mode, the

azimuthal variations present in the spoke mode present unsteadiness that precludes this analysis

from being appropriately applied in this mode.

3.6 Thruster Repair Configuration

At the beginning of the research period, it was noted that the anode gas flow inlet line

was slightly loose. This was assumed to be a design feature of the thruster to help reduce strain

on the internal plumbing. However, during the course of testing this assumption was proven

incorrect, as this component broke entirely, leaving the inlet line detached from the anode gas

distributor within the thruster, as seen in the top left of Figure 3.21. The original line was 1/8 in

stainless steel, coupled to the anode gas distribution plumbing with a coupler that was slightly

larger than 1/8 in in diameter. The pattern of the break in this joint prevented a direct

reattachment of the original line so a repair was attempted using a new inlet line. New 1/8 in line

did not fit well into the coupler, so a length of 1/16 in line was inserted into the coupler and was

centered in the coupler using a ferrule from a VCR connection. This assembly was affixed to the

coupler and all gaps around the new line were sealed using 3M TC-2810 thermally conductive

epoxy. To add stiffness, the original 1/8 in line was sheathed around the new line and joined to

the coupler using the same epoxy. This repair is shown in Figure 3.22. Using a length of 1/8 in

Tygon tubing and the appropriate Swagelok and VCR adapters, the 1/16 in line was connected to

the gas feed in the chamber and testing was resumed.
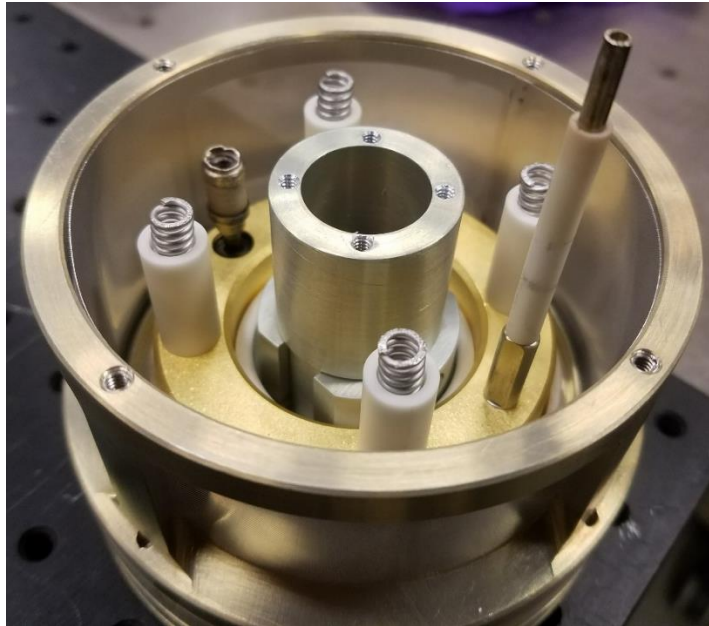
Figure 3.21: Damaged Propellant Inlet

Figure 3.22: Repair Attempt 1: taken during epoxy cure time

The thruster was successfully fired in this configuration running on Xenon for about 30 minutes, but the discharge went out abruptly with no obvious cause. The thruster did not easily start again on Xenon at this time. Another thruster was being fired subsequently using Krypton, so the lines were purged and switched to Krypton; because previous research that had ruled out the use of Krypton as the propellant for the BHT-600-PM was likely conducted while the anode feed line was damaged, an attempt was made to run the thruster on Krypton. The thruster was successfully started using Krypton, but rather high anode and cathode mass flow rates were required, around 45 and 4 SCCM, respectively. The discharge, once again, went out with no obvious cause, so testing was halted. Once out of the vacuum chamber, inspection of the thruster revealed that the epoxy appeared darker in color, and a small crack had propagated around part of the epoxy seal, as seen in Figure 3.23. Because the damage appeared minor, the crack was filled in with additional epoxy so more data runs could be conducted. A longer cure time was allowed this time to eliminate the possibility that incomplete curing increased the epoxy seal's susceptibility to damage.

Figure 3.23: Damage Sustained by First Repair Attempt

The thruster again successfully fired using Xenon, but the discharge again went out abruptly after about 45 minutes and testing was halted. Inspection of the unit afterward revealed even more severe discoloration of the new epoxy layer. The epoxy also appeared to have separated slightly from the feed line in the radial direction, as seen in Figure 3.24, which possibly left a gap for the propellant to escape, preventing sufficient mass flow from reaching the channel to support discharge. At this point, testing was halted permanently, as it was clear that these fixes would be insufficient.
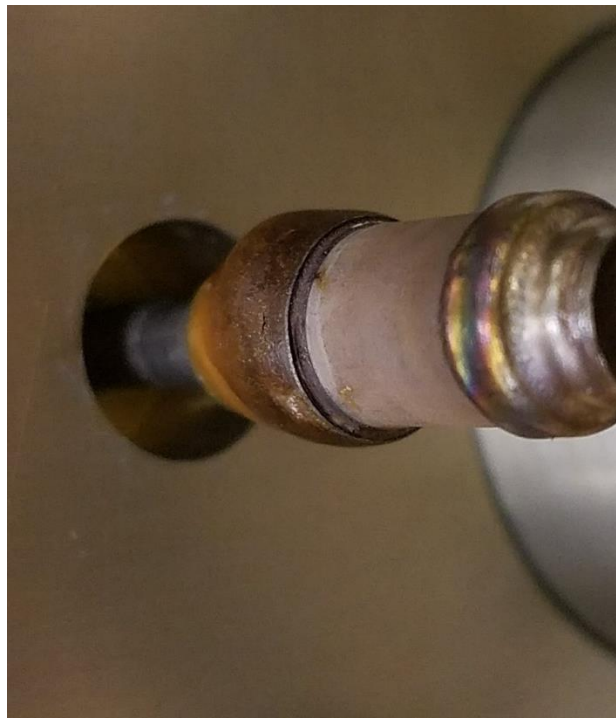
Figure 3.24: Damage Sustained by Second Repair Attempt

The data presented henceforth were taken during the brief periods of successful operation of the thruster. The manufacturer recommends several hours of operation prior to conducting experiments to allow the thruster to outgas and the discharge to stabilize. The longest successful firing event during the present research was one of the first attempts and lasted less than an hour; the goal of this attempt was to determine appropriate firing parameters and ensure functionality

of the test equipment and instrumentation, so no proper data collections were completed at this time. In subsequent successes, the thruster only fired for 45 minutes or less; while some data were collected during these sessions, they may not be wholly representative of operating conditions for the thruster and may contain some differences from a fully stabilized plume. Additionally, the extent of the damage to the inlet gas feed is not known for all data collection periods. The impact of this damage is unknown, but likely includes the necessity for higher anode gas flow rates due to the escape of propellant from the gas feed before entering the channel. These are the data that will be presented in Chapter IV, with the caveat that analysis of this data will not constitute a full characterization of the thruster for the above reasons.

3.7 Chapter Summary

The intended methodologies for experimentation and analysis of collected data were presented in this chapter. These include operating a Hall Effect Thruster and collecting optical emission data, Hall current data, and plasma potential variations at very high sample rates and in a time-correlated manner. Delays in testing caused by equipment failures and maintenance and laboratory improvements, which will be discussed in the next chapter, the data able to be collected were severely limited. Furthermore, the data that was collected may have been taken while the thruster was damaged to some degree and was almost certainly taken before the thruster discharge was able to achieve stable operation, which implies the data presented here will not represent a full characterization of a properly functioning thruster. The data that was collected, however, may provide some insight into similarities and differences between the permanent and electromagnet thruster models. This will be further explored in subsequent chapters.

IV. Analysis and Results

4.1 Chapter Overview

While the previous chapter described the planned course of action for operating the thruster and collecting and analyzing data, this chapter will outline the actual events that occurred during the research period. The somewhat limited data gathered during this period will also be presented.

4.2 Achieving Successful Thruster Operation

The following sections will detail the path taken to achieve successful thruster operation as well as several observations made along the way.

4.2.1 Experimentation Delays

Before the planned start of the research period, during a handover demonstration being given by previous researchers using the BHT-600-PM, the BHC-1500 hollow cathode being used was not igniting as expected. To remedy this, the cathodes available were sent to the manufacturer to be refurbished. This process took much longer than anticipated—the cathodes were not returned, and therefore experimentation could not be started, until the vacuum chamber was taken out of operation to allow the addition of a chamber extension. This process also took longer than expected, so a significant delay was experienced before experimentation could begin. Furthermore, as described in Chapter III, a significant effort had to be made to get the vacuum chamber back to a fully operational state after this extension installation, adding yet more delay before any experimentation could be performed.

4.2.2 Troubleshooting Thruster Discharge Ignition

Once the chamber was returned to its fully operational state, the thruster in its complete operational configuration, as seen in Figure 3.3, was installed on the thruster translational stand

and the chamber was pumped down. Also installed in the chamber at this time was another student's research article, a Busek Pseudolinear Hall Effect Thruster. When the chamber reached an appropriate pressure, the gas feed lines were purged with Xenon, and the cathode conditioning procedure was performed, which involves slowly heating the cathode while purging the lines with neutral gas to prevent the cathode from being shocked by a combination of high intensity heat and the presence of atmospheric contaminants, which can poison the cathode and shorten its lifetime. During this attempt, it was observed that no mass flow appeared to be entering the chamber from the mass flow controller being used for the cathode mass flow; this was evident because even a much greater-than-required mass flow commanded yielded no visible increase in Xenon's partial pressure in the chamber, as measured by the RGA. The cathode was connected to a different mass flow controller and the process was resumed the following day.

After the conditioning procedure was completed, the cathode mass flow was increased to the value that had yielded good performance with previous thrusters, about 1.5 SCCM, and a potential of about 625 V was applied to the cathode keeper. After about two minutes, the cathode ignited, which is observed in the BPU-600 control program as a decrease in keeper voltage to about 40 V and an increase in keeper current to about 0.2 A. Mass flow was then introduced to the anode at a rate of about 27.5 SCCM; this flow was allowed a few minutes to stabilize, then a discharge voltage of 250 V was applied to the thruster. This did not yield any observable change on the BPU control program, but the channel was not physically observed at this time to check for energized Xenon glow. At this point, the downside of having a fixed magnetic field from permanent magnets was fully realized, as previous research had shown that thruster startup was easily achieved by decreasing the electromagnet power, an option not available for the thruster under study. After various combinations of discharge voltage and anode mass flow rates were

attempted to no avail, troubleshooting was halted to allow an attempt at running the Pseudolinear Hall Effect Thruster.

The following day, the Pseudolinear Hall Effect Thruster was successfully started with little effort using Krypton. This eliminated a number of possible faults as causal to the failure of the BHT-600-PM to start, including power supply and conditioning, BPU-600 control program errors, and gas feeds external to the vacuum chamber. In light of the success of the other thruster, another attempt was made to start the BHT-600-PM, a few days later, while the chamber was still pumped down. Because the cathode had remained in near-vacuum conditions, conditioning was not required to be re-accomplished, and the cathode heater was set to 6.5 A. After a few minutes, the keeper voltage was applied, and the cathode ignited within three more minutes. The standard anode and cathode flow rates and discharge voltage were applied, but the discharge still did not ignite. At this point, it was considered to examine the thruster channel for signs of energized Xenon, as described in Chapter II. Previous research had suggested that this "glowing gas blob" was indicative of a state close to discharge, but not yet achieving adequate ionization in the channel [29]. As seen in Figure 4.1, this gas glow was observed at this time, which eliminated a few more potential causes for ignition failure and encouraged the researchers to continue attempting to achieve ignition.

Figure 4.1: Energized Xenon Emission in Thruster Channel

A more methodical approach was used to increase the anode flow rate and discharge potential, and eventually success was found by increasing anode mass flow to about 40 SCCM, much higher than the flow rate suggested by Busek, and by slowly increasing the commanded discharge potential, starting at 250 V and increasing until the discharge ignited [25]. Brief periods of ignition were observed at slightly lower mass flows and discharge potentials around 270 V, but extended thruster operation was achieved by mass flows around 40 SCCM and discharge voltages commanded to about 275 V or higher. This operation is shown in the photos in Figure 4.2; the photos are taken at different exposure settings to highlight different features of the thruster.
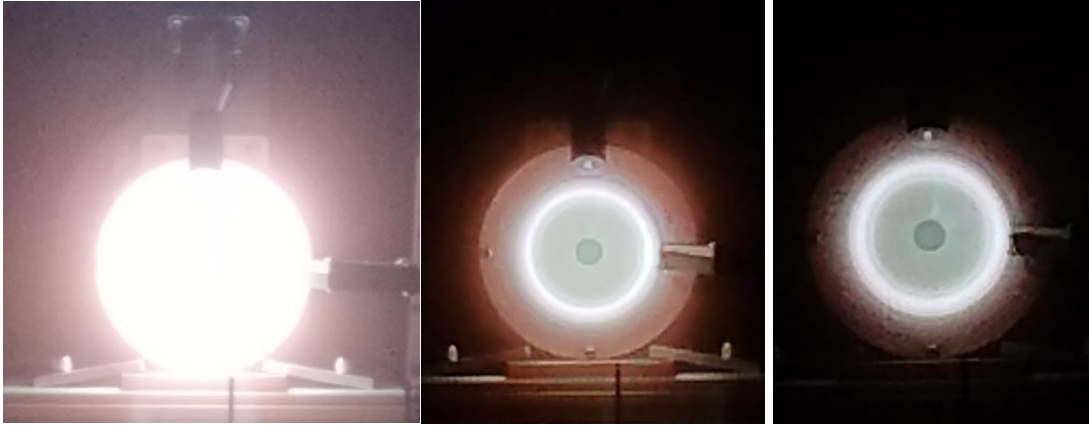
Figure 4.2: Thruster Operation on Xenon, various camera exposure settings

When extended operation was attained, an attempt was made to modify the operating

conditions to achieve standard operational mode, in which the plasma discharge is voltage-

limited. In its current operation, the thruster was using a discharge power of about 225 W,

considerably lower than its design power of 600 W. In an attempt to make the discharge voltage-

limited, the anode mass flow and commanded discharge voltage were decreased; again, however,

the shortfall of having permanent magnets showed itself, as previous thrusters were able to

obtain voltage-limited discharge by an increase in magnetic field strength. With these

adjustments, the discharge went out a few times, but was re-established by increasing the

parameters again. After some time, care was taken not to decrease either tunable parameter too

much, as having a running thruster, even at non-operational conditions was preferable to making

the discharge go out.

The thruster was allowed to run at a commanded discharge potential of 250 V and an

anode mass flow rate of about 38 SCCM; in this state the thruster had an actual discharge voltage

of about 70 V and a discharge current of about 3.2 A, maintaining the discharge power of about

225 W that was exhibited during this whole attempt. During operation, the BPU-600 control

program froze and crashed, but the thruster kept operating. At this time, a number of high speed

videos were taken; the intent was for these to be used for gain calibration, centering, and focusing of the camera, but due to the lack of data collected subsequently, they will be considered later in this chapter. Magnetic field data were also attempted to be collected, but the magnetic sensor array was not being recognized by the data collection PC for that sensor, and the thruster discharge went out before this could be troubleshot. The emissive probe was not prepared for data collection as it was desired to collect data on a stabilized plume and not risk burning out the filament before that point; as a result, no plasma potential data was collected in this session. Because the thruster control program was not responsive, no cause could be determined for the discharge extinction. After about 10 minutes of the discharge cycling on and off due to adjustments being made, the flow rate and discharge voltage were left alone, allowing the thruster to run continuously at about 225 W, as described above, for about 45 minutes before going out. The thruster was allowed to cool, and the chamber was brought up to atmospheric pressure.

4.2.3 Thruster Tuning

The thruster was successfully fired on two more occasions before the thruster inlet feed was catastrophically damaged. During these sessions, emphasis was placed on attempting to tune the thruster to achieve voltage-limited discharge. Achieving initial thruster discharge ignition was difficult, as in the first session, but after it was achieved the thruster was successfully tuned to operate at a discharge potential as commanded in the BPU-600 control program. This was accomplished by adjusting the mass flow rate to the anode, while ensuring that the mass flow to the cathode remained around the suggested 10 % of the anode flow.

During the first of these sessions, while the thruster was warming up, the magnetic sensor was troubleshot and believed to be fixed. A few test samples were taken during this time that

looked promising, but later analysis revealed that the data was not successfully recorded. Before any other datasets could be collected, the discharge went out unexpectedly with no apparent cause. Upon attempting to restart the thruster, the BPU-600 control program crashed, requiring a restart of the PC. Data collection was halted at this point to allow the other thruster to run.

During the second run, it was noted that a higher-than normal anode flow rate, almost 45 SCCM, was required to start the thruster. Voltage-limited discharge was achieved, but shortly afterward the discharge went out abruptly. It was noted at this point that no energized gas glow could be seen within the channel, regardless of the mass flows and discharge voltage used. This was when the catastrophic damage to the gas inlet feed was discovered, and the repairs described in Chapter III were attempted. No data were collected before this occurred on that run.

4.2.4 Repaired Thruster Performance

After the first repair attempt, the thruster was successfully started for two periods less than 45 minutes each. The first run was on Xenon, and it was noted that appreciably lower anode mass flow, about 30 SCCM, enabled thruster ignition, though discharge voltage had to be increased as before. Another interesting difference post-repair was that the thruster discharge was voltage-limited from the time of ignition; no tuning was required. The discharge was allowed to run to determine if the repair would allow extended operation, but the discharge went out after about 45 minutes. The discharge was not easily reignited, and at this point, it was again observed that no gas glow was visible. Images from this run, such as the one in Figure 4.3, appeared slightly different than photos of previous runs, as in Figure 4.2. While camera exposure settings and the position of the thruster in the chamber may have had some effect on this, the discharge appeared more distinctly blue, as expected from Xenon emission. This is thought to be due to better gas delivery to the anode in the repaired configuration.
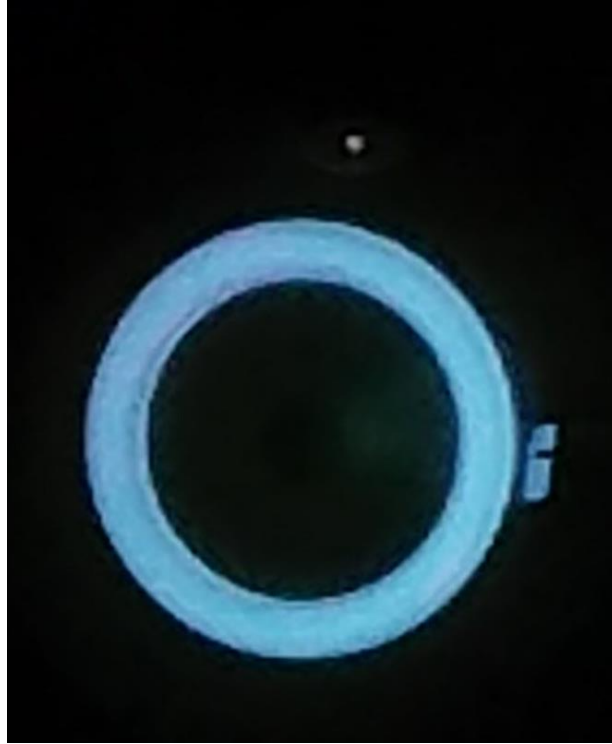
Figure 4.3: Repaired Thruster Running on Xenon

4.2.5 Thruster Running on Krypton

At this point, the gas lines were being purged on Krypton for use on the other Hall Effect

Thruster being studied, and a thought occurred that some level of damage to the anode gas feed

may have been pre-existing, as noted in Chapter III. This may have affected results of previous

research that concluded the thruster design was not suitable for running on Krypton, so it was

attempted again [29]. As seen in Figure 4.4 and evidenced by the distinct violet emissions

therein, this attempt found relatively easy success; the thruster discharge ignited with much the

same process as when Xenon was used, except higher mass flow rates had to be commanded to

both cathode and anode than were needed for Xenon operation. This discharge, however, only

lasted a few minutes before going out abruptly. Again, attempts to re-ignite the discharge were

fruitless, not even yielding gas glow in the channel.
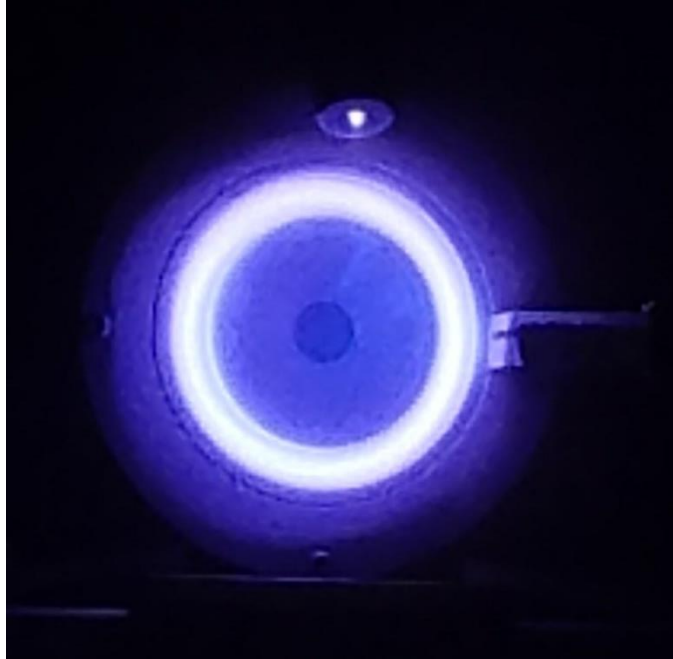
Figure 4.4: Repaired Thruster Running on Krypton

Unfortunately, because these runs were intended to be a functionality check to verify the

thruster repair was adequate, they were run while the thruster translational stand was positioned

for a different type of measurement for the Pseudolinear Hall Effect Thruster. This positioning

was not suitable for taking high speed video data, and no magnetic field or emissive probe data

were taken because the thruster discharge did not last long enough for the plume to stabilize.

4.2.6 Final Attempt

As discussed in Chapter III, damage was discovered on the epoxy that constituted the

initial repair attempt, but it was unclear if some force experienced in handling or set-up had

caused some of the damage or if it was from operating conditions, so the area was patched again

with epoxy and allowed to cure longer. In this configuration, the thruster was run again on

Xenon, with results similar to after the first repair, with a lower anode mass flow than had been

required previous to the repair and voltage-limited discharge from ignition. During the warm-up

period a number of high speed videos were recorded, and a few magnetic sensor readings were

commanded. The emissive probe was also warmed up, but the thruster discharge, once again, went out abruptly before any measurements could be taken. With no gas glow visible in the channel, testing was concluded for the session so the thruster could be inspected again. When further damage to the anode gas feed repair was revealed, testing was permanently halted, as it was clear that in-house repairs performed on the thruster would be insufficient to allow proper thruster operation.

4.3 Data Collection Summary

As described previously, out of the three intended data sources—optical emissions, magnetic field data, and plasma potential—only the first two were collected. When the data were processed and analysis was attempted, it was discovered that during the attempts at collecting magnetic field data during the second and fifth data runs, only four of the 12 manual trigger events that were commanded produced data files. Of those four data files, only one, the last collection attempted, actually contained any data. The mechanism behind this malfunction is unknown; it may be related to the hardware issues experienced previously or the fact that the recording events had to be manually triggered instead of triggered by the oscilloscope. To add further misfortune, when this dataset was processed with the calibration data for the magnetic sensor, the resulting products showed extremely low magnitudes for the calculated values, and no discernible patterns, where a breathing mode was expected. It is believed that the signal to noise ratio of this sensor was not high enough in the current configuration and that the only good data acquisition is comprised exclusively of noise in the sensor. Therefore, the remainder of this chapter will focus on analysis of high speed video data.

4.4 Optical Emission Analysis

As outlined in Chapter III, high speed video data were acquired of the thruster exhaust at a frame rate of 1 Mfps, with each video containing 102 frames. In all, 36 videos of thruster operation were acquired. Of these, 21 videos adequately captured the optical emissions of the thruster with suitable contrast for analysis. Most of these videos capture the thruster exhibiting a breathing mode, but a few capture something resembling a spoke mode. For each of these videos, the video was unrolled into a channel plot, and plots of normalized intensity at -90°, 0°, and 90° azimuths with respect to time were generated. A selection of these will be presented in the following sections; the rest can be seen in Appendix A.

4.4.1 Breathing Mode

The following discussion will include presentation of unrolled video channel plots from the current research, analysis of optical intensity variations at select azimuths, and comparison of these results to data from the electromagnet version of this thruster.

Figure 4.5 shows an unrolled video plot of the thruster exhibiting a breathing mode during the first successful run of the thruster. At this point the thruster had been running for about 20 minutes. Because this video was not triggered by the oscilloscope on a rising breath in the discharge current, the recording started in the middle of a breath. This limits the available data for analysis, but breathing frequency was approximated to be 28 kHz. Also visible in this plot are some variations in intensity around the channel that do not vary much with time. These are also evident in Figure 4.6, the plot of intensity at select azimuths, as the peak intensities at 0° and -90° are lower than at 90°. These variations are not believed to be indicative of any additional anomalies in the plasma, but rather artifacts introduced by poor camera focusing and pointing, as these parameters were still being tuned at the time.
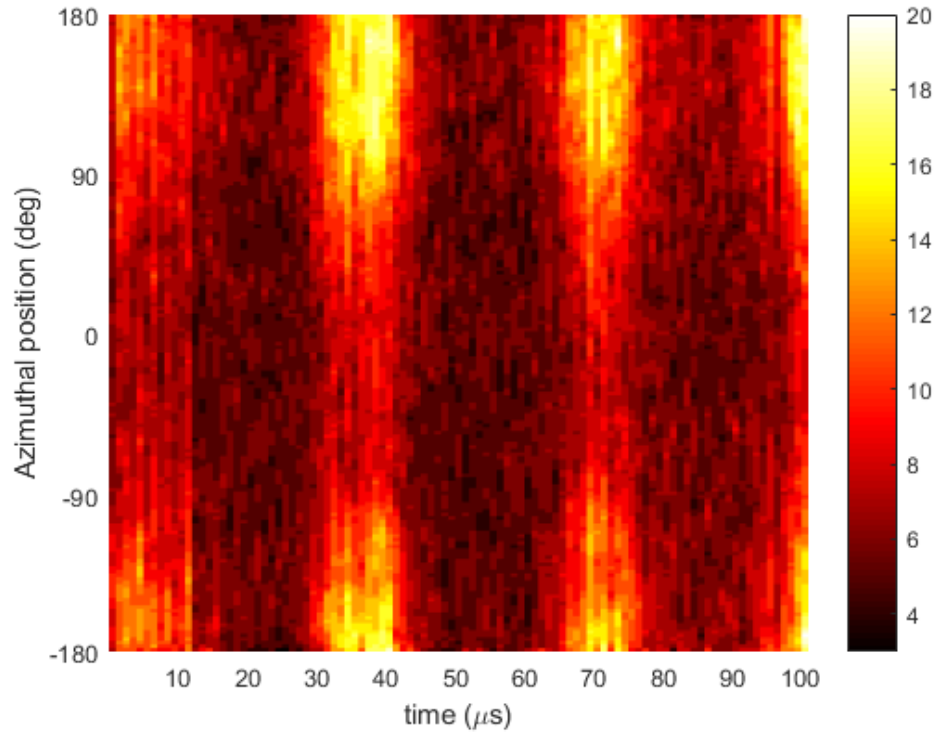
Figure 4.5: Breathing Mode Test 1 Unrolled Video, $V_D = 75$ V, $I_D = 3.2$ A

Despite the variation in intensity at the peaks between azimuths, it is clear from Figure 4.6 that

the peaks in intensity for each azimuth occur at the same time, which confirms there is not a

significant azimuthal component to the changes in intensity, as expected in a breathing mode.
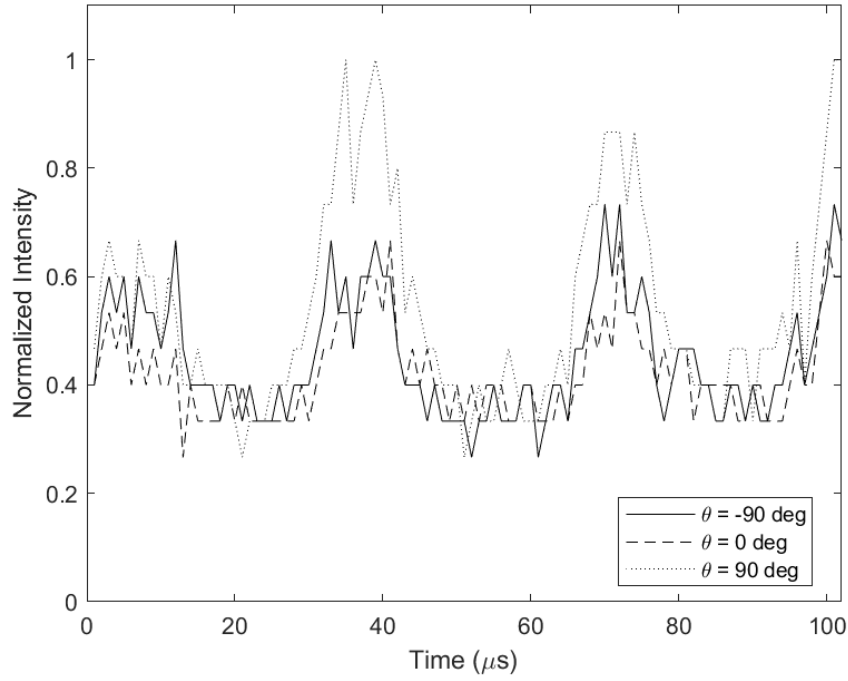
Figure 4.6: Breathing Mode Test 1 Intensity Plot, $V_D = 75$ V, $I_D = 3.2$ A

Figure 4.7 is an unrolled video that was taken less than a minute after Figure 4.5. It is plagued

by a similar issue regarding the number of breaths observable due to the initial state of the

discharge when recording commenced, but by similar analysis, it appears to have a frequency of

about 25 kHz. It is also a clearer image, with less of the variations seen in the previous plot.

Figure 4.8 also confirms less azimuthal variation in peak intensity as well as no distinguishable

azimuthal variations in time of peak intensity, once again confirming the breathing mode.
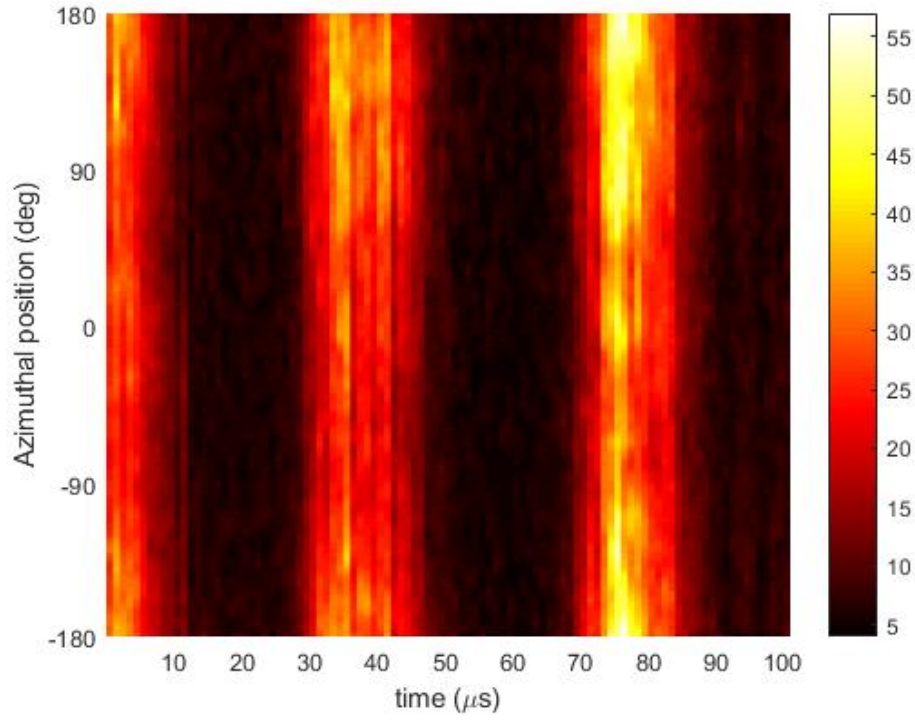
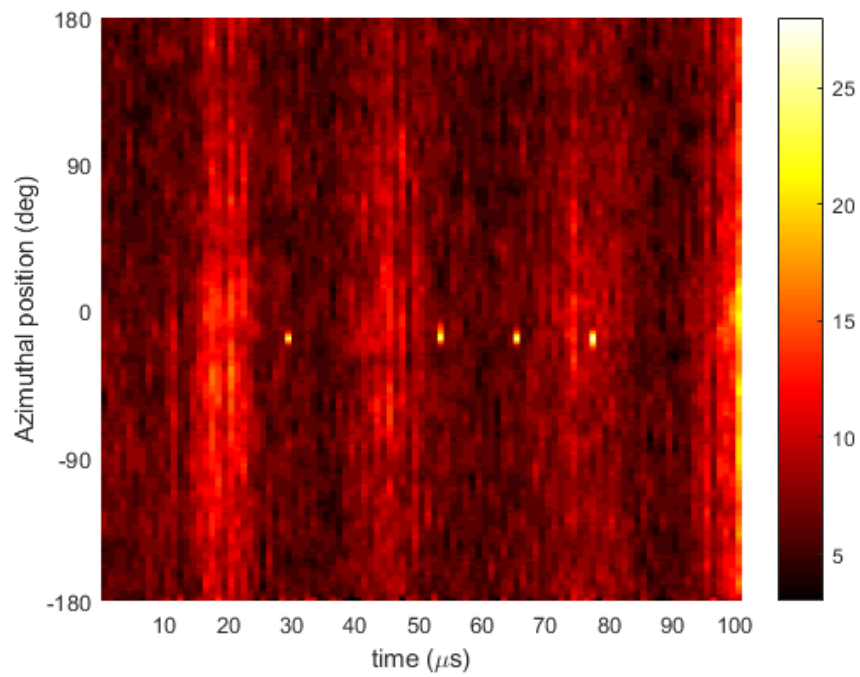Figure 4.7: Breathing Mode Test 2 Unrolled Video, V_D = 75 V, I_D = 3.2 A
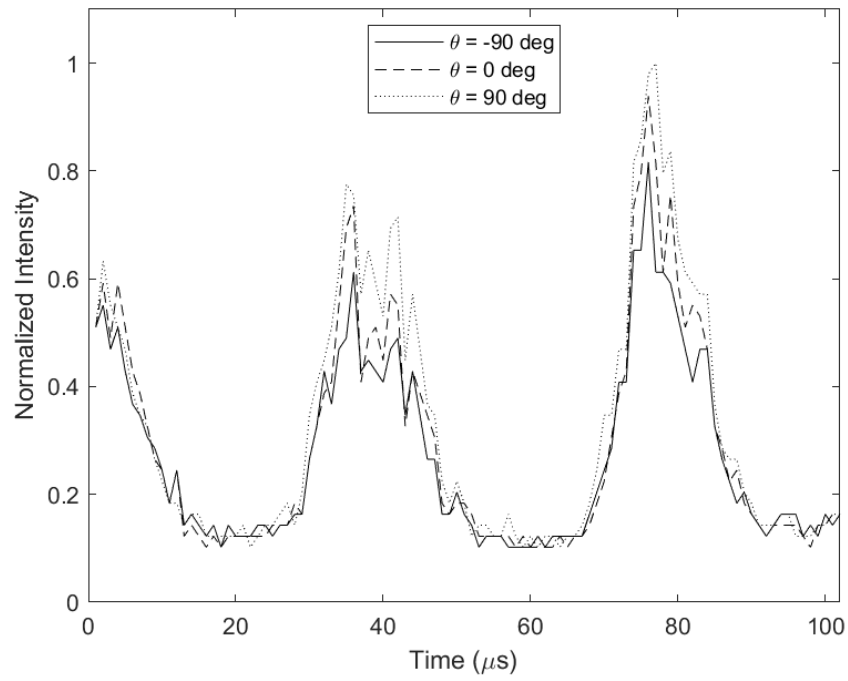
Figure 4.8: Breathing Mode Test 2 Intensity Plot, V_D = 75 V, I_D = 3.2 A

Between these first two tests the breathing mode frequency changed some, from 28 kHz to 25 kHz, but the uncertainty is rather high in determining these frequencies due to very small sample sizes. Longer duration high sample rate video collection would be required to make stronger conclusions.

About 10 minutes after the video represented in Figure 4.5 was taken, Figure 4.9's source video was collected. Figure 4.9, along with its associated intensity plot for selected azimuths, in Figure 4.10, has much narrower, brighter emissions with sharper edges and more space between them. While some of this may be due to increased sharpness enabled by increased operator experience and camera adjustments that were made, it is believed that this particular mode was also the harbinger of discharge extinction, as the discharge went out within 7 minutes of this mode being recorded. The breathing mode frequency here was found to be about 24 kHz. Subsequent videos from the same experimentation session show similar increased contrast and severity of rises and falls, suggesting that this mode did in fact lead to the discharge going out.
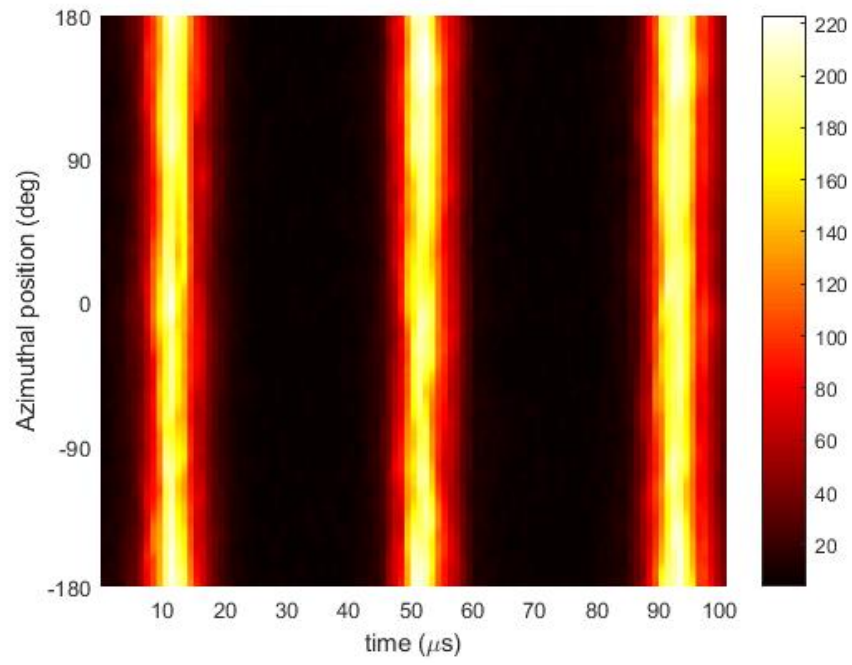
Figure 4.9: Breathing Mode Test 5 Unrolled Video, $V_D = 70$ V, $I_D = 3.2$ A
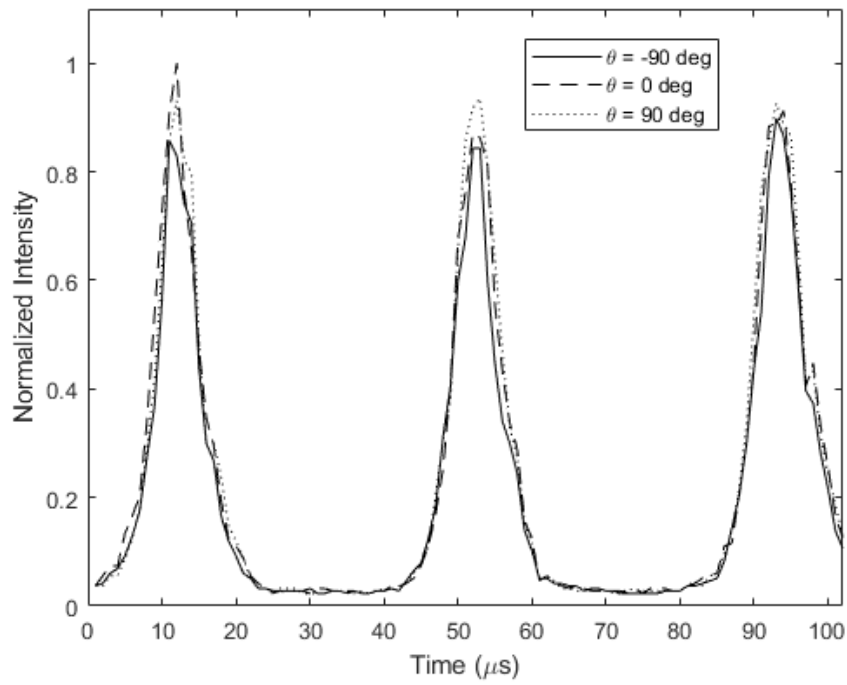
Figure 4.10: Breathing Mode Test 5 Intensity Plot, $V_D = 75$ V, $I_D = 3.2$ A

Table 4.1 shows approximate breathing mode frequency for the 19 samples and documents the amount of time passed since the first video in each session was taken. During the first session, the breathing frequency is observed to vary more significantly among earlier values. After about 10 minutes have passed since the first video was taken, the breathing mode frequency settles around 23-24 kHz. As previously mentioned, this more constant breathing frequency could be indicative of thruster operation or other conditions, such as temperature, stabilizing. At the 10-minute mark in Table 1, the thruster had been running for approximately 30 minutes, which is at the very bottom of the range of recommended thruster operating times to achieve a stable plasma plume. It is also of note, however, that in this session, the thruster did not reach the typical operating mode characterized by voltage-limited discharge. This may have affected the breathing mode characteristics.

While Session 1 saw improved stability in the breathing frequency over time, Session 2 contains significant variations across the board. Fewer data points are available, but there is a noticeable downward trend in the breathing frequency, possibly indicating that the thruster required a longer warm-up period in its repaired configuration and did not achieve the same level of stability that was attained in Session 1 before it went out.

Table 4.1: Approximate Breathing Mode Frequencies

Test	Time (min:sec)	Breathing Frequency (kHz)
Session 1		
1	00:00	28
2	00:41	25
3	00:57	27
4	01:13	25
5	09:32	25
6	09:52	26
7	10:07	24
8	10:21	24
9	10:39	23
10	11:05	24
11	15:35	23
Session 2		
12	00:00	35
13	05:01	33
14	06:56	32
15	12:31	35
16	17:07	41
17	22:14	37
18	31:56	33
19	41:36	29

As shown in Figures 4.11 and 4.12, which correspond to Test 17, the thruster has not started to exhibit the stronger, more severe breathing mode seen in Test 5, though the thruster had been operating for nearly the same amount of time in these. This may be indicative of some success in the thruster repair, though the differences cannot explicitly be attributed to that, as the thruster was in significantly different operating regimes during these Sessions. In Session 1, the thruster was operating at about 225 W discharge power and was not discharge voltage limited; in Session 2 the thruster was operating very near standard operating conditions, about 600 W and discharge voltage limited.

Figure 4.11: Breathing Mode Test 17 Unrolled Video, $V_D = 250$ V, $I_D = 2.4$ A
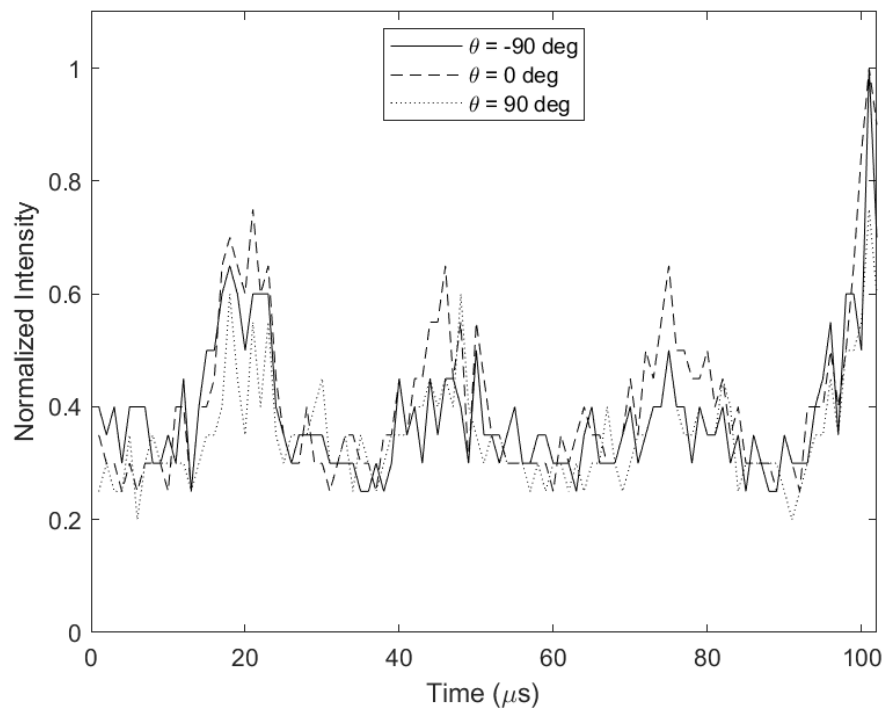
Figure 4.12: Breathing Mode Test 17 Intensity Plot, $V_D = 250$ V, $I_D = 2.4$ A

Figure 4.11 also contains bright spots at a few timestamps located just below the 0°

azimuth. These are visible in the raw video footage as small areas of bright pixels, as seen in

Figure 4.13. It is unclear whether this is some error or noise in the camera or some other

anomaly, but it is not related to the thruster operation. It is possible, however, that this

phenomenon is negatively impacting the post-processing results, leading to the less defined

images in Test 17. When that azimuth is removed in the intensity plot, however, a fair amplitude

difference is still available between peaks and valleys in brightness, so analysis is not too

severely impacted.
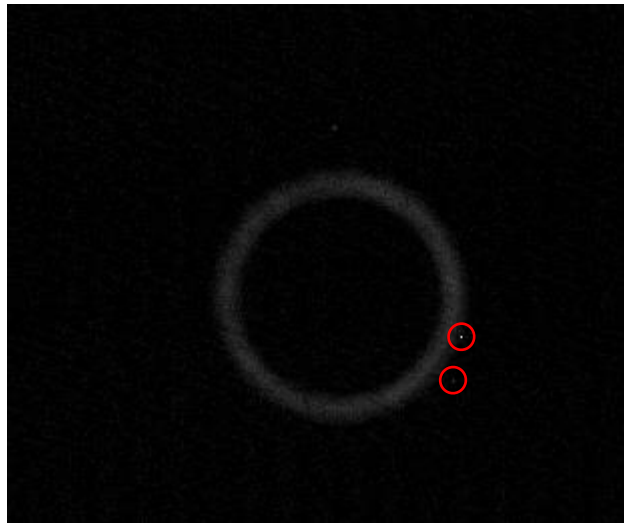
Figure 4.13: Frame from Breathing Mode Test 17 Video: anomalous bright spots circled in red

Tests 18 and 19, which represent slightly longer thruster operation than Test 5 from

Session 1, did show sharper breaths with more space between them, as shown in Test 19's results

in Figure 4.14 and 4.15. This may indicate that the thruster was starting to enter this extinction

mode after just a slightly longer run than before the thruster was repaired.
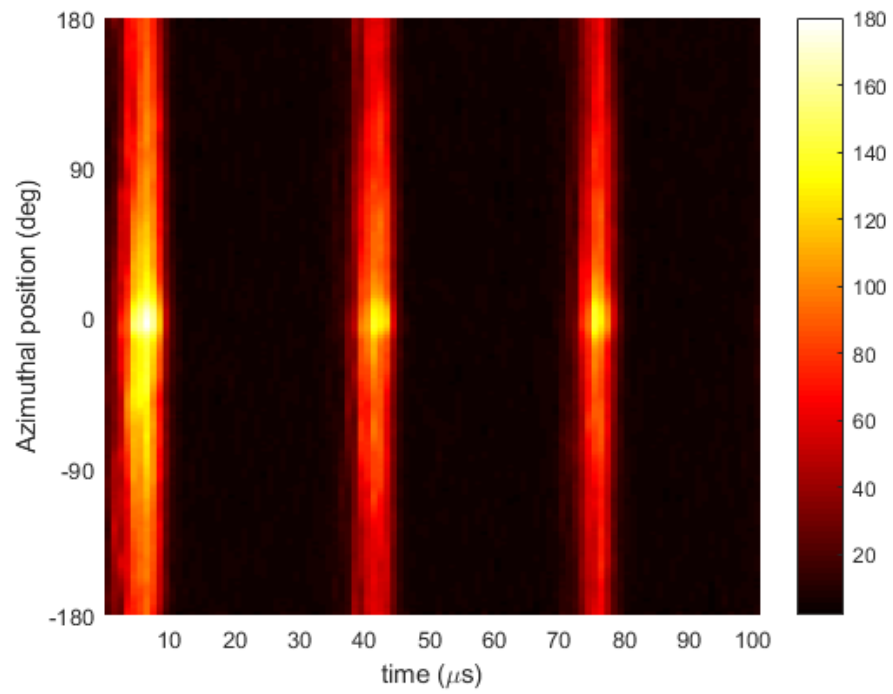
Figure 4.14: Breathing Mode Test 19 Unrolled Video, $V_D = 250$ V, $I_D = 2.4$ A
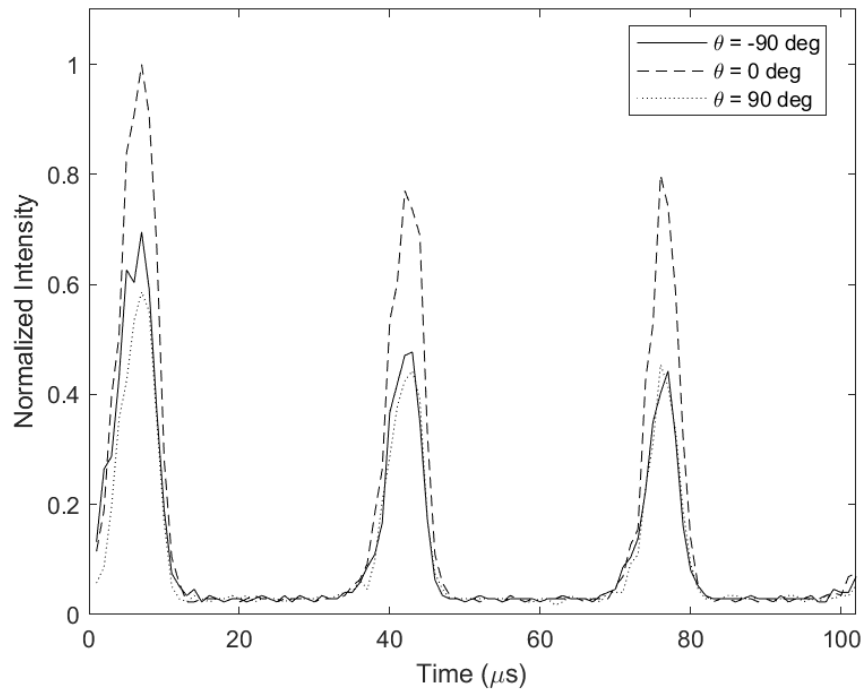
Figure 4.15: Breathing Mode Test 19 Intensity Plot, $V_D = 250$ V, $I_D = 2.4$ A

4.4.2 Breathing Mode Conclusions

Data from Session 1 of breathing mode video collections, which were collected over a period of 15 minutes and represent data from about 20 minutes of thruster operation to about 35 minutes of thruster operation, show a trend toward breathing mode frequency stabilization as time passes, on the order of 30 minutes from thruster start. In this case, the breathing frequency settled around 23-24 kHz. This is well within the established oscillation frequency range of 1-30 kHz for Hall Effect Thruster breathing mode [13]. The video data also appear more defined, with sharper breaths and more space between them in the later samples, indicating a deeper or more severe breathing pattern is occurring. This is thought to be indicative of imminent thruster extinction and appears to be unique to the thruster under study as no such mode was noted by Cunningham [3]. This phenomenon is thought to be caused by an insufficient propellant flow rate to the ionization zone in the channel; in the case of this thruster this is most likely due to the damage on the gas inlet feed, as described below.

In Session 2, video data were collected over a 42-minute period, spanning from about 2 minutes after thruster start to about 44 minutes after thruster start. The stabilization of the breathing frequency was not fully realized in this Session, and higher frequency breathing was observed throughout the session, though the frequency appeared to be trending downward in later videos. The frequencies observed were in the same range as those observed by Cunningham but are above the maximum of the range suggested by Choueiri [3,13]. This may have been due to a number of differences between the Sessions, most notably the inclusion of a repair in the inlet gas feed of the thruster and the actual thruster operating parameters, as the thruster ran at voltage-limited discharge with a discharge power of about 600 W in Session 2, as opposed to the 225 W operation in Session 1.

While the severe breathing mode exhibited toward the end of each Session appears indicative of an imminent extinction of the plasma discharge, no causal mechanism is immediately obvious. In the context of the current research, it is proposed that the damage to the gas inlet feed may be a contributor to this phenomenon. It is believed that some damage, such as a small crack, existed in the anode gas feed line from the beginning of the current research period, and after each post-repair operation, damage in the form of cracks or expansion of the epoxy to break the seal between the old feed line and the new were found. Therefore, it is conceivable that, after a certain duration of thruster operation, around 30 minutes in this case, sufficient thermal stresses and possibly pressure-induced stresses caused expansion and/or widening of these cracks. As they widened, more propellant escaped behind the thruster channel, decreasing the effective mass flow to the anode. With less neutral gas flow in the channel, fewer electron collisions occur, causing a decrease in ionization rate. The lower effective neutral gas flow to the anode may have made the breathing mode more severe by more easily being ionized, indicated by the more abrupt, shorter periods of high intensity optical emissions. Similarly, it may have taken longer for the channel to be filled with enough neutral gas to cause a sharp increase in ionization rate again, marked by the longer dark periods between breaths. After some time in this mode, the effective mass flow to the anode may not have been sufficient to support this cyclic ionization mechanism anymore, causing the thruster discharge to go out.

This theory also lends itself to supporting one prevailing theory that the breathing mode is related to the inability of gas diffusion to keep up with the ionization rate, as described in Chapter 2. The refill rate of Xenon in the channel can be approximated as the thermal velocity of the neutral Xenon, equal to $\sqrt{RT}$, or about 140 m/s, assuming the Xenon supply is around 300 K,

divided by the ionization region length, about 3-5 mm. This predicts refill cycles around 30 kHz, which corresponds to the breathing frequencies observed in this and past research [3,14].

4.4.3 Spoke Mode

The mode in which spokes are easily visible was not able to be intentionally induced in the course of the present research for two primary reasons. The first reason is that very little operational time was accomplished, and all of this time was considered thruster warm-up time, so the desired modes were not being actively sought. The second reason is that only discharge voltage and anode mass flow rate were available as tuning parameters because of the non-adjustable magnetic field, whereas past research has made use of discharge voltage and magnetic field variations to make spokes more visible [3]. When these parameters were adjusted in the present research, however, the discharge usually went out before any changes in operating mode were observed. Therefore, it is unclear whether a true spoke mode is inducible in the thruster under study. In past research, spokes have been observed in multiple azimuths, rotating about the channel at about the same rate [3]. This can be seen as the diagonal striations in Cunningham's plots, as in Figure 4.16.
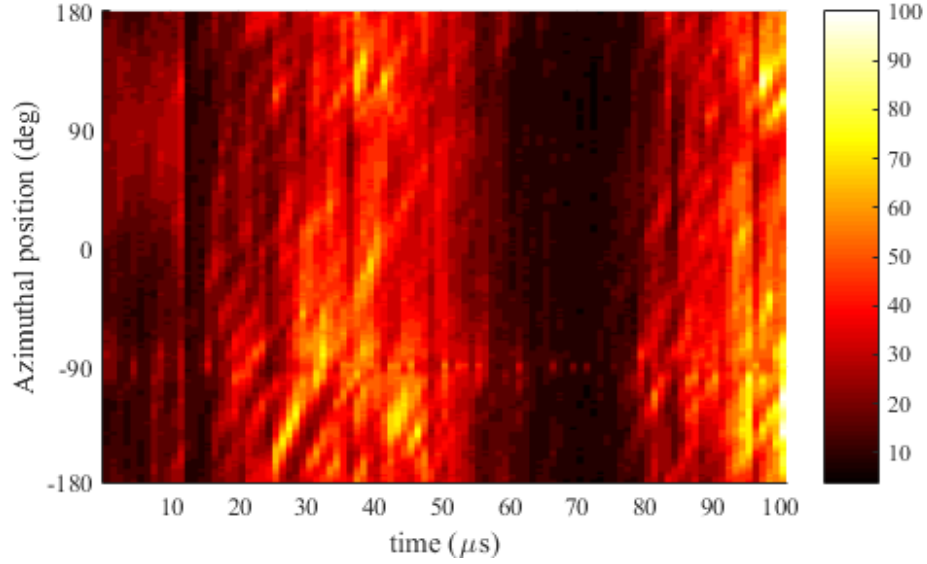
Figure 4.16: Spoke Mode Unrolled Video from Cunningham [3]

While this mode was not seen in the current research, a somewhat similar mode was observed very soon after thruster startup during the first data collection period. While this is thought to be a phenomenon related to thruster warm-up, it is worth noting that the two videos taken during this mode were taken about five minutes apart but show similar features. These videos' unrolled plots are shown in Figures 4.17 and 4.19, and their corresponding intensity plots at selected azimuths are seen in Figures 4.18 and 4.20.
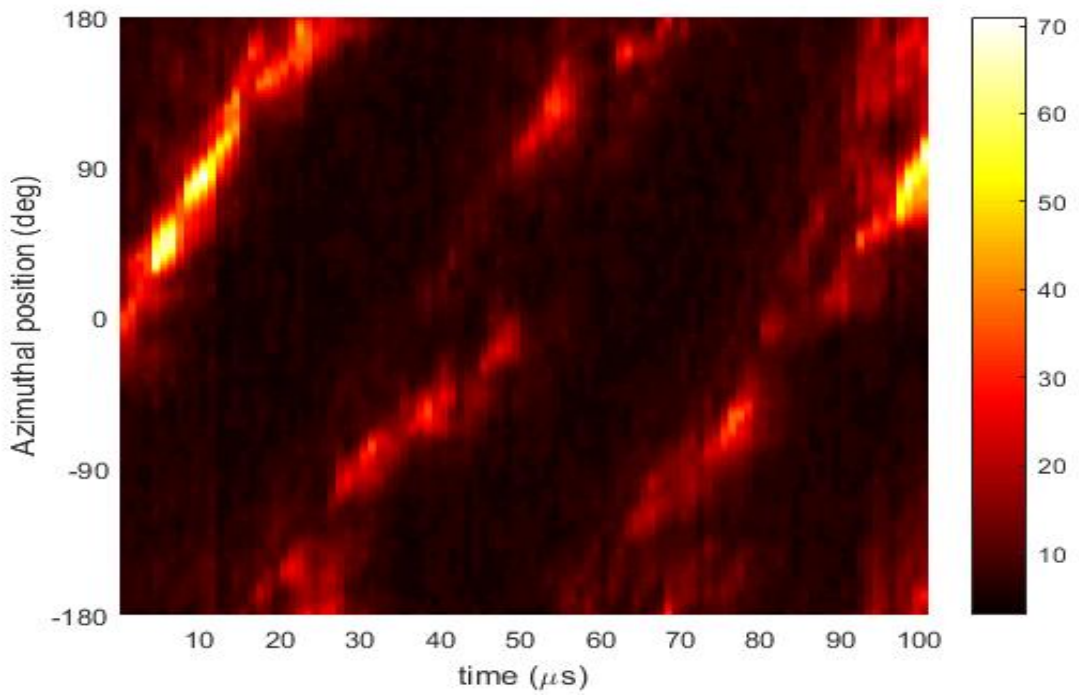
Figure 4.17: Spoke Mode Test 1 Unrolled Video, $V_D = 80$ V, $I_D = 3.2$ A
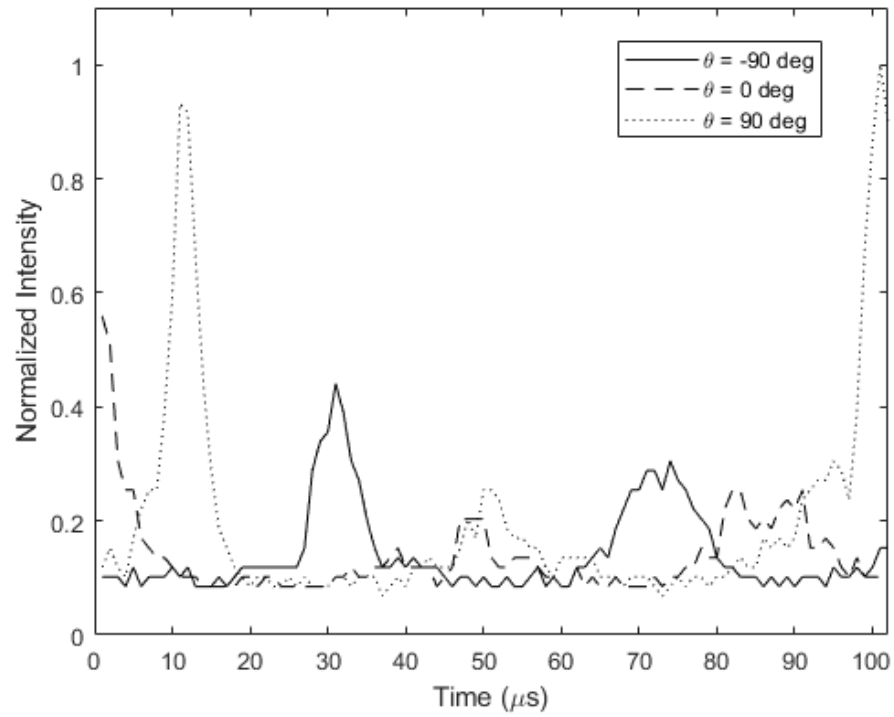
Figure 4.18: Spoke Mode Test 1 Intensity Plot, $V_D = 80$ V, $I_D = 3.2$ A
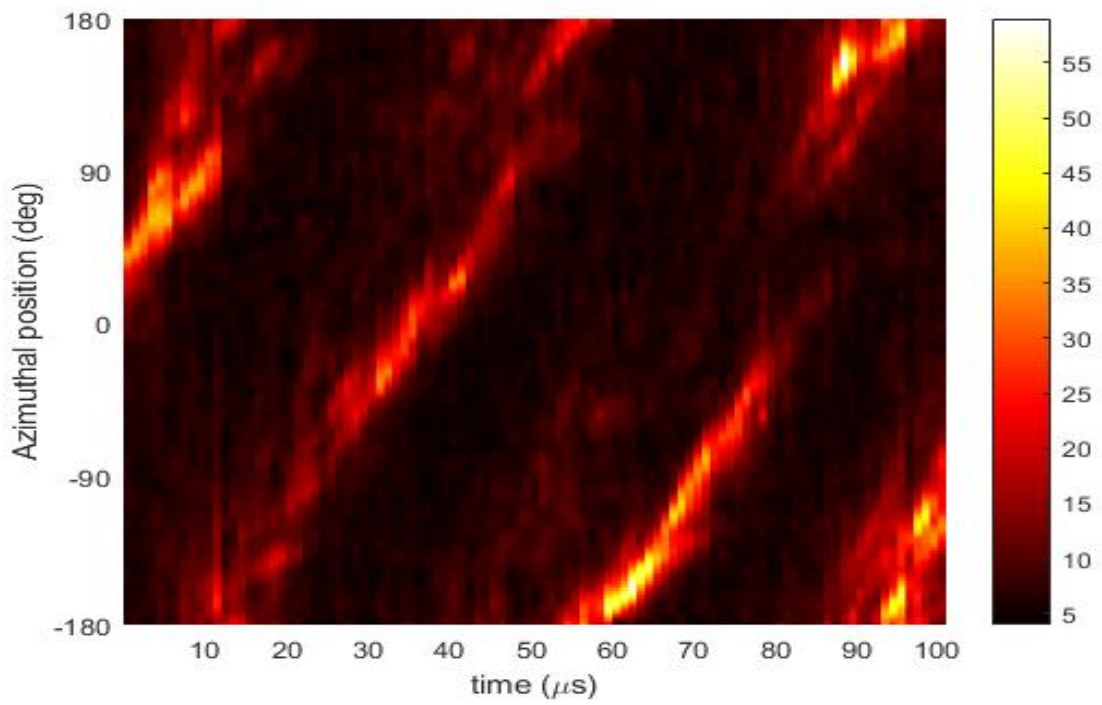
Figure 4.19: Spoke Mode Test 2 Unrolled Video, $V_D = 80$ V, $I_D = 3.2$ A
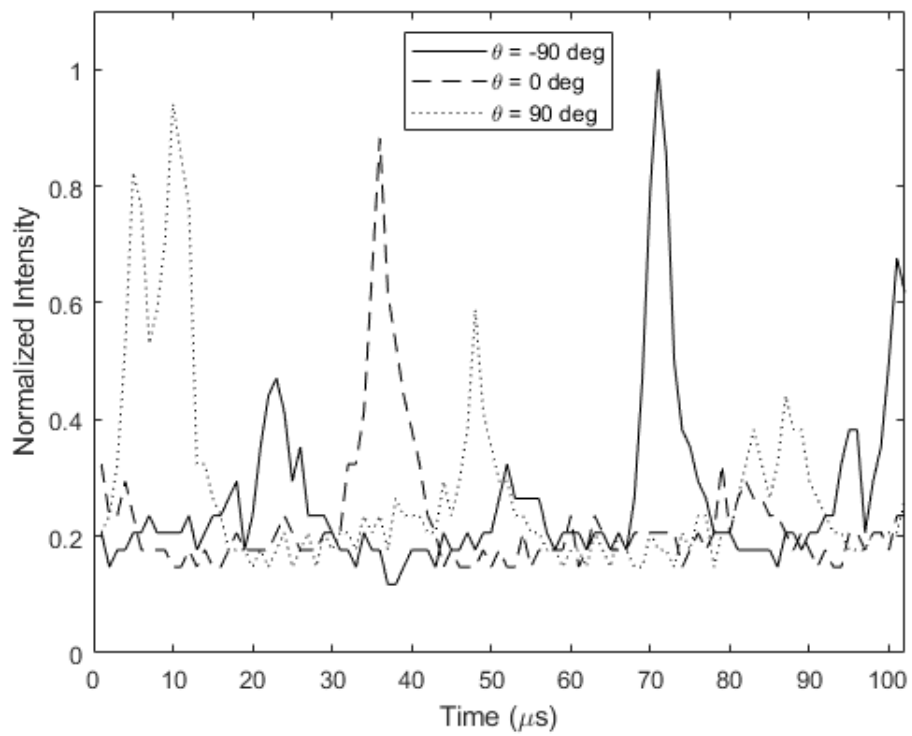
Figure 4.20: Spoke Mode Test 2 Intensity Plot, $V_D = 80$ V, $I_D = 3.2$ A

Clearly, the primary difference between the phenomenon observed here and the classically defined spoke mode as seen in Cunningham's research is that only one area of brightness is observed as opposed to multiple spokes travelling together. This affords one major benefit regarding analysis in that it is not necessary to be cautious in ensuring the same spoke is being followed, as there is only one spoke to follow. In both unrolled videos, the spoke appears to break up and reform at some point in its path, but this is believed to be an artifact of the unrolling process. The spoke in Test 1 appears to travel with a frequency of about 20 kHz, and in Test 2 the spoke has a frequency of about 22 kHz. These frequencies match well with Sekerak *et al's* observed average of about 20 kHz and fall within the range observed from spokes in Cunningham's research, which goes from 16.6 kHz to 27.7 kHz [30,3]. The spoke also travels in the $\vec{E} \times \vec{B}$ direction, as seen from traditional spokes in many previous studies, including Cunningham, Janes and Lowder, Liu, and Sekerak [3,9,15,30]. During data collection in the current research, no low-emissions period was observed in the presumed underlying breathing mode. Because of this, the single spoke was confirmed to propagate around the entire channel, making it meaningless to try to determine spoke generation points. While this may provide some additional evidence supporting Cunningham's theory that spoke structures can travel about the channel even in low optical emission periods, it is far from conclusive given the differences in the observed spoke modes between his research and the present study.

Unfortunately, the data collected here without correlated Hall Current or plasma potential data to provide additional insight does not provide much new information about causal mechanisms for the spokes seen here. Without additional measurements, it is also difficult to say with certainty whether the mode observed here can be accurately described as a spoke mode.

V. Conclusions

5.1 Summary of Data Collection and Analysis

The goal of the present research was to successfully operate the BHT-600-PM and find operating modes that induced breathing and spoke modes as seen in past research so similar data could be collected and analysis performed; the differences between the permanent magnet and electromagnet thruster studied by Cunningham could then be identified, possibly revealing some details about the physics behind these plasma instabilities. Because of the issues encountered getting the thruster to discharge reliably and for long periods of time, further complicated by damage sustained to the thruster during operation, very limited data was collected. Chapter 4 outlines this data and the analysis thereof, which consisted of unrolling high-speed video into projected channel plots and analyzing intensity at various azimuths. The frequencies of the breathing mode and spoke mode were also found.

5.2 Significance of Research

The thruster under study in the present research has the potential to be very useful in operational use due to its use of permanent magnets over electromagnets. The benefits permanent magnets introduce include significant mass savings, both due to the significantly lower mass of the permanent magnets compared to electromagnet coils and the need for slightly less substantial power supply and conditioning equipment, as no power is required by the permanent magnets. The power savings also found in this are somewhat small relative to the large power requirements of other thruster components, but some savings are realized.

The major negative impact of the permanent magnets that was observed in this research was the inability to tune the magnetic field. During testing, this led to difficulty achieving discharge and also increased the effort required to manipulate the characteristics of the discharge

for experimental purposes. During testing, it is also believed that damage to the thruster's inlet gas feed also led to difficulty achieving and maintaining discharge. In operational use, this would be of little significance assuming the magnetic field is conducive to starting the discharge in its operationally intended mode.

There is also some concern about thermal loads in the thruster, though very little data was collected to support this. The major observation in this area was that thermal loads appeared to contribute to the damage found on the gas inlet feed, but it is unclear which came first, the damage or the thermal loads. If the damage came first it is possible that the leaking of propellant behind the anode may have contributed to higher heat loads in that region, creating a self-perpetuating cycle of damage. If there are higher than expected heat loads in the thruster, however, permanent damage in the form of demagnetization of the Samarium-Cobalt magnets may occur.

5.3 Future Work

Due to the limited data collected in the present research, the most obvious path forward is to have the thruster properly repaired and inspected for further damage or any malfunctions that may have contributed to the original damage. If this can be done, the thruster could again be analyzed using the correlated data collection techniques proposed above. If further research is completed with the BHT-600-PM, it is highly suggested that a temperature monitoring system is put in place to ensure operating limits are not being exceeded. It is also suggested that, unless further analysis supports continued use of Krypton as the propellant, Xenon should be used to ensure the thruster is run in its intended operating conditions and unexpected stresses are not induced. Possible improvements on the data acquisition and analysis plan of the present research mostly lie in improving the reliability of the instrumentation used so that equipment

malfunctions do not hinder research progress as was experienced here; a few other variations could prove useful as well. These changes could be applied to studying the BHT-600-PM or any other thruster that a researcher wants to characterize in this manner.

One possible variation would be to determine a new method for measuring Hall Current that does not rely on the steady current assumption. This may be possible with altered analysis that eliminates this assumption or with new equipment that measures Hall Current without the need for collecting and converting magnetic field data. This would allow analysis of Hall Current during azimuthal variations, as in the spoke mode, which could significantly improve understanding of underlying mechanisms in this mode.

A few additional variations that may be useful regard the high-speed camera. An imaging sensor that has greater sensitivity has the potential to allow better observation of periods of low optical emission, such as between breaths in the discharge. Better resolution in these periods during spoke mode operation may reveal whether spoke structures propagate during these low emission times. While some higher frequency phenomena may exist and would benefit from a camera capable of a higher sample rate, the current features under study would not significantly benefit from this. Instead, a camera capable of recording more sequential frames would be more useful as it would provide larger sample sizes, allowing better frequency analysis and examination of features through longer thruster operation periods. Finally, an imaging solution with both high frequency sampling and good spectral resolution could allow distinction between emissions from excited neutrals, ion formation, and ion recombination.

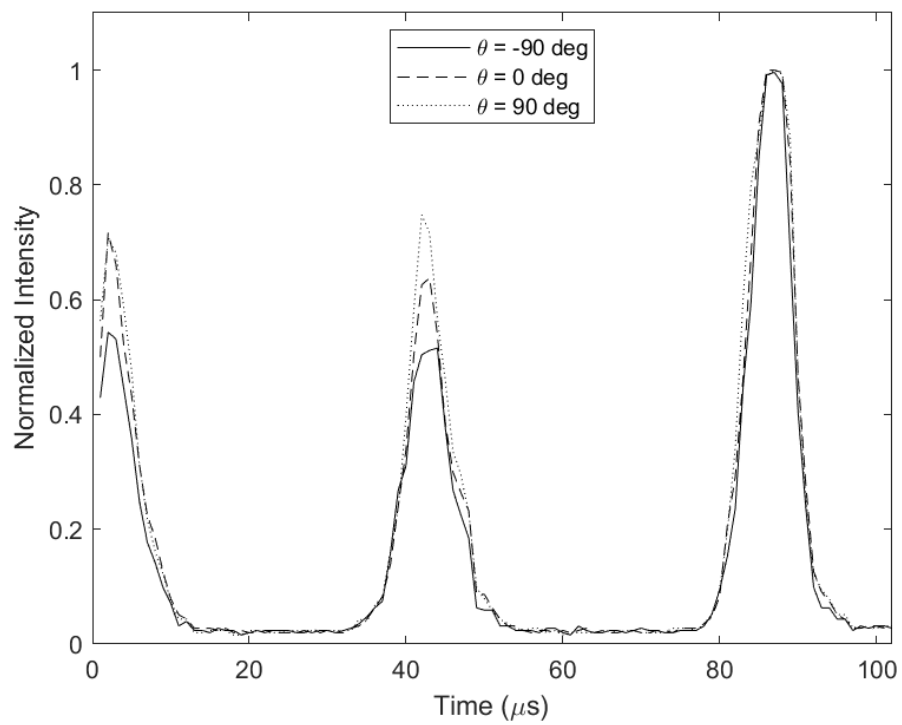# Appendix A. Unrolled Videos and Intensity Plots

Breathing Mode Test 1, $V_D = 75$ V, $I_D = 3.2$ A
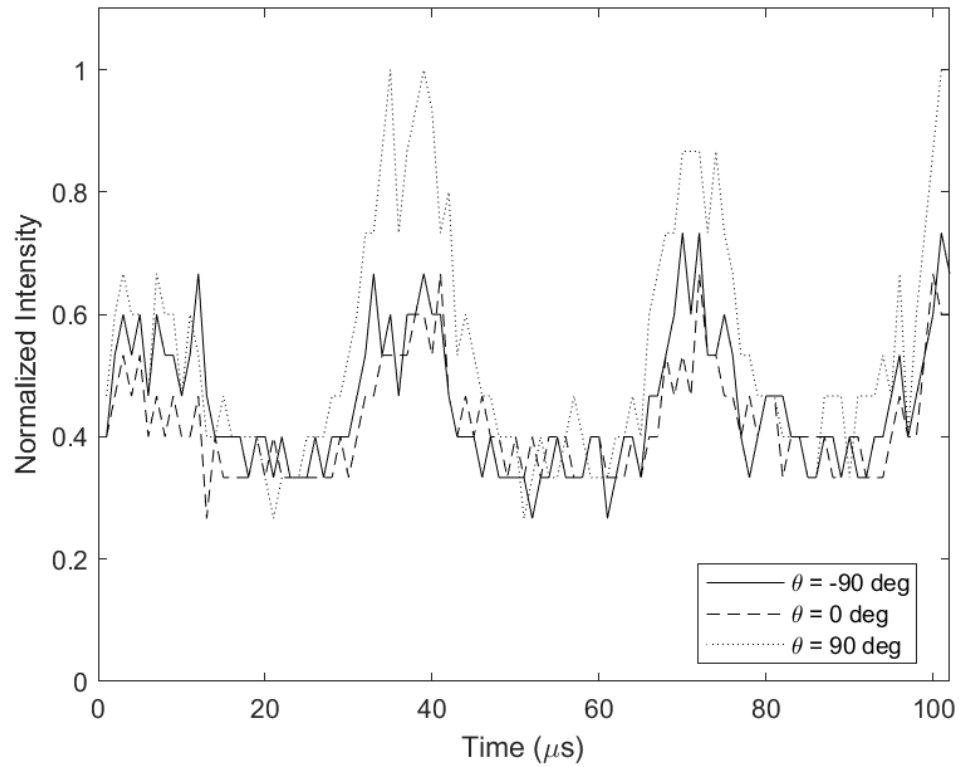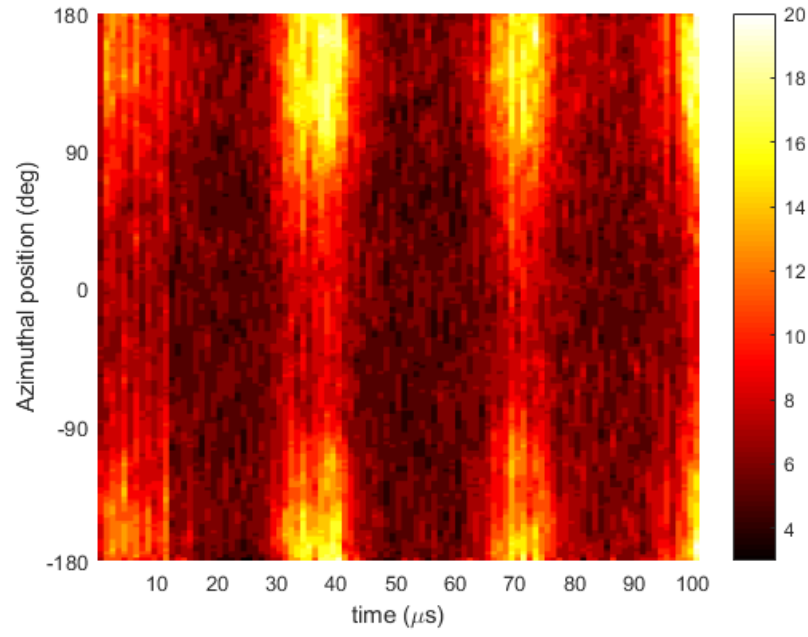
Breathing Mode Test 2, V_D = 75 V, I_D = 3.2 A
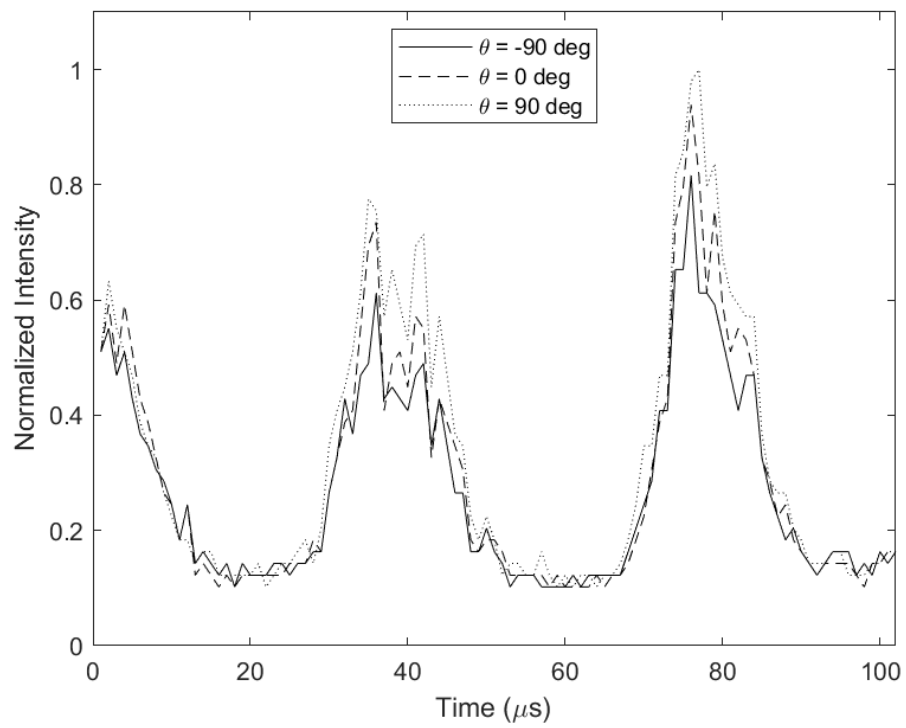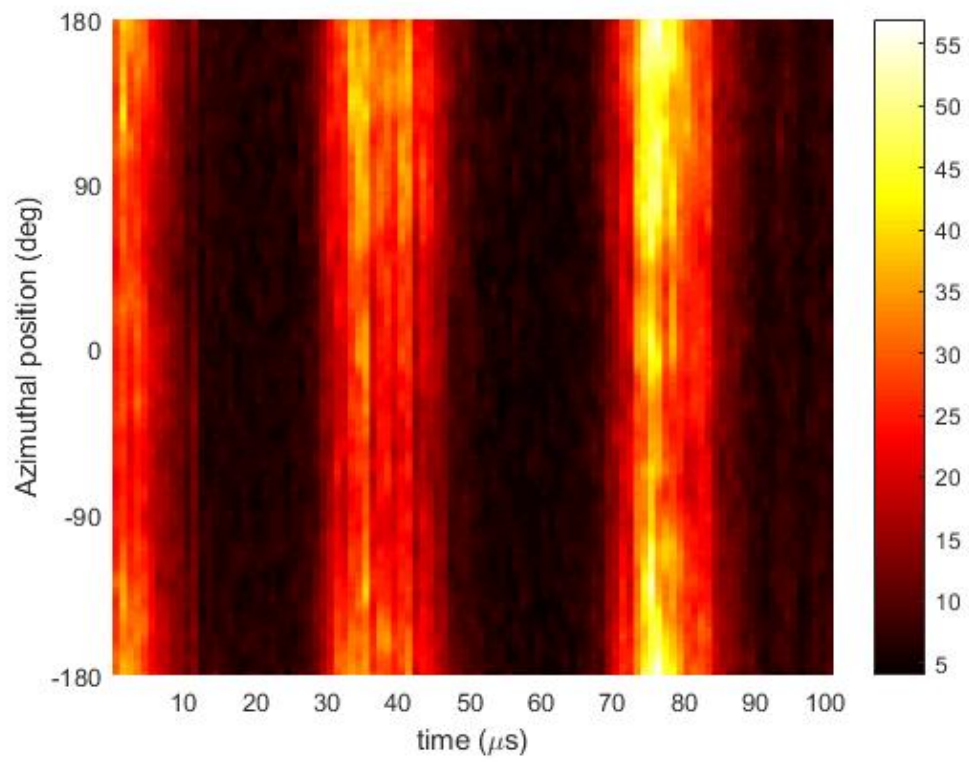
Breathing Mode Test 3, V_D = 75 V, I_D = 3.2 A
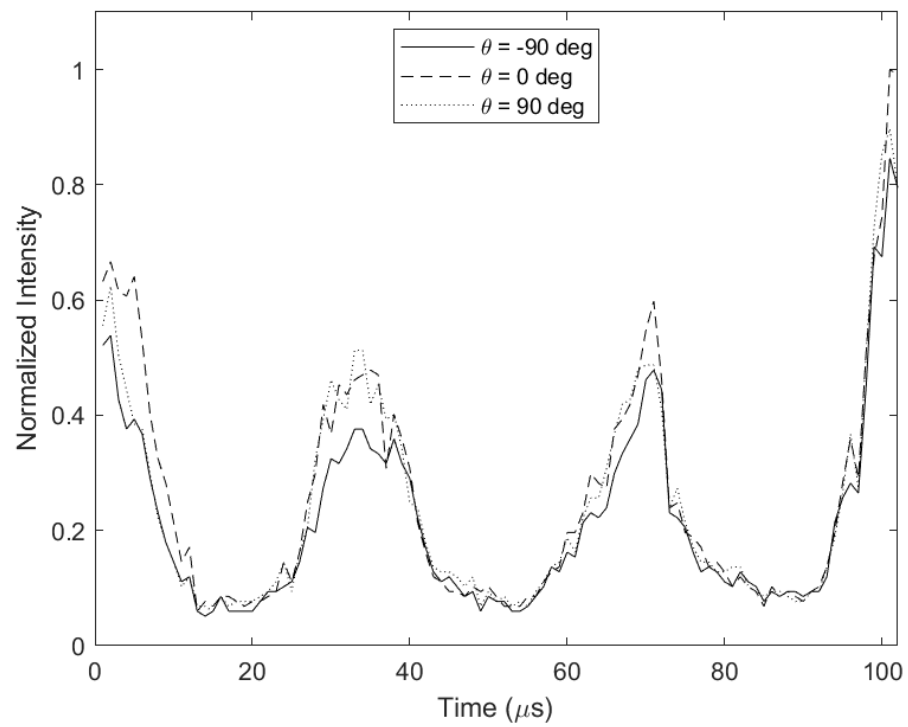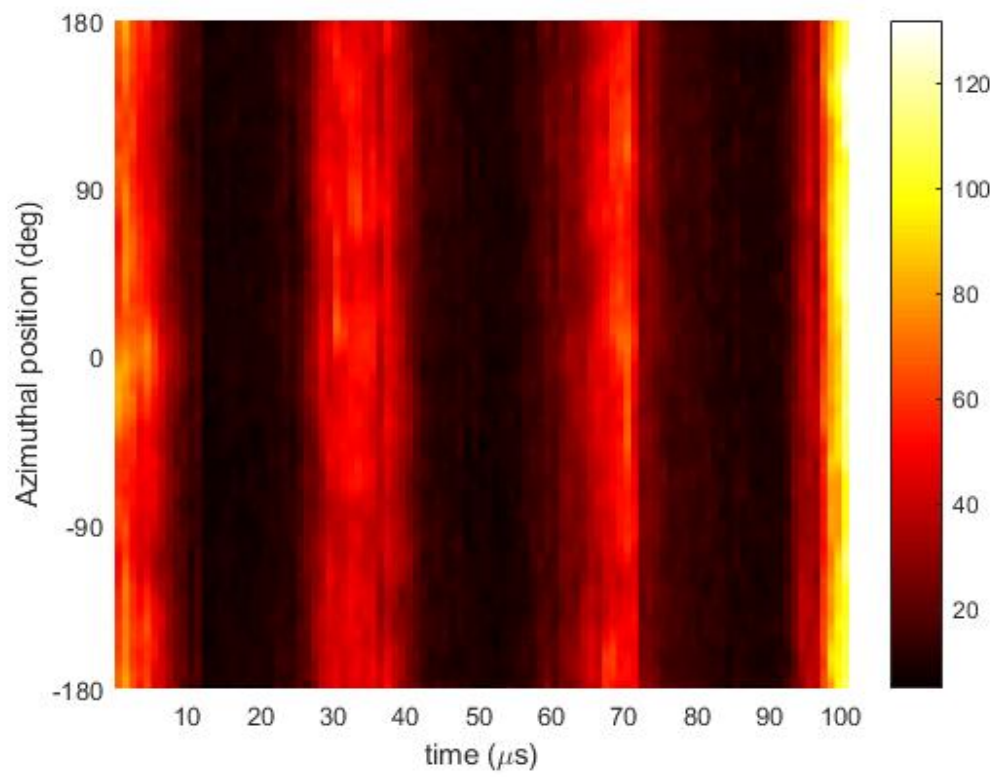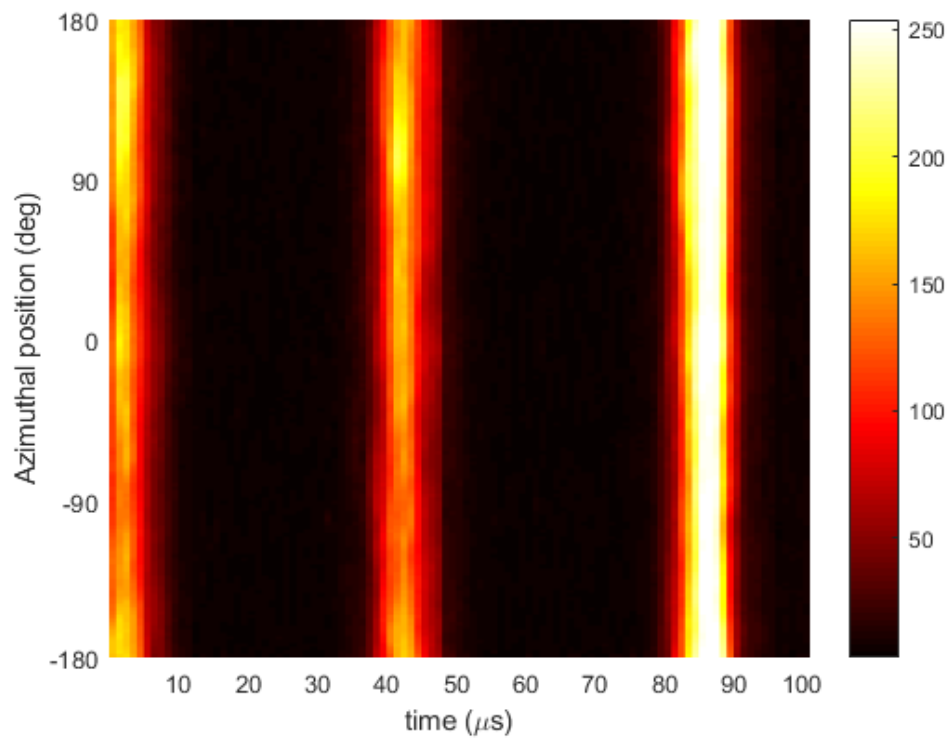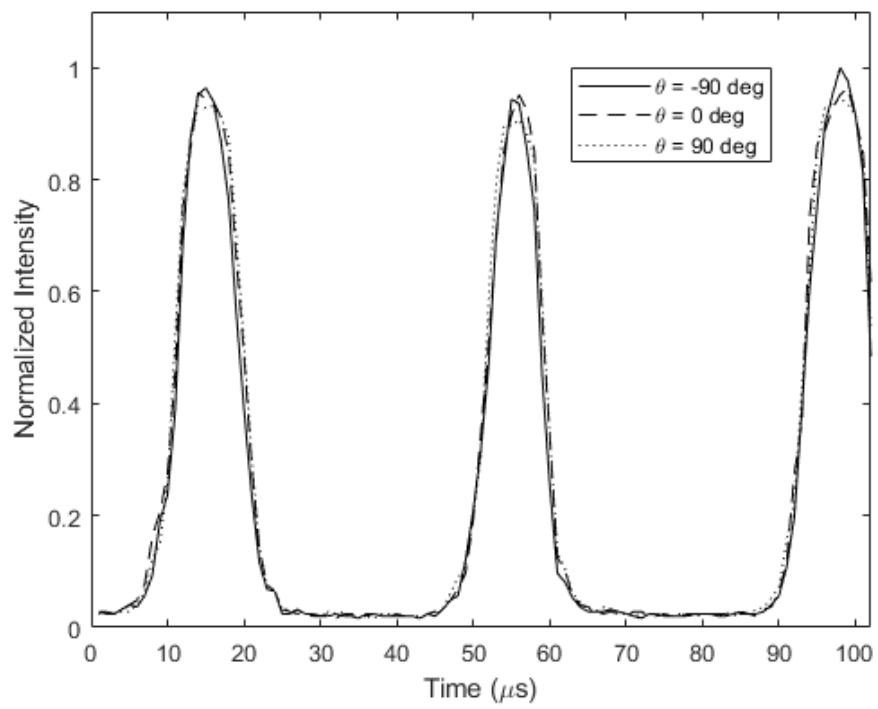
Breathing Mode Test 4, V_D = 73 V, I_D = 3.2 A
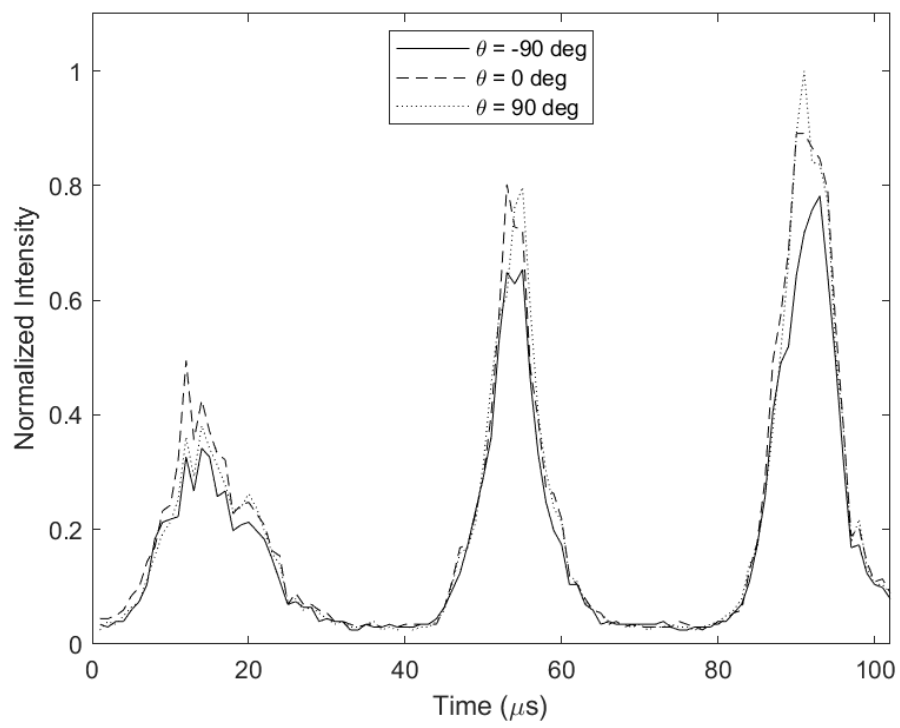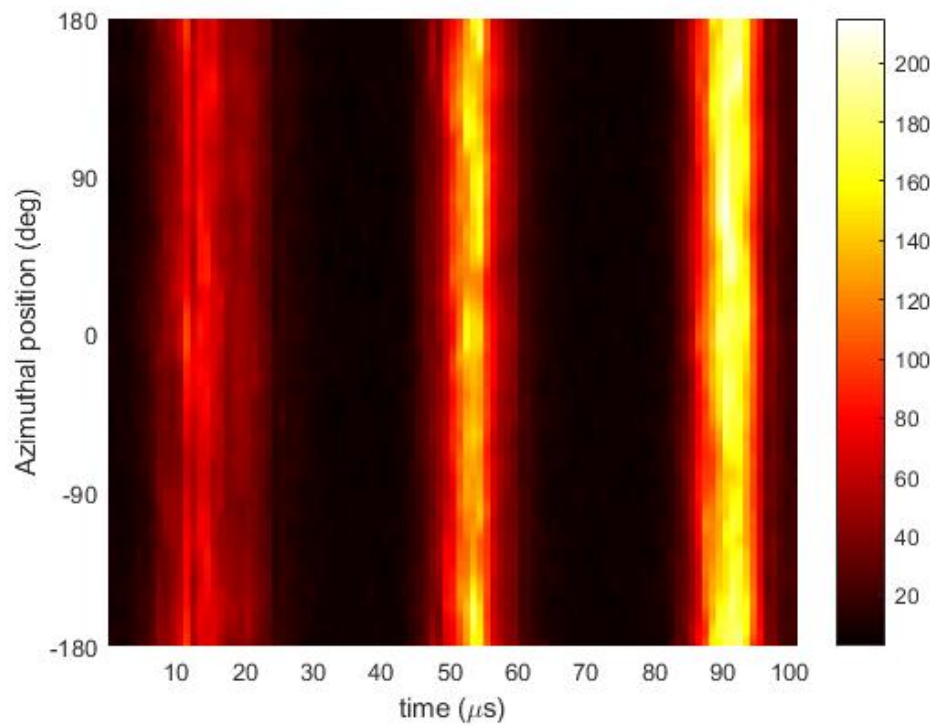
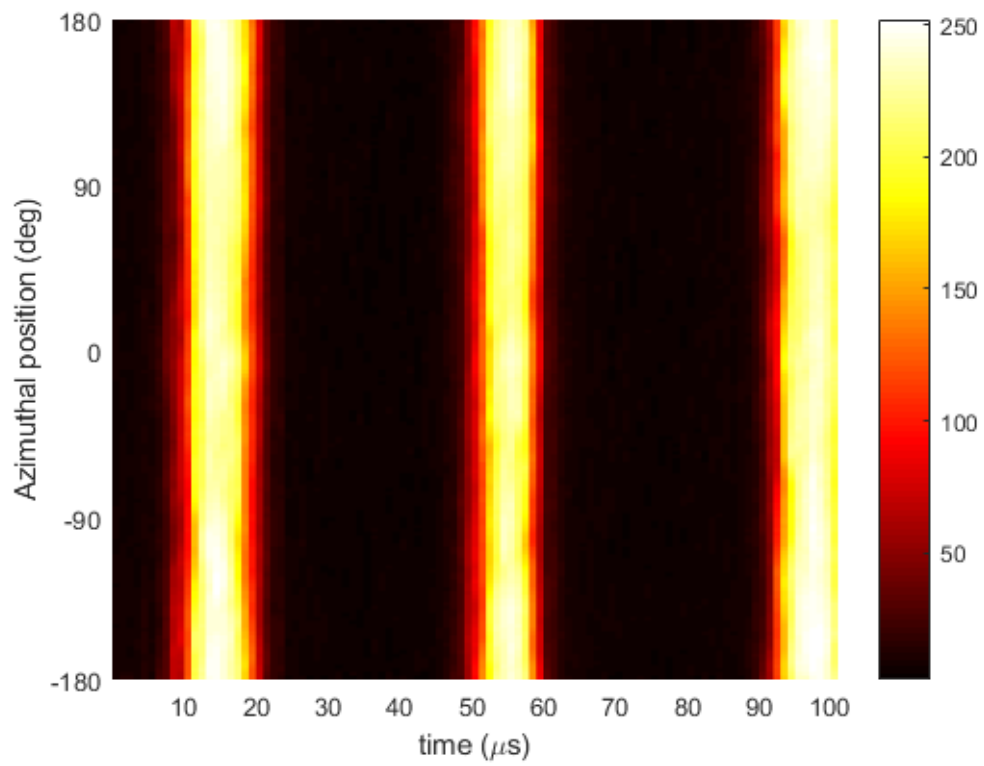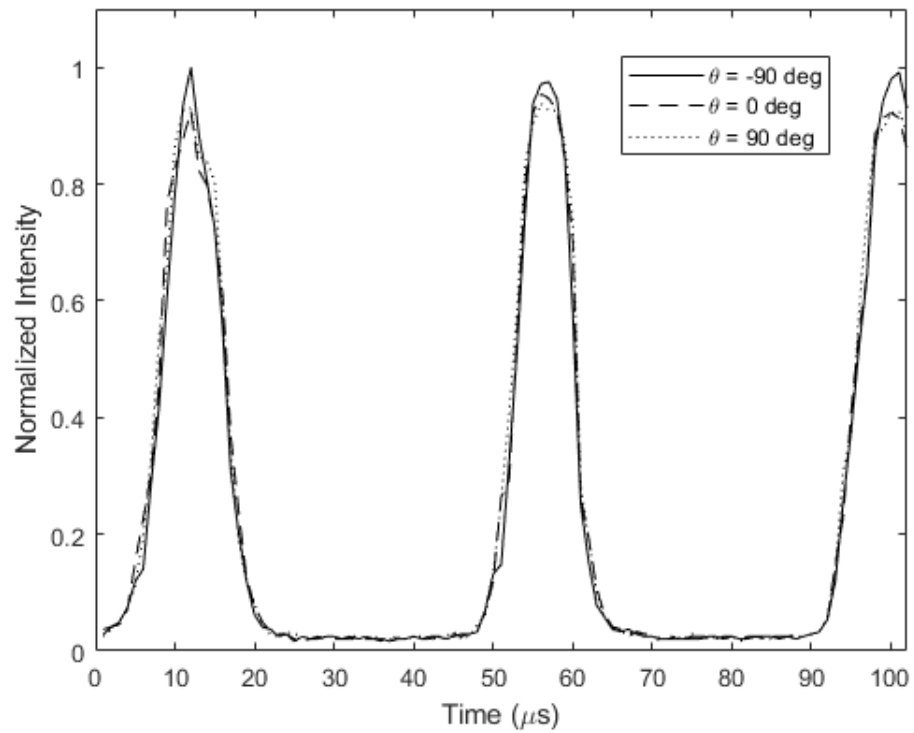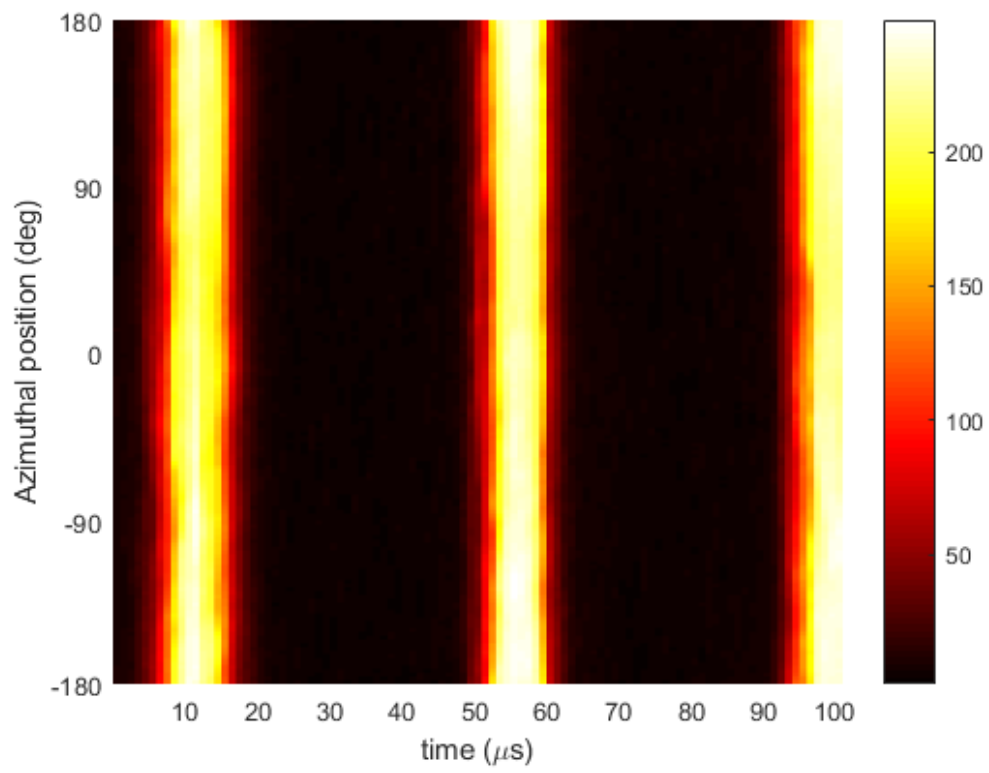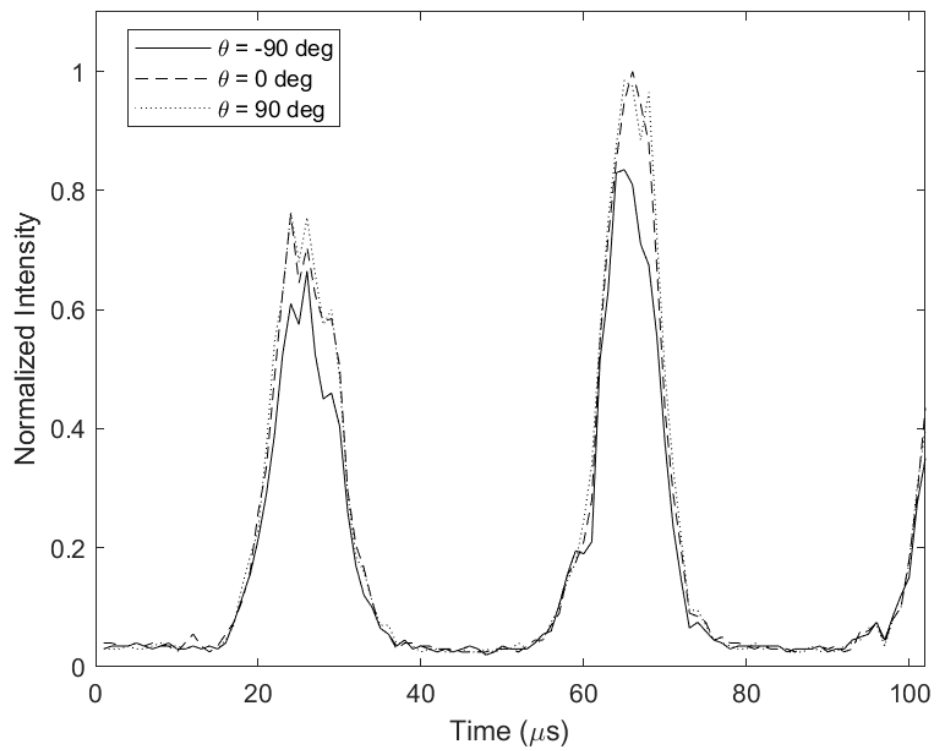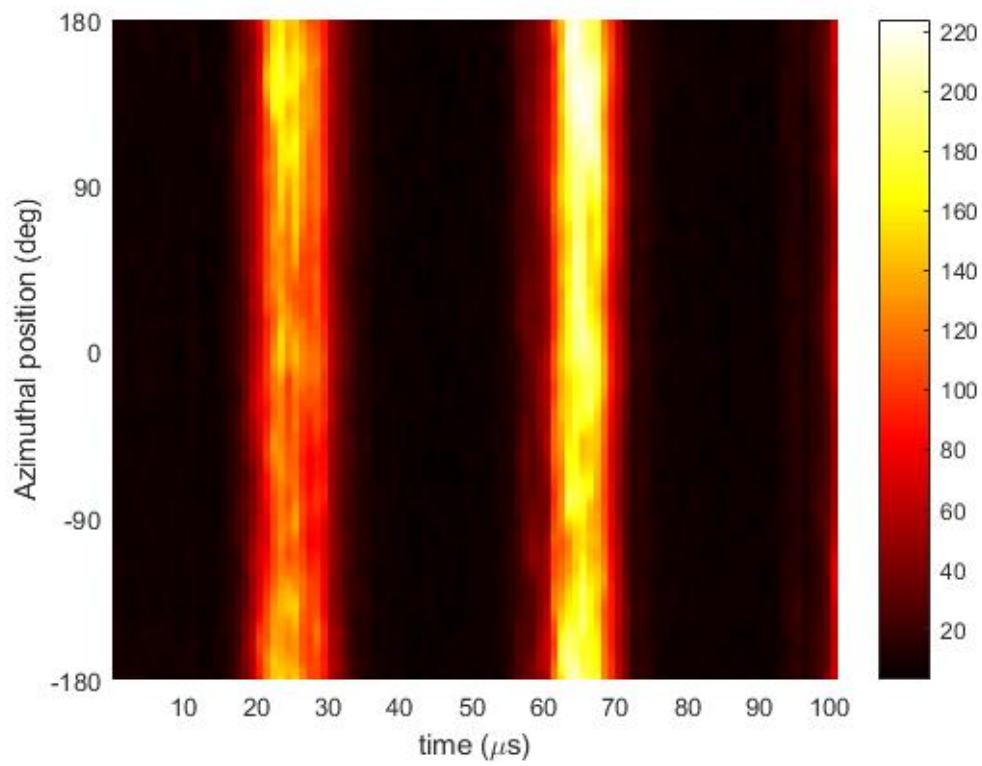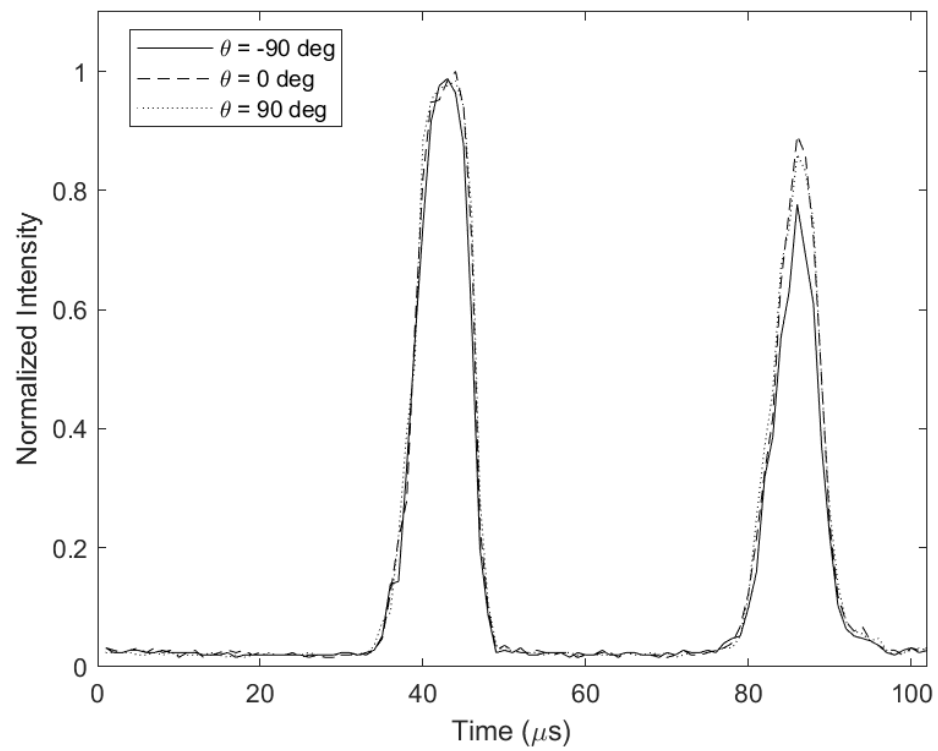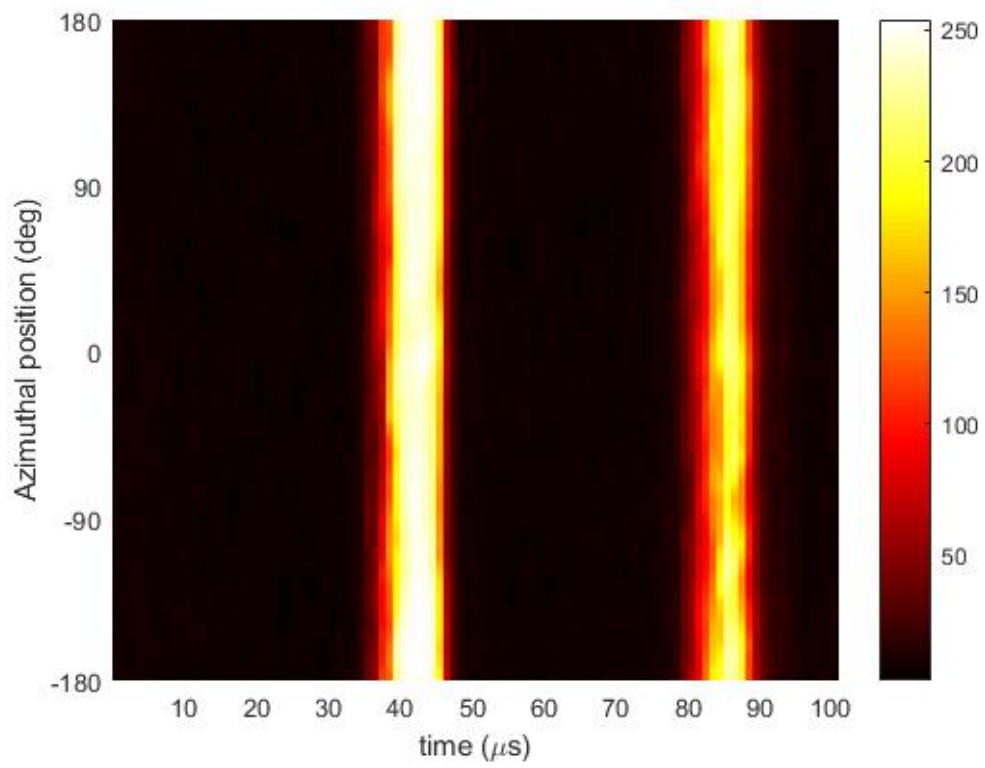Breathing Mode Test 5, V_D = 70 V, I_D = 3.2 A
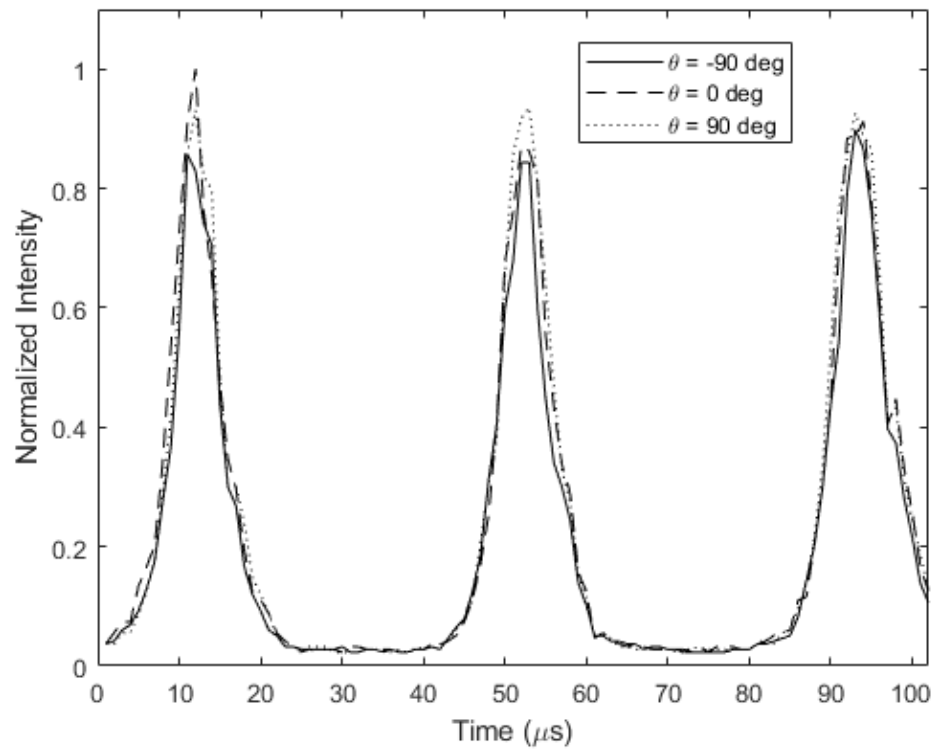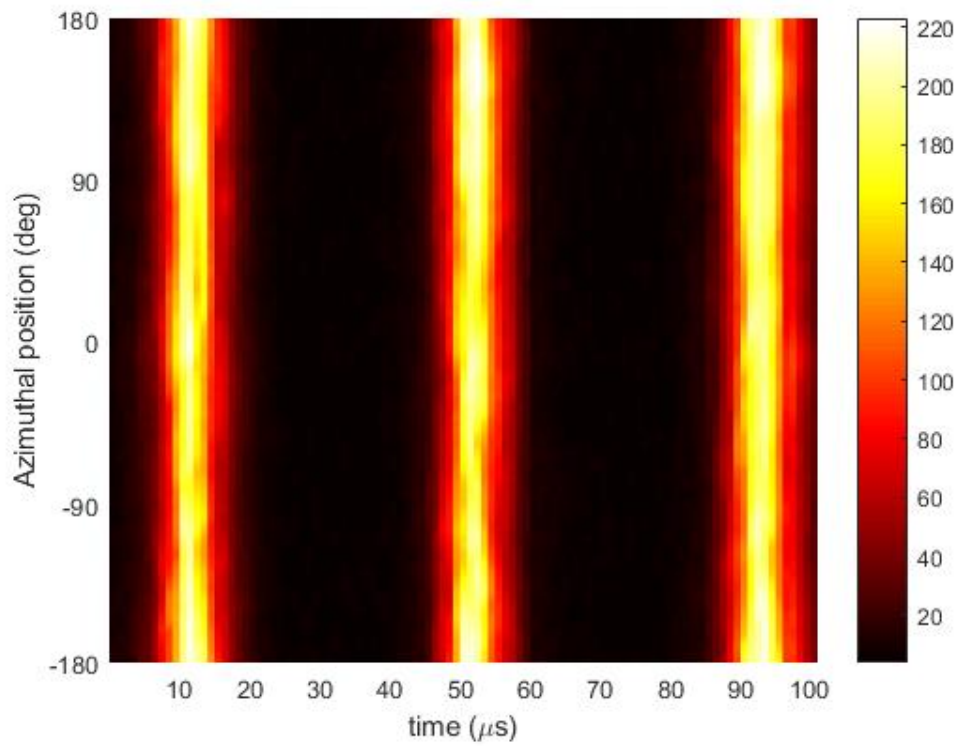
Breathing Mode Test 6, V_D = 70 V, I_D = 3.2 A
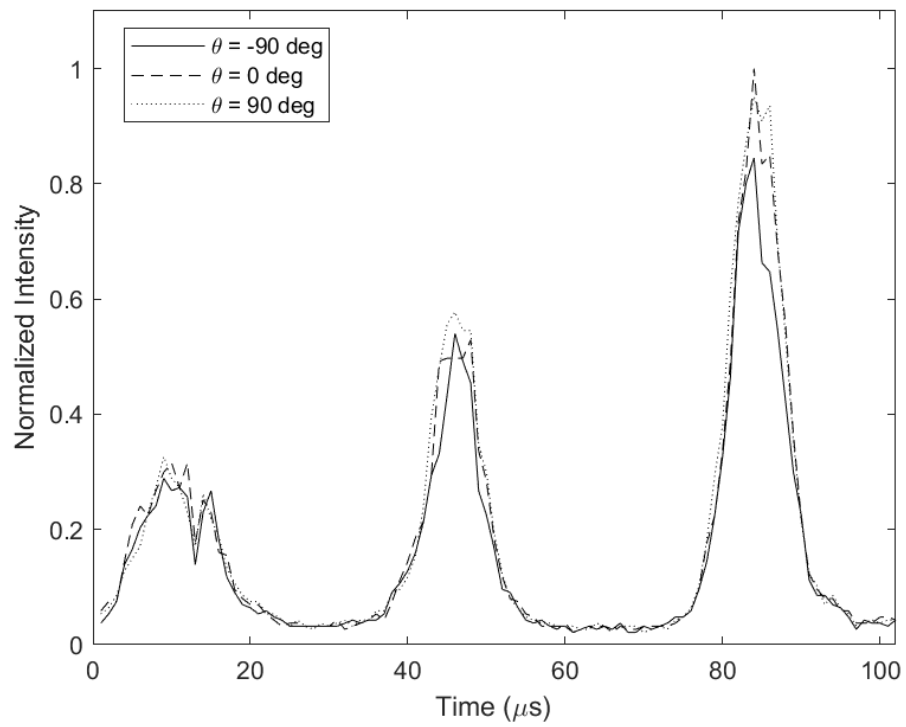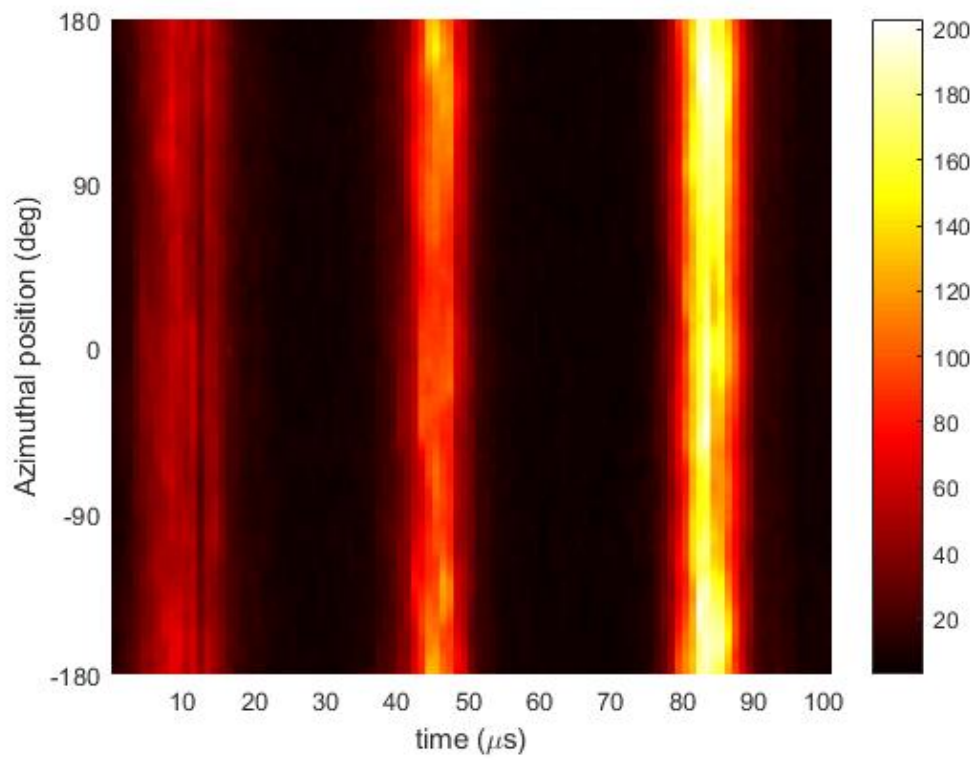
Breathing Mode Test 7, V_D = 70 V, I_D = 3.2 A

Breathing Mode Test 8, $V_D = 70$ V, $I_D = 3.2$ A
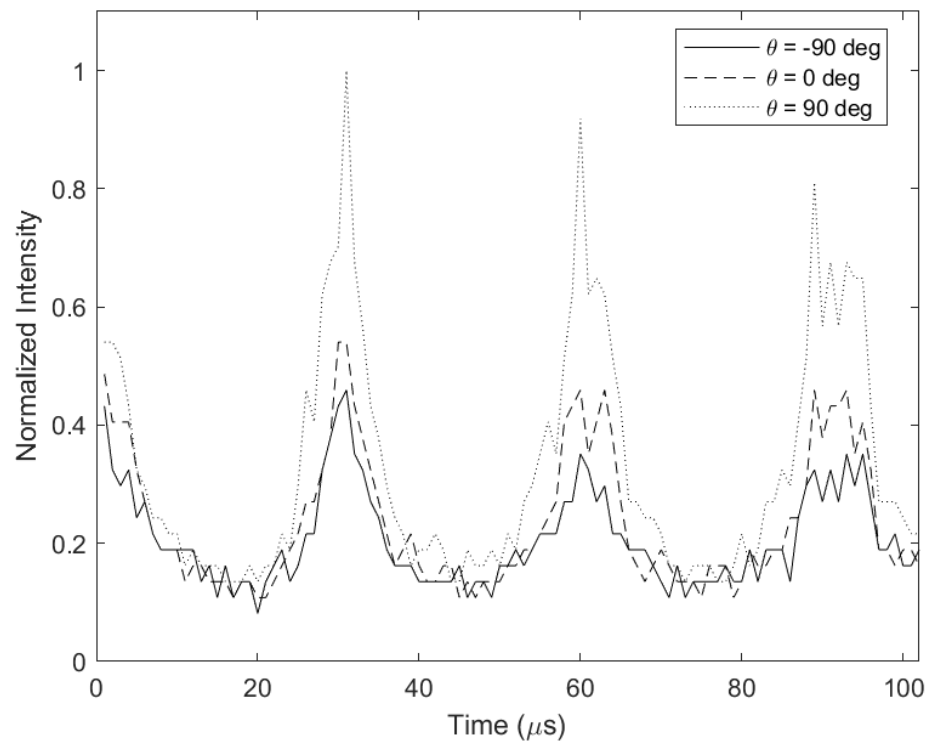
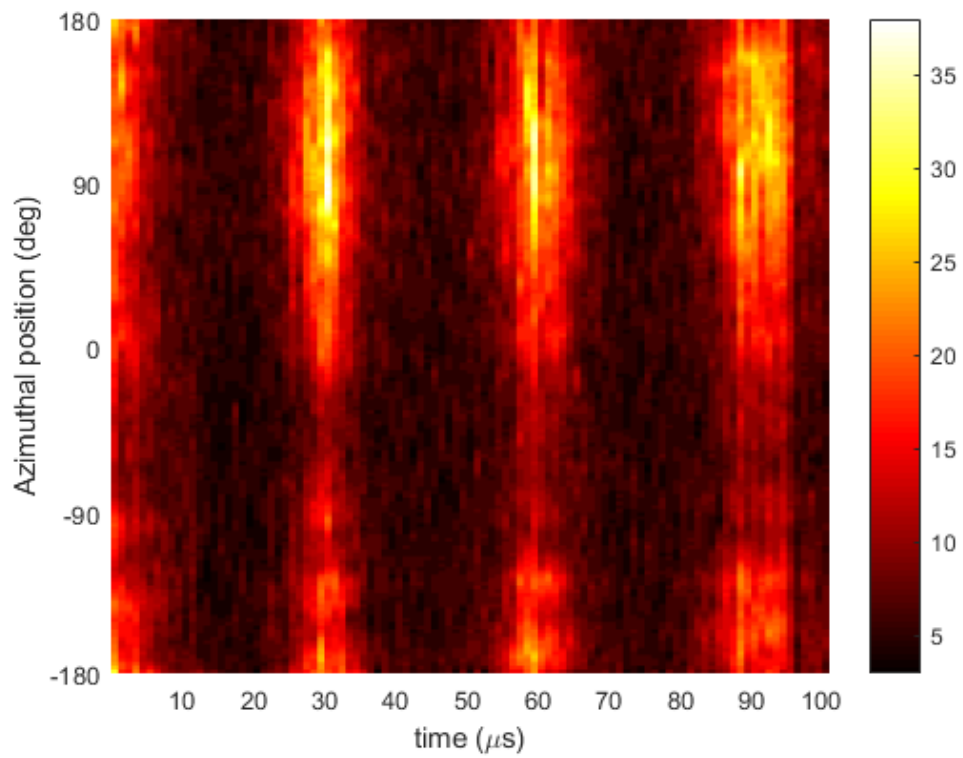Breathing Mode Test 9, $V_D = 70$ V, $I_D = 3.2$ A

95

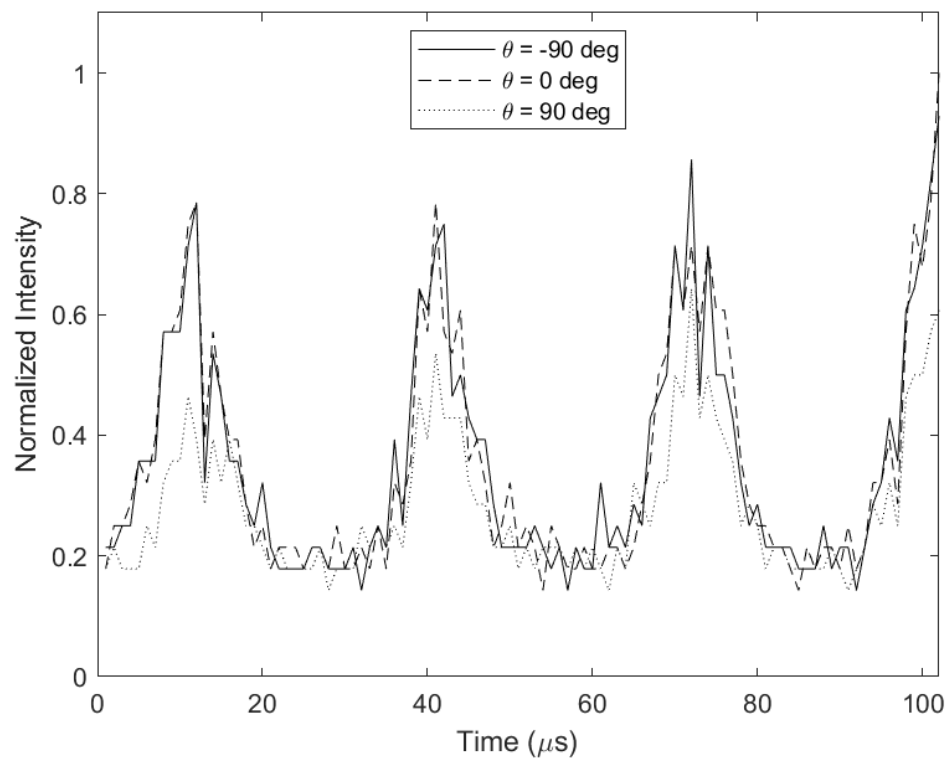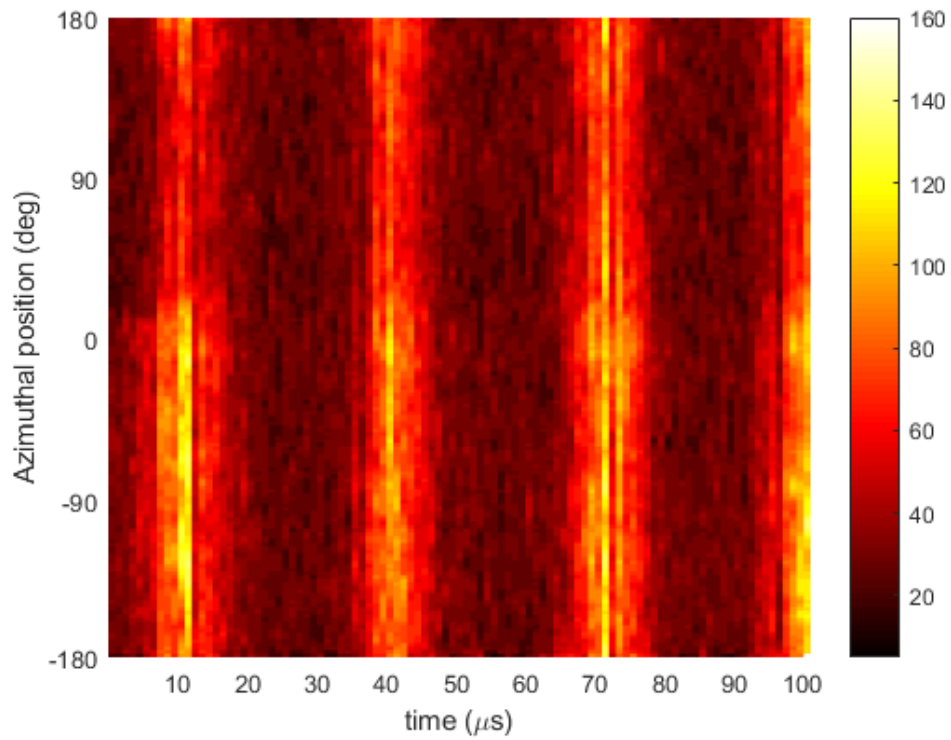Breathing Mode Test 10, $V_D = 70$ V, $I_D = 3.2$ A

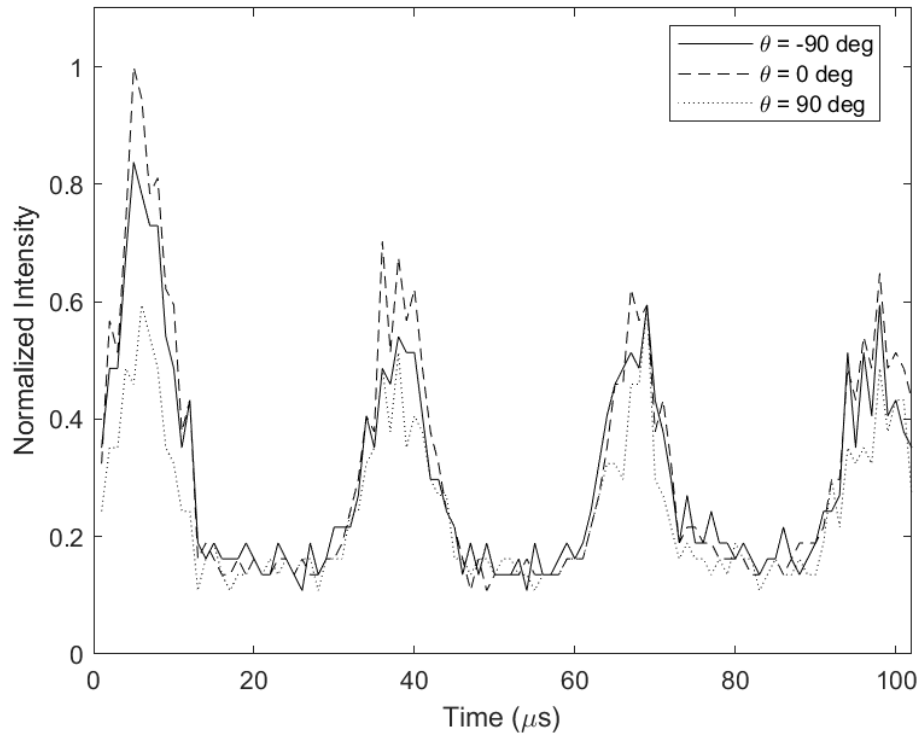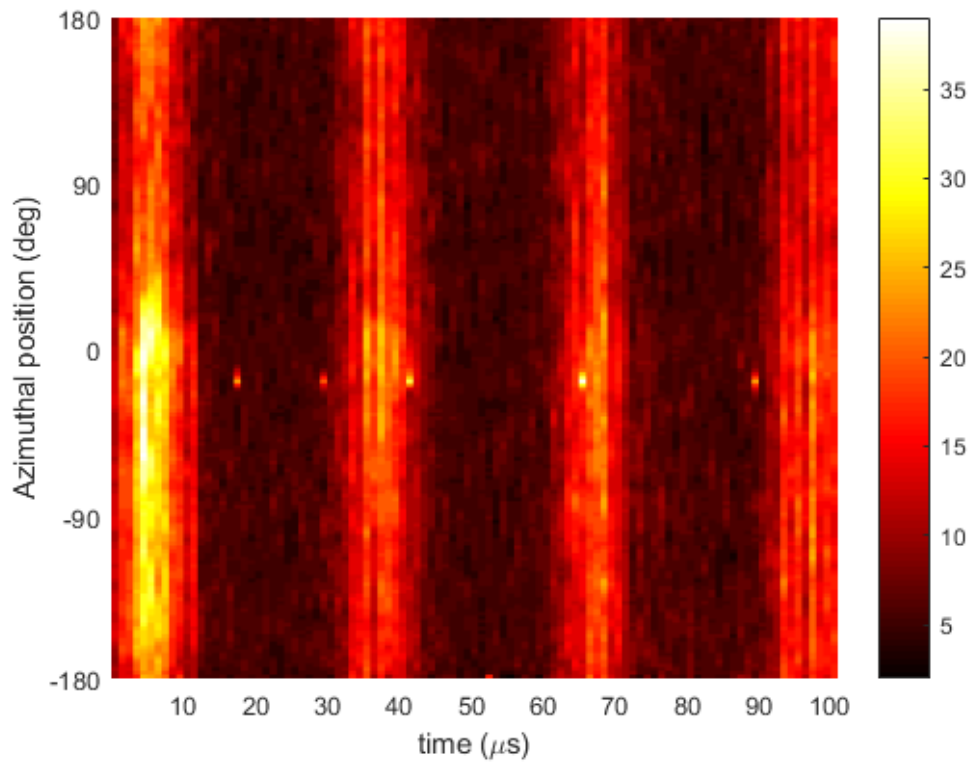Breathing Mode Test 11, $V_D = 70$ V, $I_D = 3.2$ A

Breathing Mode Test 12 (Beginning of Session 2), $V_D = 250$ V, $I_D = 2.4$ A

Breathing Mode Test 13, $V_D = 250$ V, $I_D = 2.4$ A

Breathing Mode Test 14, V_D = 250 V, I_D = 2.4 A

Breathing Mode Test 15, V_D = 250 V, I_D = 2.4 A
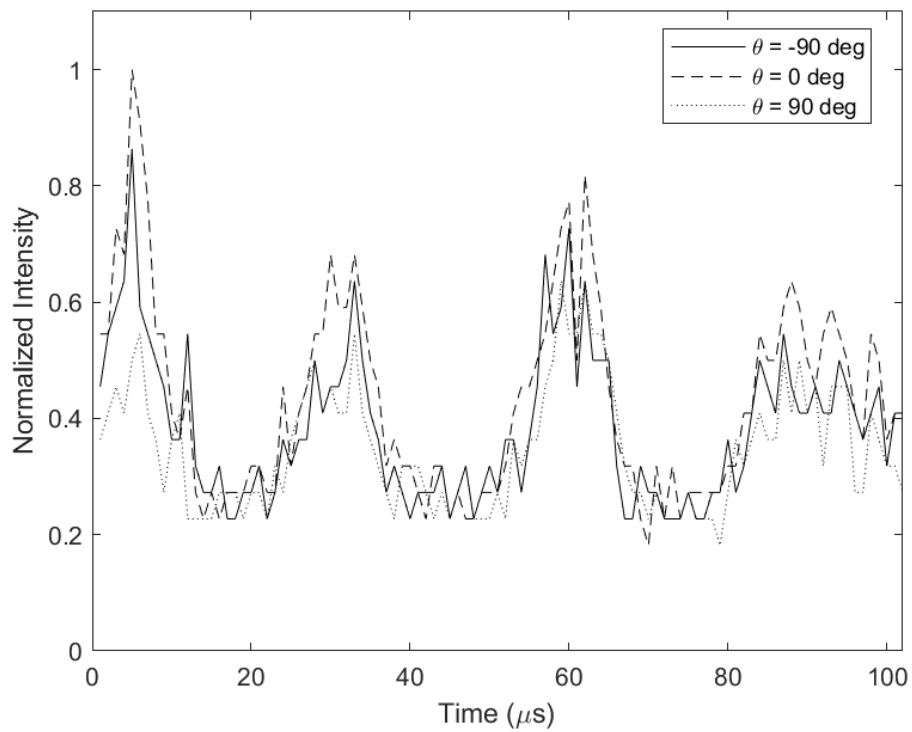
Breathing Mode Test 16, $V_D = 250$ V, $I_D = 2.4$ A
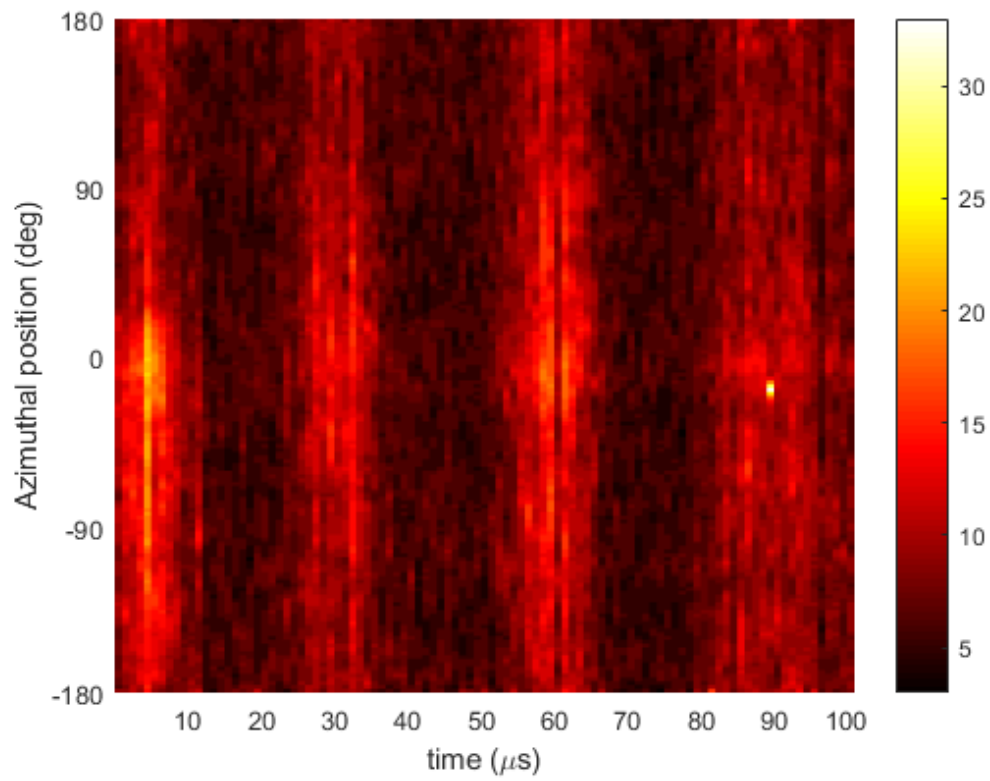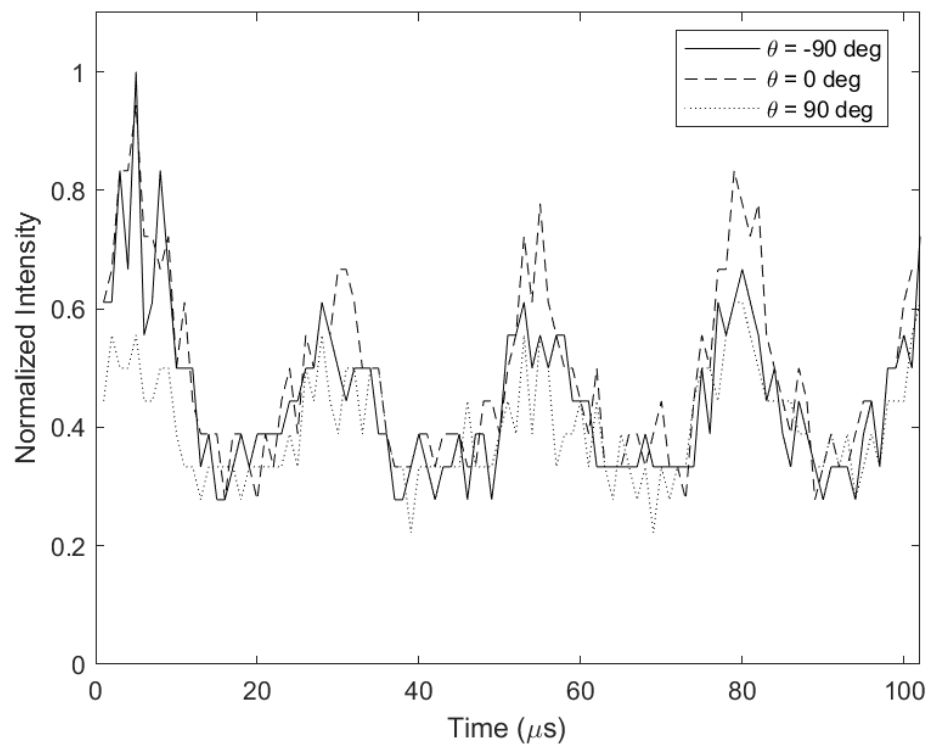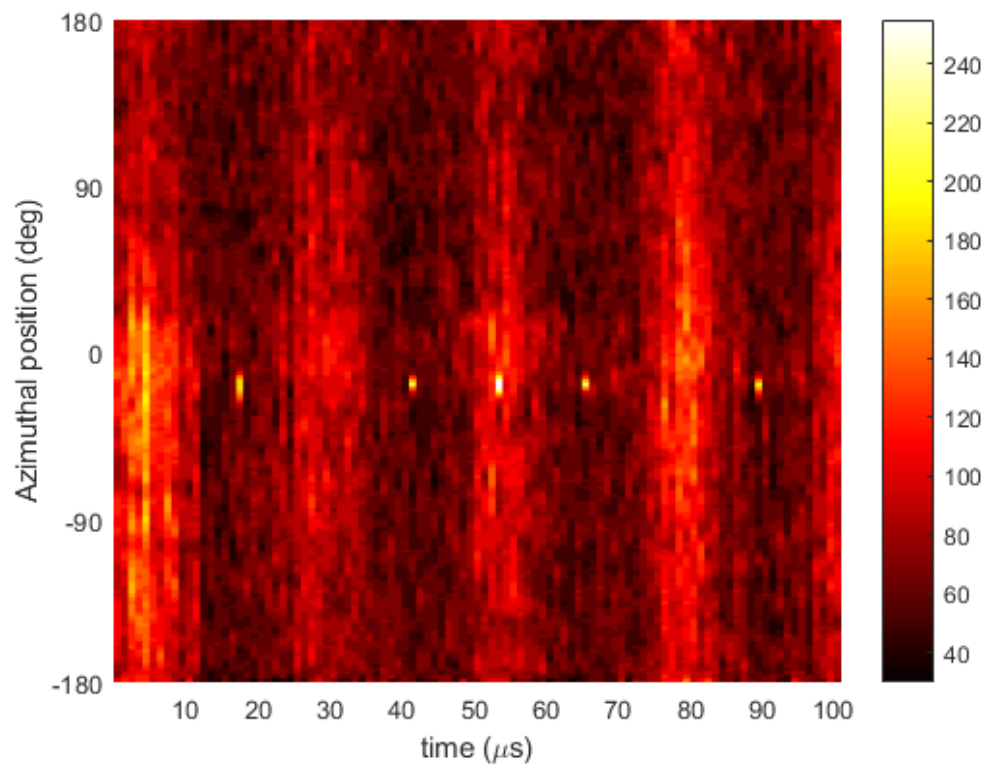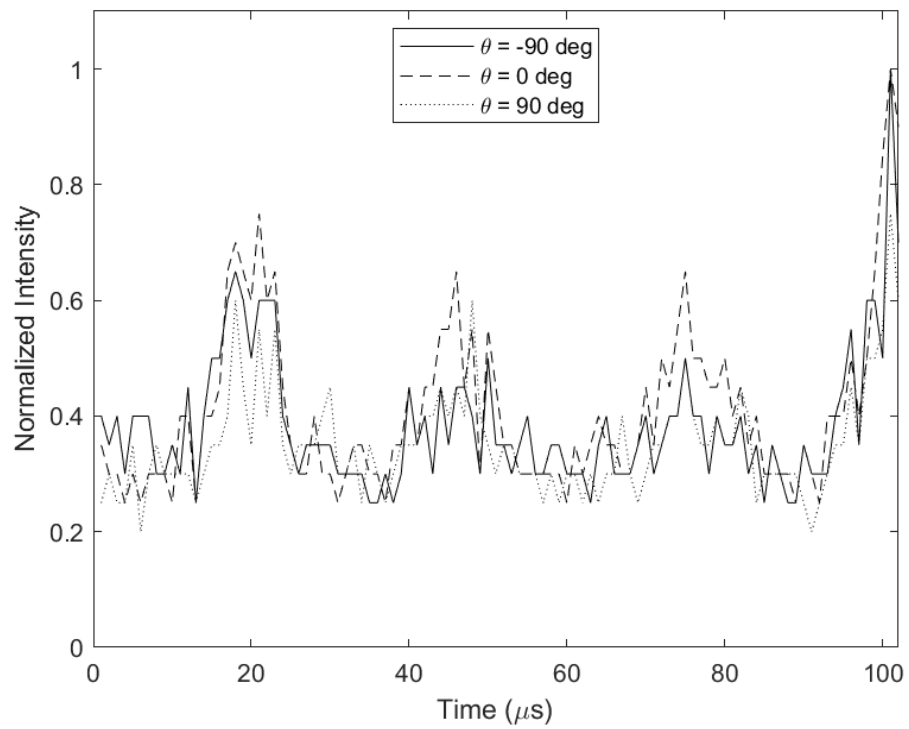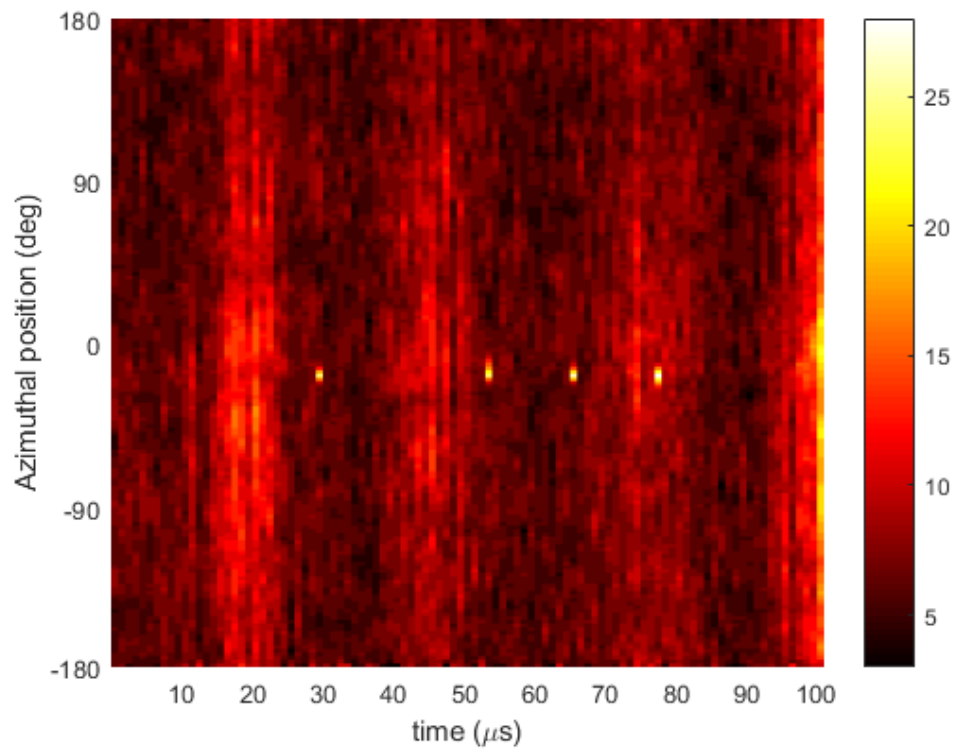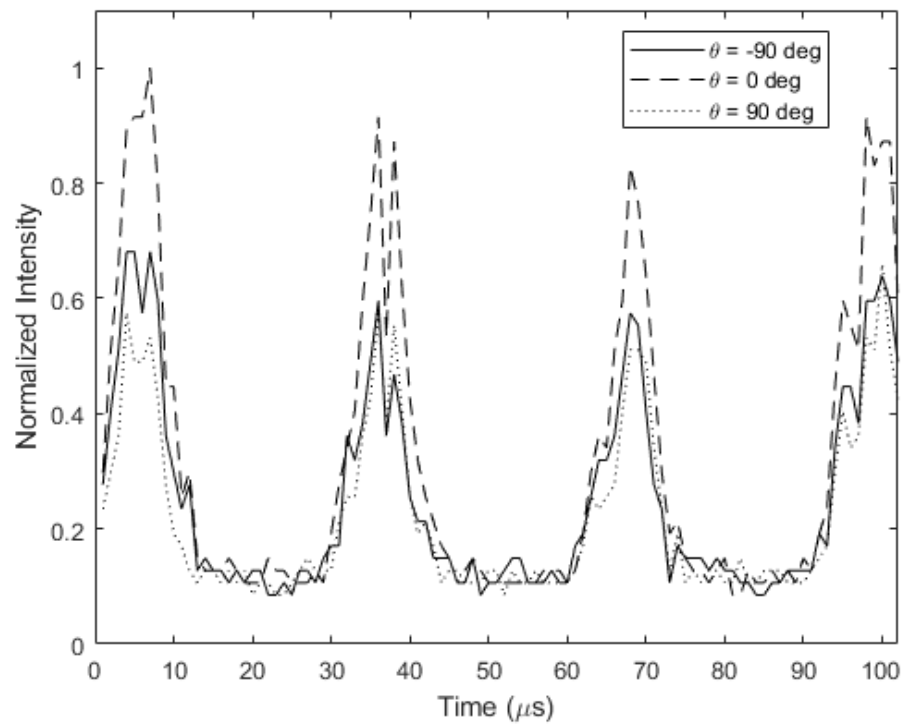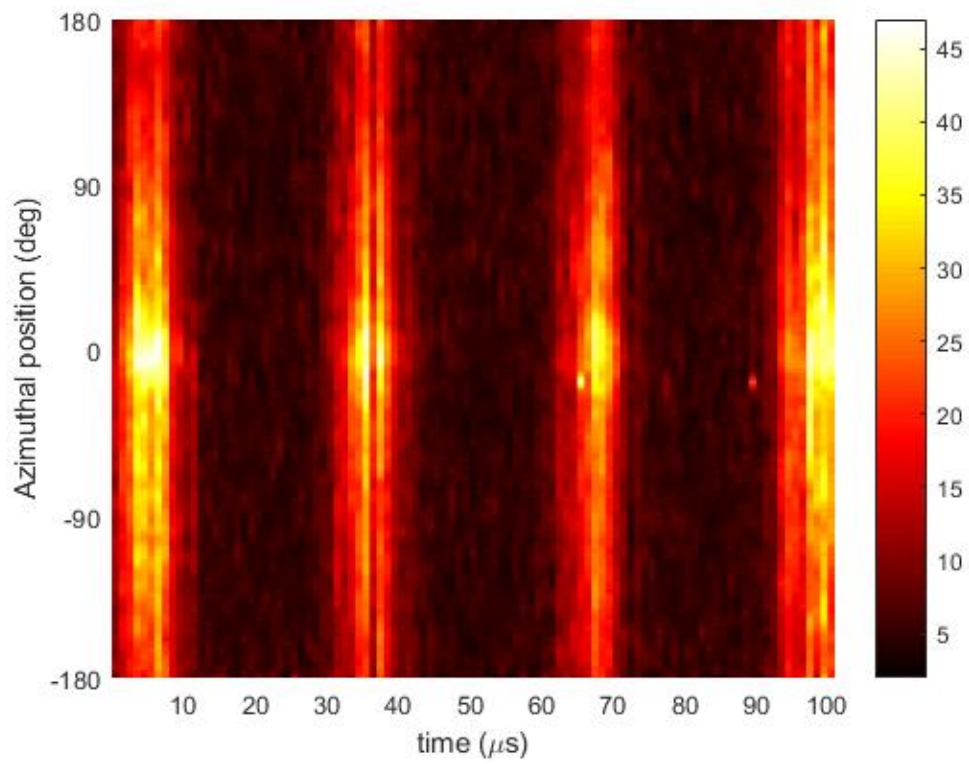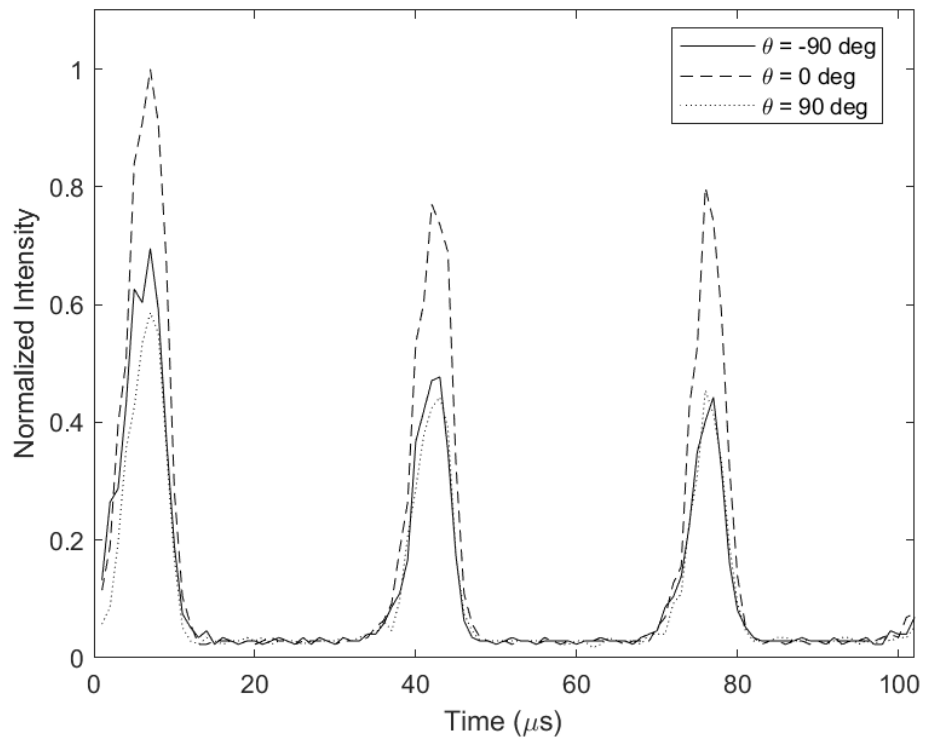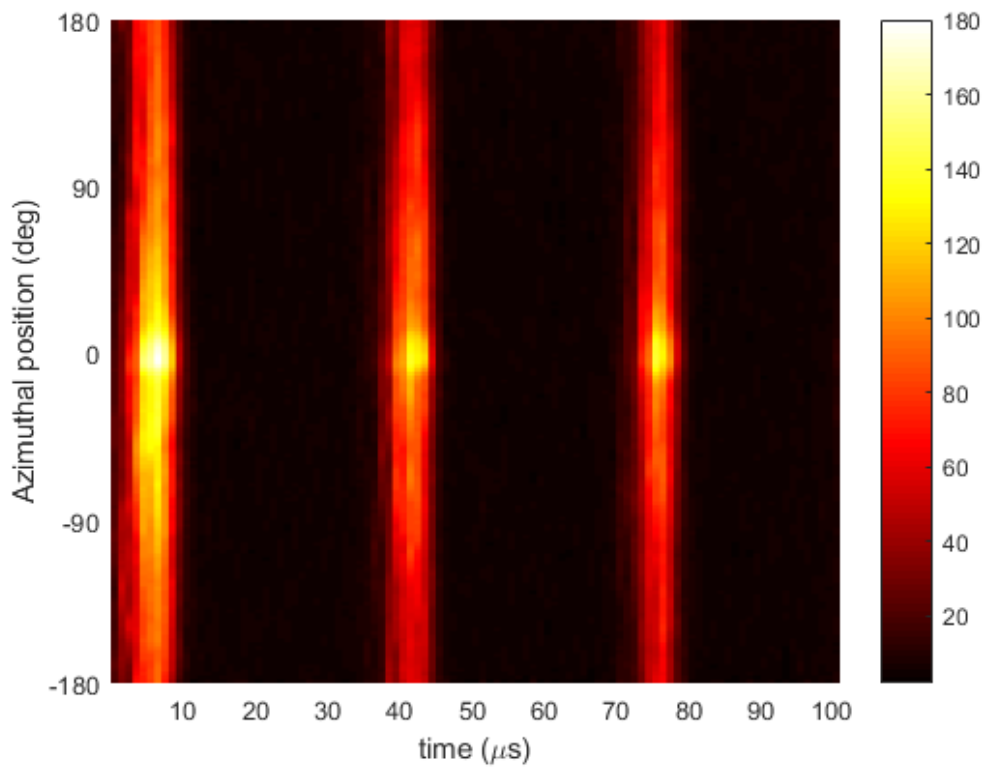
Breathing Mode Test 17, V_D = 250 V, I_D = 2.4 A

Breathing Mode Test 18, V_D = 250 V, I_D = 2.4 A

Breathing Mode Test 19, V_D = 250 V, I_D = 2.4 A

Appendix B. Computer Code

B.1 Matlab Video Unwrapping Code

B.1.1 Unwrapper.m

```matlab
% Projects an image of the channel of a Hall thruster onto several columns
% of pixels, interpolating the rows which are missing using natural nearest
% neighbor interpolation. Crops the output to only contain the channel.
% Written by: David Cunningham, modified by Samuel Wright
% INPUT VARIABLES:
%   Image: Image, designed to be a 2-D matrix of uint8 values (intensities)
%       Other formats may cause issues.
%   r_in: Int, The column index of the first column of pixels that will be in
%   the output image.
%   r_out: Int, The column index of the last column of pixels that will be in
%   the output image.
%   center: [row col] Int, pixel coordinates of thruster center
%   Imsize: [row col] Int, size of image in pixels
% OUTPUT VARIABLES:
%   I: Image with dimension tres x (r_out-r_in), designed to be a 2-D
%   matrix of uint8 values.
% Meshgrid and interpolation code adapted from code found at
% URL: http://stackoverflow.com/a/12926591
% updated to work with newer MATLAB functions
%
% Use at own risk
% function I = Unwrapper(Image, r_in, r_out, center, emissive)

function I = Unwrapper(Image, r_in, r_out, center, Imsize, emissive)
%%%%%%%%%%%% set image size and values %%%%%%%%%%%%
% Image=imread(Image);

if emissive
    Image(184:196,151:162) = 1;
end




%%%% THIS SECTION ADAPTED FROM  URL: http://stackoverflow.com/a/12926591 and
is omitted to avoid licensing issues.

% Convert to integers
Unroll = uint8(Unroll);
% crop
Unroll = imcrop(Unroll,[r_in, 0, r_out-r_in, 240]);
I = Unroll;
imagesc(I);
end
```

B.1.2 Unwrap_Video.m

```matlab
% Converts a Hall thruster video into a .tiff image with each column of
% pixels representing a frame in time (if averaging is true) and each row
% of pixels representing a set azimuthal location on the thruster channel
% (how big a section depends on the setup of Unwrapper.m). Saves image to
% video directory.
% INPUT VARIABLES:
% WhichTest: STRING, designating which test in the series of tests to
% use. This is a variable due to the need to convert many tests at
% once (see Unwrap_All)
% date: STRING, format 'YYYY_MM_DD', date of testing to go with file
% folder structure convention.
% averaging: BOOLEAN, if true averages all radial locations to one pixel.
% If false, the output image is the entire channel projection from

% each frame stacked with the inner channel wall of a frame touching
% the outer wall of the previous frame.
% Written by: David Cunningham, modified by Samuel Wright
% Use at own risk
function Unwrap_Video(WhichTest,date,averaging,emissive)
%%%%%%%%%%%%%%%%%% Video Parameters %%%%%%%%%%%%%%%%%%
% To be set for each day of testing, or each time the camera is moved.
% It is recommended to fine tune these parameters with direct calls to
% Unwrapper.m using a test frame. Once the thruster channel appears as a
% straight line, input those values below.
% chanIn = 45; % first row of projected image to be cropped (inner channel
radius)
% chanOut = 65; % last row of projected image to be cropped (outer channel
radius)
% Xcenter = 163; % pixel coordinate of thruster center (column)
% Ycenter = 125; % pixel coordinate of thruster center (row)

chanIn = 41; % first row of projected image to be cropped (inner channel
radius)
chanOut = 50; % last row of projected image to be cropped (outer channel
radius)
Xcenter = 163; % pixel coordinate of thruster center (column)
Ycenter = 126; % pixel coordinate of thruster center (row)
%%%%%%%%%%%%%%%%%% Initialize Variables %%%%%%%%%%%%%%%%
% oldDir = cd(strcat('INSERT FOLDER
PATH',date,'\TIFF\Test_',WhichTest,'_Video'));
breathing'));
% testsize = Unwrapper(imread(strcat('Test_',WhichTest,'_Video_',...
%     num2str(1,'%03i'),'.tiff')), chanIn,chanOut,[Ycenter,Xcenter],...
%     [260,312],emissive);
testsize=Unwrapper(imread(strcat(WhichTest,'_',num2str(1,'%03i'),'.tiff')),ch
anIn,chanOut,[Ycenter,Xcenter],[260,312],0);
Images = uint8(zeros(size(testsize,1),size(testsize,2),102));
if averaging
    BigPicture = uint8(zeros(size(testsize,1),102));
    avgstring = 'Pixels_condensed';
else
    avgstring = 'Full_Width';
end
%%%%%%%%%%%%%%%%% Read in each frame, unroll it, add it to output image %%%%
```

```matlab
for i = 1:102
    % note the image may have gain applied here.
    Images(:,:,i) =
Unwrapper(imread(strcat(WhichTest,'_',num2str(i,'%03i'),'.tiff')),chanIn,chan
Out,[Ycenter,Xcenter],[260,312],emissive);
    if ~averaging
        if i == 1
            for j = 1:size(Images,1)
                BigPicture(j,:,1) = uint8(Images(j,:,i));
            end
        else
            for j = 1:size(Images,1)
                holder(j,:) = uint8(Images(j,:,i));
            end
            BigPicture = [BigPicture holder];
        end
    elseif averaging
        for j = 1:size(Images(:,1,1))
            BigPicture(j,i) = uint8(mean2(Images(j,:,i)));
        end
    end
end
%%%%%%%%%%%%%%% Display and Save %%%%%%%%%%%%%%
imshow(BigPicture)
imwrite(BigPicture,
strcat('Test_',WhichTest,'_Unrolled_',avgstring,'.tiff'));
cd(oldDir);
```

B.1.3 Make_Surface_From_Unrolled.m

```matlab
% create surface plot from unrolled video, set up for 1Mfps, 2 deg/pixel
% INPUT VARIABLES:
% WhichTest: STRING, designating which test in the series of tests to
% use. This is a variable due to the need to convert many tests at
% once
% date: STRING, format 'YYYY_MM_DD', date of testing to go with file
% folder structure convention.
% save: BOOLEAN, if true saves output image to .fig file
% color: BOOLEAN, if true uses Matlab hot colormap on surface
% gain: Int, gain multiple to apply to output
% Written by: David Cunningham, modified by Samuel Wright
% Use at own risk
function Make_Surface_From_Unrolled(WhichTest,date,save,color, gain)
% WhichTest = '10';
% oldDir = cd(strcat('INSERT FOLDER PATH',WhichTest,'_Video'));
I = gain*imread(strcat('Test_',WhichTest,'_Unrolled_Pixels_condensed.tiff'));
% I=gain*imread(strcat('faster breathing_
surf(I,'EdgeColor','none');
view(2);
array = 0:0.01:1;
map = [array;array;array];
colormap(map')
xlim([1,102]);
ylim([1,180]);
ax = gca;
ax.XTick = 11:10:101;
ax.XTickLabel = {'10','20','30','40','50','60','70','80','90','100'};
ax.YTick = [1,45,90,135,180];

ax.YTickLabel = {'-180','-90','0','90','180'};
xlabel('time (\mus)');
ylabel('Azimuthal position (deg)');
if color
    colormap hot
end
% title(strcat('Test ',WhichTest,' \Theta vs. t Plot'));
if save
    cd(strcat('E:\Research Data\Analyzed Data\',date,'\PC Plots'));
    savefig(strcat('Unrolled_Plot_',WhichTest));
    print(strcat('Unrolled_Plot_',WhichTest),'-dtiff');
end
cd(oldDir)
```

B.1.4 individual_azimuths.m

```matlab
% This script reads in a series of unwrapped plots and pulls azimuths of
% interest, plotting intensity over time for each.
% Written by: Samuel Wright

clearvars; close all; clc

cd(Insert Path Here)
for i=1:19
    I=imread(strcat('Test',num2str(i),'.tiff'));
    Id=double(I);
    figure
    maxes=[max(Id(180/4,:)),max(Id(180/2,:)),max(Id(3*180/4,:))];
    maxI=max(maxes);
    plot(Id(180/4,:)/maxI,'k')
    hold on
    plot(Id(180/2,:)/maxI,'k--')
    plot(Id(3*180/4,:)/maxI,'k:')
    axis([0,102,0,1.1])
    xlabel('Time (\mus)')
    ylabel('Normalized Intensity')
    legend('\theta = -90 deg','\theta = 0 deg','\theta = 90
deg','Location','Best')

    clear I Id
    saveas(i,strcat('Test',num2str(i),'az.tiff'))
end
```

Bibliography

[1] D. M. Goebel and I. Katz, Fundamentals of Electric Propulsion: Ion and Hall Thrusters, Hoboken, New Jersey: JPL Space Science and Technology Series, Wiley, 2008.

[2] A. E. Gonzales, M. K. Scharfe, J. W. Koo and W. A. Hargus, "Comparison of Numerical and Experimental Time-Resolved Near-Field Hall Thruster Plasma Properties," in AIAA Joint Propulsion Conference, Atlanta,Georgia, July- Aug 2012.

[3] David A. Cunningham. Localized Plasma Measurement During Instability Modes In a Hall Thruster. Master's thesis, Air Force Institute of Technology, March 2016.

[4] G. P. Sutton and O. Biblarz, Rocket Propulsion Elements Eighth Edition, Hoboken, New Jersey : John Wiley & Sons, Inc. , 2010.

[5] Chen, F. F., Introduction to Plasma Physics, Plenum, New York, New York, 1974.

[6] Jahn, Robert G., Physics of Electric Propulsion, Dover Publications, Mineola, New York, 2006.

[7] H. Evans, J. Lange and J. Schmitz , The phenomenology of Intelligence-focused Remote Sensing, New York, NY: Riverside Research , 2014.

[8] Sekerak, M. J., Plasma Oscillations and Operational Modes in Hall Effect Thrusters, Ph.D. thesis, University of Michigan, Ann Arbor, Michigan, 2014.

[9] Janes, G. S. and Lowder, R. S., "Anomalous Electron Diffusion and Ion Acceleration in a Low-Density Plasma," Physics of Fluids, Vol. 9, No. 6, June 1966, pp. 1115-1123.

[10] Morozov, A. I., "Wall Conduction in a Highly Magnetized Plasma," Journal of Applied Mechanical and Technical Physics, Vol. 9, No. 3, 1968, pp. 19 - 22.

[11] Gascon, N., Dudeck, M., and Barral, S., "Wall Material Effects in Stationary Plasma Thrusters," Physics of Plasmas, Vol. 10, No. 10, 2003, pp. 4123 - 4136.

[12] Boniface, C., Garrigues, L., Hagellar, G. J. M., Boeuf, J. P., Gawron, D., and Mazouffre, S., "Anomalous Cross Field Electron Transport in a Hall Effect Thruster," Applied Physics Letters, Vol. 89, 2006, pp. 161503-1 – 161503-3.

[13] Choueiri, E. Y., "Plasma oscillations in Hall thrusters," Physics of Plasmas, Vol. 8, No. 4, April 2001, pp. 1411-1426.

[14] Boeuf, J.-P. and Garrigues, L., "Low frequency oscillations in a stationary plasma thruster," Journal of Applied Physics, Vol. 84, 1998, pp. 3541.

[15] Liu, D., Huffman, R. E., Branam, R. D., and Hargus, W. A., "Ultrahigh Speed Images of Hall Thruster Azimuthal Instabilities," IEEE Transactions on Plasma Science, Vol. 42, No. 10, 2014, pp. 2656 - 2657.

[16] Escobar, D. and Ahedo, E., "Low frequency azimuthal stability of the ionization region of the Hall thruster discharge. I. Local analysis," Physics of Plasmas, Vol. 21, 2014.

[17] M. S. McDonald, A. D. Gallimore, B. A. St. Pierre and C. K. Bellant, , "Measurement of Cross-Field Electron Current in a Hall Thruster Due to Rotating Spoke Instabilities," in 47th AIAA/ASME/SAE/ASEE Joint Propulsion Conference & Exhibit, San Diego, California, 31 July - 03 August 2011.

[18] Smith, A. W. and Cappelli, M. A., "Time and space-correlated plasma potential measurements in the near field of a coaxial Hall plasma discharge," Physics of Plasmas, Vol. 16, 2009.

[19] Kemp, R. F. and Sellen, J. M. J., "Plasma Potential Measurements by Electron Emissive Probes," Review of Scientific Instruments, Vol. 100, 1966, pp. 455-461.

[20] Mazouffre, S., Pétin, A., Kudrna, P., and Tichý, M., "Development of a High-Frequency Emissive Probe System for Plasma Potential Measurements in a Hall Thruster," IEEE Transactions on Plasma Science, Vol. 43, 2015, pp. 29 - 34.

[21] D. J. Griffiths, Introduction to Electrodynamics 3rd edition, Upper Saddle River, New Jersey : Prentice Hall Inc , 1999.

[22] Rubin, B., Kapulkin, A., and Guelman, M., "Research on Optimization of On-board Magnetic Diagnostics System of Hall Thruster Plasma," The 29th International Electric Propulsion Conference, Princeton, New Jersey, October 2005.

[23] Mullins, C. R., Martinez, R. A., Williams, J. D., Farnell, C. C., Farnell, C. C., Liu, D., and Branam, R. D., "Non-Invasive Hall Current Distribution Measurement in a Hall Effect Thruster," The 51st AIAA/SAE/ASEE Joint Propulsion Conference, No. AIAA 2015-4005, Orlando, Florida, July 2015.

[24] Rubin, B., Analysis and Numerical Experimentation of Onboard Diagnostic Systems for Hall Thrusters, Ph.D. Thesis, Technion-Israel Institute of Technology, Haifa, Israel, 2006.

[25] Busek Co. Inc., "BHT-600-PM Permanent Magnet Hall Thruster Installation and Operating Manual," Natick, MA, 2016.

[26] D. Liu, Two-Dimensional Time-Dependent Plasma Structures of a Hall Effect Thruster, Dayton : Air Force Institue of technology , 2011.

[27] D. LTilley, K. H. De Grys and R. M. Meyers, "Hall thruster-cathode coupling," in 35th Joint Propulsion Conference and Exhibit, Los Angeles Ca, 1999.

[28] Busek Co. Inc., "Busek Hollow Cathodes," 2013. [Online] Available: http://www.busek.com/index_htm_files/70008509B.pdf.

[29] Nicholas L. Hyatt, "Hall Effect Thruster Characterization through Potential, Magnetic, and Optical Measurements," Master's thesis, Air Force Institute of Technology, March 2017.

[30] Sekerak, M. J., Longmier, B. W., Gallimore, A. D., Brown, D. L., Hofer, R. R., and Polk, J. E., "Azimuthal Spoke Propagation in Hall Effect Thrusters," The 33rd International Electric Propulsion Conference, Washington, D.C., October 2013.

<table>
<tr><td colspan="3" align="center">REPORT DOCUMENTATION PAGE</td><td colspan="2" align="center">Form Approved
OMB No. 0704-0188</td></tr>
</table>

REPORT DOCUMENTATION PAGE			*Form Approved* *OMB No. 0704-0188*	

Public reporting burden for this collection of information is estimated to average 1 hour per response, including the time for reviewing instructions, searching existing data sources, gathering and maintaining the data needed, and completing and reviewing this collection of information. Send comments regarding this burden estimate or any other aspect of this collection of information, including suggestions for reducing this burden to Department of Defense, Washington Headquarters Services, Directorate for Information Operations and Reports (0704-0188), 1215 Jefferson Davis Highway, Suite 1204, Arlington, VA 22202-4302. Respondents should be aware that notwithstanding any other provision of law, no person shall be subject to any penalty for failing to comply with a collection of information if it does not display a currently valid OMB control number. **PLEASE DO NOT RETURN YOUR FORM TO THE ABOVE ADDRESS.**

1. REPORT DATE *(DD-MM-YYYY)* 22-03-2018	**2. REPORT TYPE** Master's Thesis		**3. DATES COVERED** *(From - To)* August 2016 – March 2018
4. TITLE AND SUBTITLE Characterization and Analysis of Plasma Instabilities in a 600 W Permanent Magnet Hall Thruster			**5a. CONTRACT NUMBER**
			5b. GRANT NUMBER
			5c. PROGRAM ELEMENT NUMBER
6. AUTHOR(S) Wright, Samuel D., Captain, USAF			**5d. PROJECT NUMBER**
			5e. TASK NUMBER
			5f. WORK UNIT NUMBER
7. PERFORMING ORGANIZATION NAME(S) AND ADDRESS(ES) Air Force Institute of Technology Graduate School of Engineering and Management (AFIT/EN) 2950 Hobson Way, Building 640 WPAFB OH 45433-8865			**8. PERFORMING ORGANIZATION REPORT NUMBER** AFIT-ENY-MS-18-M-308
9. SPONSORING / MONITORING AGENCY NAME(S) AND ADDRESS(ES) Air Force Office of Scientific Research Energy Attn: Dr. Mitat Birkan 875 N. Randolph, Ste 325 Arlington, VA 22203 mitat.birkan@us.af.mil			**10. SPONSOR/MONITOR'S ACRONYM(S)** AFOSR
			11. SPONSOR/MONITOR'S REPORT NUMBER(S)

12. DISTRIBUTION / AVAILABILITY STATEMENT
DISTRUBTION STATEMENT A. APPROVED FOR PUBLIC RELEASE; DISTRIBUTION UNLIMITED.

13. SUPPLEMENTARY NOTES
This material is declared a work of the U.S. Government and is not subject to copyright protection in the United States.

14. ABSTRACT
Electric propulsion is an important technology for the future of space operations and exploration. Within the range of electric propulsion devices, Hall Effect Thrusters provide a balance of thrust and specific impulse well-suited for many Earth-centric missions. Hall Effect Thrusters have been studied extensively, but the intimate details of the plasma behavior within the thruster exhaust plume are still not well understood. Furthering this knowledge may be key to improving thruster design to yield better performance and longer lifetimes. To this end, experiments were conducted to measure visible emissions, plasma potential, and Hall Current from a 600 W permanent magnet Hall Effect Thruster in operation modes that exhibited two well-known plasma behaviors—breathing and azimuthal spokes. Multiple delays and issues with the thruster and laboratory equipment severely limited data collection during the present research, but a number of visible emissions data samples were collected. Data revealed the breathing mode exhibited in the permanent magnet thruster is similar to that in a previously studied electromagnet thruster. Additionally, a trend in the breathing mode was observed that appears to lead to discharge extinction. An azimuthally-varying mode was also identified and compared to the spoke mode exhibited by the electromagnet thruster.

15. SUBJECT TERMS
Hall Thruster, Hall Effect Thruster, Electric Propulsion, Ionization, Plasma

16. SECURITY CLASSIFICATION OF:			**17. LIMITATION OF ABSTRACT**	**18. NUMBER OF PAGES**	**19a. NAME OF RESPONSIBLE PERSON** Dr. Carl Hartsfield, AFIT/ENY
a. REPORT U	**b. ABSTRACT** U	**c. THIS PAGE** U	UU	129	**19b. TELEPHONE NUMBER** *(include area code)* (937)255-3636 x4667 carl.hartsfield@afit.edu

<div align="right">

Standard Form 298 (Rev. 8-98)
Prescribed by ANSI Std. Z39.18

</div>